Earth-Science Reviews 214 (2021) 103477

Contents lists available at ScienceDirect

Earth-Science Reviews

journal homepage: www.elsevier.com/locate/earscirev

Extending full-plate tectonic models into deep time: Linking the Neoproterozoic and the Phanerozoic

Andrew S. Merdith [a,*], Simon E. Williams [b], Alan S. Collins [c], Michael G. Tetley [a], Jacob A. Mulder [d], Morgan L. Blades [c], Alexander Young [e], Sheree E. Armistead [f], John Cannon [g], Sabin Zahirovic [g], R. Dietmar Müller [g]

[a] UnivLyon, Université Lyon 1, ENS de Lyon, CNRS, UMR 5276 LGL-TPE, Villeurbanne F-69622, France
[b] State Key Laboratory of Continental Dynamics, Department of Geology, Northwest University, Xi'an, China
[c] Tectonics and Earth Systems (TES) Group, Department of Earth Sciences, The University of Adelaide, Adelaide, SA 5005, Australia
[d] School of Earth, Atmosphere and Environment, Monash University, Clayton, Victoria 3168, Australia
[e] GeoQuEST Research Centre, School of Earth, Atmospheric and Life Sciences, University of Wollongong, Northfields Avenue, NSW 2522, Australia
[f] Geological Survey of Canada, Canada & Metal Earth, Harquail School of Earth Sciences, Laurentian University, 601 Booth Street, Ottawa, Ontario, Sudbury, Ontario, Canada
[g] Earthbyte Group, School of Geosciences, University of Sydney, Sydney, New South Wales 2006, Australia

ARTICLE INFO

Keywords:
Palaeogeography
Rodinia
Gondwana
Plate tectonics
Neoproterozoic

ABSTRACT

Recent progress in plate tectonic reconstructions has seen models move beyond the classical idea of continental drift by attempting to reconstruct the full evolving configuration of tectonic plates and plate boundaries. A particular problem for the Neoproterozoic and Cambrian is that many existing interpretations of geological and palaeomagnetic data have remained disconnected from younger, better-constrained periods in Earth history. An important test of deep time reconstructions is therefore to demonstrate the continuous kinematic viability of tectonic motions across multiple supercontinent cycles. We present, for the first time, a continuous full-plate model spanning 1 Ga to the present-day, that includes a revised and improved model for the Neoproterozoic–Cambrian (1000–520 Ma) that connects with models of the Phanerozoic, thereby opening up pre-Gondwana times for quantitative analysis and further regional refinements. In this contribution, we first summarise methodological approaches to full-plate modelling and review the existing full-plate models in order to select appropriate models that produce a single continuous model. Our model is presented in a palaeomagnetic reference frame, with a newly-derived apparent polar wander path for Gondwana from 540 to 320 Ma, and a global apparent polar wander path from 320 to 0 Ma. We stress, though while we have used palaeomagnetic data when available, the model is also geologically constrained, based on preserved data from past-plate boundaries. This study is intended as a first step in the direction of a detailed and self-consistent tectonic reconstruction for the last billion years of Earth history, and our model files are released to facilitate community development.

1. Introduction

Plate tectonics is a unifying theory of modern geology, explicitly connecting the evolution and processes that bridge the mantle, lithosphere, hydrosphere and atmosphere. Tectonic forces control the rates of uplift and erosion where continents collide or separate (England and Molnar, 1990) and modulate the flow of energy between oceans, lithosphere and mantle as continental configurations evolve (Bebout, 1995; Karlsen et al., 2019; Müller et al., 2008). Evolving plate tectonic configurations also determine changes in how species are distributed across different landmasses (McKenzie et al., 2014; Meert and Lieberman, 2008) and infer the rates of chemical flux between the Earth's surface and the deep interior (Gernon et al., 2016; Jarrard, 2003).

Global reconstructions have traditionally focussed on the positions of the major continents and geological terranes preserved within them. Data acquired from modern oceans provide an effective constraint on the breakup of the supercontinent Pangea over the last ca. 200 Ma, and form the basis of continuous models of plate configurations from the

* Corresponding author.
E-mail address: Andrew.merdith@univ-lyon1.fr (A.S. Merdith).

https://doi.org/10.1016/j.earscirev.2020.103477
Received 2 October 2020; Received in revised form 15 December 2020; Accepted 16 December 2020
Available online 24 December 2020
0012-8252/Crown Copyright © 2021 Published by Elsevier B.V. All rights reserved.

Mesozoic to present (e.g. Müller et al., 2016; Seton et al., 2012). These 'full-plate' reconstructions use geological and geophysical data to determine the configurations and motions of both continental and oceanic lithosphere, and the nature of the plate boundaries that separate neighbouring plates. Together with the development of free software tools (Boyden et al., 2011; Müller et al., 2018), full-plate reconstructions permit quantitative estimates of tectonic processes through time within a continuous, consistent kinematic framework, opening up portions of Earth's history to quantitative analysis (e.g. Bower et al., 2013; Brune et al., 2017; Dutkiewicz et al., 2019; Hounslow et al., 2018; Karlsen et al., 2019; Merdith et al., 2019a).

Plate tectonic processes are thought to have been the dominant control on Earth's palaeogeography, possibly since 3.2 Ga (Brenner et al., 2020; Brown et al., 2020a; Cawood et al., 2018a; Gerya, 2014; Palin et al., 2020). Studies of the pre-Pangean Earth have led to the proposal that Pangea was preceded by the Proterozoic supercontinents Rodinia (Dalziel, 1991; Hoffman, 1991; Moores, 1991) and Nuna/Columbia (Meert, 2002; Rogers and Santosh, 2002; Zhao et al., 2002) and earlier Archaean 'supercratons' (e.g. Bleeker, 2003; Pehrsson et al., 2013; Smirnov et al., 2013), reflecting transient aggregations of continental blocks interspersed between other phases of Earth's history when the continents were more dispersed. The absence of a pre-Mesozoic ocean floor record necessitates that reconstructing the pre-Pangean Earth relies on the fragmented geological record preserved within the continents. Early studies of Proterozoic supercontinents provide individual snapshots of continental configurations; though there are differences between competing interpretations. More recently, attempts have been made to reconcile Neoproterozoic continental motions within a continuous kinematic framework (Cawood et al., 2020; Collins and Pisarevsky, 2005; Li et al., 2008). To further infer the extent and nature of tectonic boundaries covering all of Earth's surface in the Proterozoic requires methodical extrapolation of available observations and is subject to major uncertainties. Despite this, these reconstructions are valuable in that they make testable predictions about regions and time periods where observations are lacking.

Full-plate models published over the last decade collectively span the last 1 Ga. However, each of these models cover different time periods or areas of the world and each model is based on different assumptions and hypotheses, and place differing emphases on subsets of the geological record. Thus, although continental motions and plate boundary evolution have been categorised in some manner for the past 1 Ga, there is no fully continuous model defining Earth's tectonic history for this time. A fundamental test of any tectonic reconstruction for the Precambrian is that the configurations of continents, terranes and plate boundaries can evolve continuously as to seamlessly merge with reconstructed configurations for more recent times that are better constrained and ultimately tied to the present-day Earth. The absence of such continuous reconstructions highlights a critical uncertainty for assessing interpretations of Neoproterozoic palaeogeography, tectonics and geodynamics.

Our key motivations for this study are three-fold. Firstly, a 1 Ga model will permit, for the first time, Neoproterozoic and Cambrian quantitative analysis that constrains (bio)geochemical and volatile fluxes, palaeoclimatic studies and the nature of earth systems, during times of biological evolution and extreme climate change (Gernon et al., 2016; Goddéris et al., 2017; Mills et al., 2011, 2019). Second, a full-plate model would be a starting point for future studies to constrain both the tectonic (e.g. supercontinent cycle (Li et al., 2019; Merdith et al., 2019b)) and geodynamic (e.g. core-lithosphere-mantle connection (Heron et al., 2020; Tetley et al., 2019)) nature and evolution of the Earth. Third, a consistent model for the Neoproterozoic and Cambrian that coherently links with younger models can be used as a framework to support future regional studies that test and enhance the resolution of the model or spawn alternative models that can be used for hypothesis testing. We stress that our reconstruction is intended to capture the main aspects of global tectonics across the last billion years and consequently lacks many details that could be incorporated for individual regions. Just as the earliest full-plate models for the Cenozoic and Mesozoic (Seton et al., 2012) and late Palaeozoic (Domeier and Torsvik, 2014) have provided valuable open-access resources for numerous other studies to test and improve, we intend that the global framework provided by our reconstruction will form the basis for future studies that will generate improved reconstructions by incorporating new or different observations and ideas.

This paper is organised as follows: first, we provide a review of the concepts behind full-plate reconstructions, including the types of observations and assumptions on which they are based. We then summarise the previously published reconstruction models and justify which elements of these existing studies we have chosen to include in our reconstruction. Finally, we present the main outcome of our study: the first continuous and self-consistent full-plate model from 1 Ga to present day with a single set of polygons, Euler rotations and plate boundaries.

2. Full-plate reconstruction models

There are two broad categories of models that can be constructed to describe Earth's tectonic or palaeogeographic history. The first category we refer to as 'continental drift' type models (Fig. 1a), as they model the motion of continents drifting across the Earth's surface and tend to explicitly reflect palaeogeography rather than tectonic evolution. The second type we refer to as 'full-plate models' (Fig. 1b), which, in addition to tracking the motion of continents, trace the evolution of plate boundaries and by implication, the evolution of tectonic plates themselves (Gurnis et al., 2012). In effect, continental drift type models are the precursor to full-plate models, but rather than supersede continental drift models, both types of models complement each other and provide different avenues for research. Continental drift type models are useful for analysing palaeomagnetic data, for contextualising regional studies or as a ground-breaking study where there is little preserved data on plate boundaries. Comparably, full-plate models are more encompassing, but are also much harder to iterate over and generate alternative models from. If one simply requires the distribution of continental crust and not of plate boundaries, then it is much easier and simpler to build a continental drift style model than categorically describe and model plate boundaries through time. However, both types of models use the same reconstruction framework.

2.1. Reconstruction framework

The essential characteristic of any plate reconstruction is the reconstruction framework (or network (Domeier and Torsvik, 2017)), which is the organisation of data used to describe the motion of rigid objects on a sphere using Euler's rotation theorem (McKenzie and Parker, 1967; Morgan, 1968). In plate reconstructions, the rigid objects in motion are the plates themselves and, in addition to requiring the temporal and spatial components of moving plates (i.e. the time period of motion, latitude, longitude and angle of rotation) the theorem also requires that each rotation be defined relative to another object. This rotation of one object relative to another forms the basis of a 'relative plate motion model'. It is also desirable for these relative rotations to be tied to something immutable within, or around, the Earth (e.g. the core, mantle, or the spin-axis) thus, transforming the model into an 'absolute plate motion model'. For the Mesozoic and Cenozoic, plates are described in a relative framework due to the preservation of oceanic lithosphere within oceans formed since the breakup of Pangea. In this way each plate's motion history is described as moving relative to another plate, with the African plate typically at the top of the hierarchy (e.g. (Ross and Scotese, 1988; Torsvik et al., 2008); Fig. 2a, b). The motion of the African plate can then be defined absolutely (though using observations from many or all plates, and not just Africa) to the deep Earth through alternative methods such as hotspot chains (Müller et al., 1993; O'Neill et al., 2005), seismic imaging of subducted slabs (van der

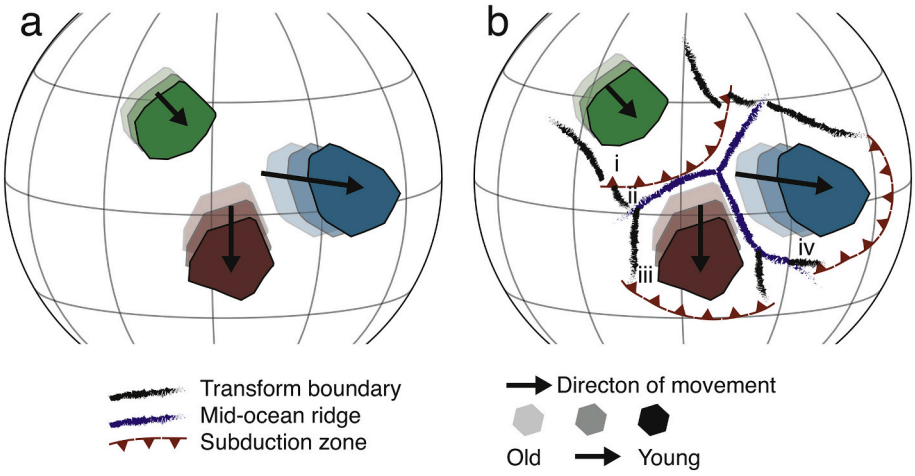


Fig. 1. Schematic comparison of evolution of plate tectonic modelling. (a) 'Continental drift'/palaeogeographic type models and (b) full-plate models; (i)–(iv) identify separate plates. Palaeomagnetic data are the primary constraint of the movement of continents in both (a) and (b) however, the inclusion of geological data into the model in (b) preserves the relative type of motion between two continents (divergence, convergence or transform) and allows for the construction of plate boundaries.

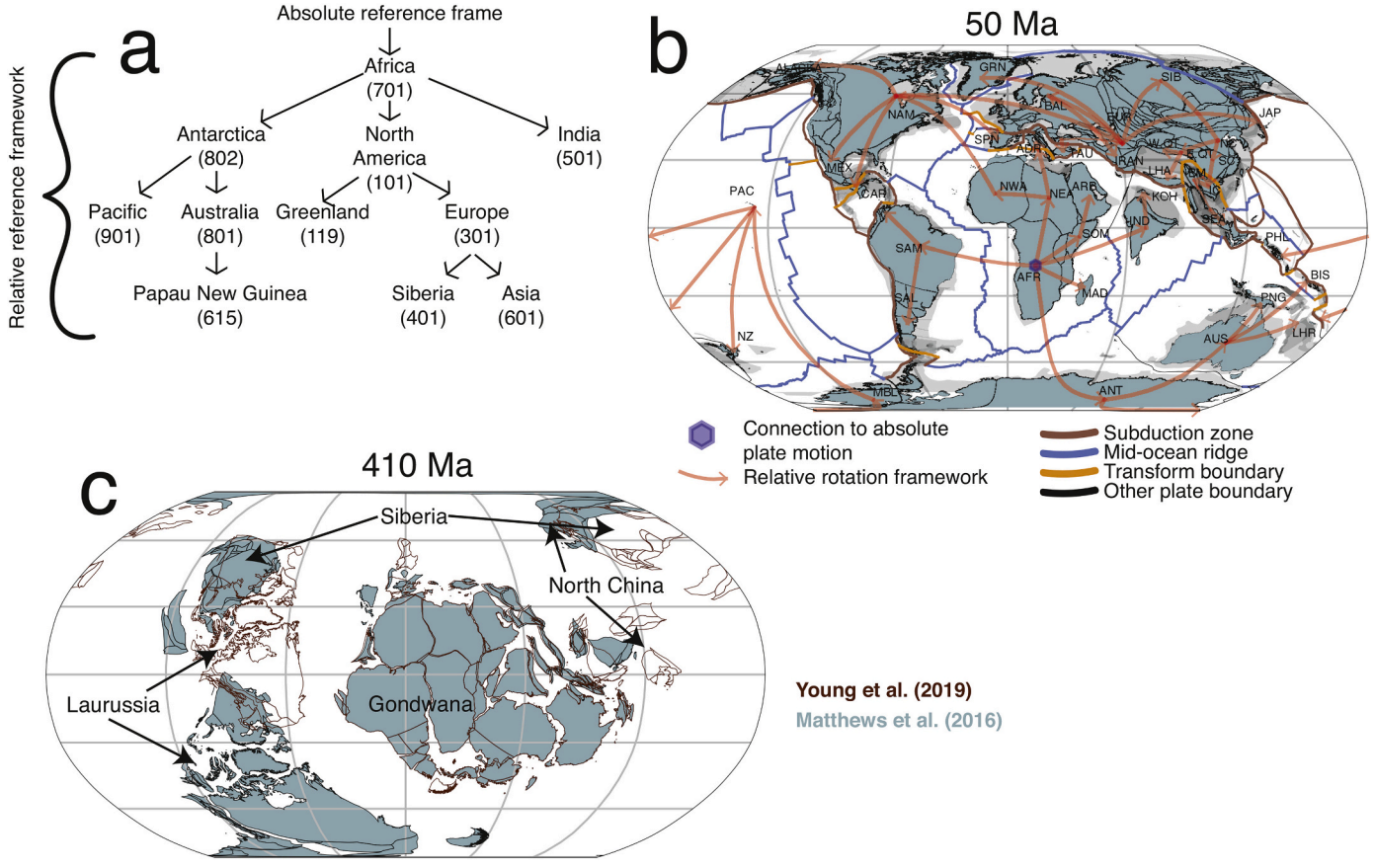


Fig. 2. Overview of the rotational framework of a relative plate motion model. (a) Schematic of the 'tree' like hierarchy (e.g. Ross and Scotese, 1988) from the Matthews et al. (2016) reconstruction, where the motion of all plates are defined relative to the African plate at 50 Ma. (b) A simplified map view of the hierarchy in (a). The African stage pole (blue hexagon) is at the top of the hierarchy and connected to the absolute plate motion model that describes the movement of the African plate (in this case, as a proxy for the entire globe) to the deep earth. (c) Example of plate motion with a continent (Africa) fixed in its present-day position. Fixed plate presentations enable observations of relative motions between the fixed continent or plate and another. Hence, they are useful to constrain relative plate motions and also compare two or more different plate models. In this instance, a key difference between the model of Young et al. (2019) and Matthews et al. (2016) is highlighted in the spatial relationship between Laurussia and Gondwana at 410 Ma. In Domeier and Torsvik et al. (2014) (which is preserved in Matthews et al. (2016)) Laurussia is proximal to southwest Gondwana while in Young et al. (2019) it is positioned to the northwest. ADR, Adria; AFR, Africa; ARB, Arabia; AUS, Australia; BAL, Baltica (cratonic Europe); BM, Burma; CAR, Caribbean; E.QT, East Qiangtang; EUR, Europe; GRN, Greenland; IC, Indochina; IND, India; JAP, Japan; KOH, Kohistan arc; LHA, Lhasa; LHR, Lord Howe Rise; MAD, Madagascar; MBL, Marie Byrd Land; MEX, Mexico; NAM, North America; NC, North China; NEA, Northeast Africa; NWA, Northwest Africa; NZ, New Zealand; PAC, Pacific; PHL, Philippines; PNG, Papua New Guinea; SAL, Salado Microplate; SAM, South America; SC, South China; SEA, Southeast Asia; SIB, Siberia; SOM, Somalia; SPN, Spain; TAU, Taurides; W.QT, West Qiangtang.

Meer et al., 2010), palaeomagnetic data (with or without true polar wander corrections, Torsvik et al., 2012) or methods jointly evaluating the characteristics of multiple constraints including plate velocities, hotspot chains and subduction trench migration (Tetley et al., 2019). Regardless of which method is chosen, the result is a global reference frame defined as a sequence of absolute motions of the African plate, which, together with the relative motions between plate-pairs arranged within a hierarchy (Fig. 2), define the absolute motions of all plates. An exception to all plates being tied to Africa occurs for the Mesozoic Pacific Ocean. Before 83 Ma (and the opening of the West Antarctic spreading centre) the motion of the Pacific plate is preserved and reconstructed absolutely to the spin axis through hotspot motion, rather than through Africa. Plate models can also be described in a purely relative framework, in which case a single continent (or plate) is fixed to its present-day position and all other continents or plates are rotated relative to the fixed plate. This approach is commonly used for localised studies or to easily highlight the difference between two contrasting models (Fig. 2c).

Before the Mesozoic era, it is not possible to use preserved, *in situ* oceanic lithosphere, hotspot motions and seismic imaging of slabs to constrain plate motion. Therefore, the logical arrangement of connections within the rotational framework changes (Domeier and Torsvik, 2017), however the general principles of plate reconstructions remain the same. For these times, the only quantitative information on the positions of plates is through palaeomagnetism, which describes the palaeolatitude of continents with respect to the Earth's spin axis. In these cases, where the absolute motions are more directly constrained than relative motions, rotation models traditionally favour a simpler hierarchy, rather than the complex hierarchies used for post-Pangea times (e.g Fig. 3a, b). The motion of major continents relative to the spin axis is determined using their own palaeomagnetic data (Fig. 3a, b). Within this data set, continents can be grouped together in localised hierarchies where there is evidence that they have remained together or close to one another or, in instances where palaeomagnetic data are lacking from some of the blocks if geological constraints permit.

Finally, although Euler's rotation theorem is based on the motion of rigid bodies, this is a simplification because the lithosphere is deformable. Recent advancements in plate modelling (Gurnis et al., 2018) have allowed for the development of deforming plate models where rigid plates are able to deform along their edges.

2.2. Palaeolatitude

Palaeolatitude is determined through the study of palaeomagnetic data and is the only method to quantitatively constrain the absolute latitudinal position of a continent for pre-Jurassic times. If sufficient data are present from a single continent, an apparent polar wander path (APWP) can be constructed that describes the motion of that continent through time (Torsvik et al., 2012). If there are very good geological constraints on the relative positioning between multiple continents, then poles from these continents can be merged to form composite apparent polar wander paths. This merging is done by rotating the poles of multiple continents into the coordinate frame of a single continent, typically found higher in the framework (e.g. Africa, Fig. 2a). If this process is done using all global data it is known as a global apparent polar wander path (GAPWaP). GAPWaPs provide the potential for a more rigorous description of the evolution of a suite of continents as more data are available.

There are, however, many caveats and uncertainties associated with GAPWaPs and APWPs that contain data sourced from more than one continent (e.g. APWP for Gondwana). In particular, they are strongly dependent on the relative position of continents, as even minor changes in these relative positions can result in large differences in the resulting wander paths. They also are directly dependent on the quality and abundance of palaeomagnetic data, thus a degree of subjectivity can be introduced by what criteria are used for selecting and filtering poles (Van der Voo, 1990; though see a new approach in Wu et al., 2020). For example, in the Gondwana APWP of Torsvik et al. (2012) (and also for the APWP we construct in this paper), there is one pole for Gondwana between 440 and 400 Ma that constrains the motion of over half of all known continental crust at the time. In the Precambrian, the geological uncertainty of exactly how two cratons (or continents) fit together limits the usefulness of GAPWaPs and APWPs that are defined by multiple continents in conjunction with one another. Instead individual APWPs can be constructed using available palaeomagnetic data for continents and then these are all balanced together globally to produce a coherent kinematic continental model (e.g. Li et al., 2008; Pisarevsky et al., 2014). In this manner, it is possible to build continental drift models purely from palaeomagnetic data.

2.3. True Polar Wander

True polar wander (TPW) is the motion of the entire solid Earth (mantle-lithosphere) with respect to the spin axis due to centrifugal forces from Earth's orbit acting on mass anomalies in the upper mantle, wherein positive anomalies are driven towards the equator and negative anomalies towards the poles (Evans, 2003). Since TPW is inherent in palaeomagnetic data, all APWP are a composite of both plate motions

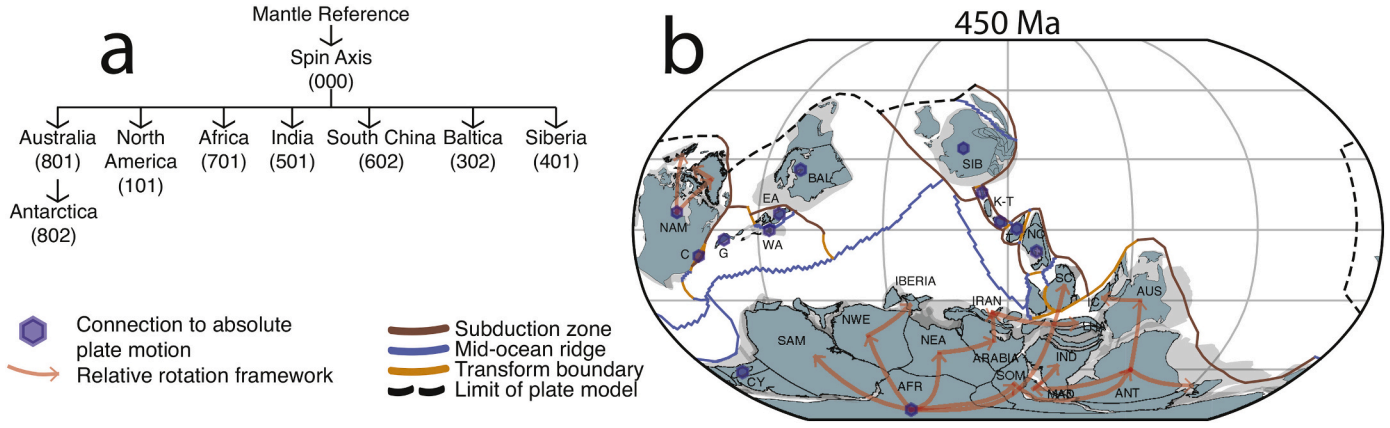


Fig. 3. Overview of the rotational framework of an absolute plate motion model. (a) Schematic of a flat hierarchy where the motion of all plates is defined relative to Africa. (b) Map view of the schematic at 450 Ma from Domeier (2018, 2016). Many different plates (blue hexagons) sit at the top of the hierarchy and connect to the deep earth. AFR, Africa; ANT, Antarctica; AUS, Australia; BAL, Baltica; C, Carolinia; CY, Cuyania; EA, East Avalonia; G, Ganderia; IC, Indochina; IND, India; K-T, Kazakh-Tianshan; LHA, Lhasa; MAD, Madagascar; NAM, North America; NC, North China; NEA, Northeast Africa; NWA, Northwest Africa; SAM, South America; SC, South China; SIB, Siberia; SOM, Somalia; T, Tarim; WA, West Avalonia.

and some component of TPW. Thus, in the strictest sense, to properly use a plate model for geodynamic modelling, a correction that removes any component of detected TPW should be applied (i.e. the mantle reference frame). Further, as the mass anomalies in the mantle are thought to arise from the flow induced by subducted oceanic lithosphere and the associated return flows, TPW excursions are closely linked to the supercontinent cycle (Zhong et al., 2007).

Raub et al. (2007) identified three types of TPW summarised briefly below, though only the latter two are relevant here. Type 0 TPW operates on short ($< 10^3$ a) timescales as a response to elastic deformation within the lithosphere arising from seismic events (Soldati et al., 2001) and so has a negligible effect on plate motions on the timescales pertinent here (Evans, 2003; Raub et al., 2007). Type 1 TPW is the most important to consider, and is broadly defined as the slow motion of the solid Earth (mantle and lithosphere) readjusting to mass anomalies in the mantle. Type 1 TPW is what is commonly detected and corrected in plate motion models (Steinberger and Torsvik, 2008; Torsvik et al., 2012) in order to constrain geodynamic relationships between deep Earth processes and tectonics (Mitchell et al., 2012). Type 2 TPW (Inertial-Interchange True Polar Wander, IITPW) was originally described by Kirschvink et al. (1997) and is a hypothesis where the mantle and crust are rapidly displaced over large distances relative to the spin axis as the moment of minimum inertia (I_{min}) approaches the maximum moment of inertia (I_{max}) resulting in an interchange between the two (i.e. I_{min} becomes I_{max} and vice versa). IITPW has been linked to supercontinent breakup as continental lithosphere and subduction zones move away from the upwelling, known as a superswell, developing beneath the supercontinent, which is assumed to remain quasi-stable (Li et al., 2004). In the model of Li et al. (2004), the superswell is likely to maintain the I_{max}, but as all the continents move away I_{min} approaches I_{max}, thus they are speculated to interchange with each other.

The primary challenge of subtracting the effects of TPW from APW paths is identifying and separating TPW components from continental motion. Methods of detecting TPW vary, either isolating it directly from palaeomagnetic data (Mitchell et al., 2012) or deconstructing the APWP of continents by comparing the kinematic motions of all continental lithosphere on the globe to isolate TPW (Steinberger and Torsvik, 2008). Both approaches require *a priori* assumptions stemming from the choice of plate model being analysed, which makes it impossible to apply a TPW correction from one model to another. For example, fitting a great circle to palaeomagnetic data following the approach of Mitchell et al. (2012) is dependent on knowing the relative continental configuration from which the palaeomagnetic data are sampled. Alternatively, deconstructing the motions of the continents after Steinberger and Torsvik et al. (2008) is dependent on constraining absolute palaeolongitude to separate TPW from apparent polar wander. In order to support their arguments, both methods are dependent on having some form of absolute palaeolongitudinal control.

2.4. Palaeolongitude

There is no well-established method to compute the absolute palaeolongitude of any given plate that is applicable to pre-Jurassic times. However, two hypotheses have been proposed for establishing absolute palaeolongitude for pre-Pangea reconstructions (Torsvik and Cocks, 2017): (i) the plume generation zone method (PGZ) (Torsvik et al., 2014) and (ii) the orthoversion model of the supercontinent cycle (Mitchell et al., 2012).

The PGZ method is based on reconstructing the surface locations of kimberlites and large igneous provinces (LIPs) to the margins of the large low shear velocity provinces (LLSVPs) (Burke and Torsvik, 2004; Torsvik et al., 2010a) situated on the core-mantle boundary (CMB) (Garnero et al., 2007; Li and McNamara, 2013). The foundation for this method is the observation that kimberlites and LIPs, when restored to a mantle reference frame at the time of eruption, are positioned preferentially above the margins of the LLSVPs (Burke and Torsvik, 2004; Torsvik et al., 2010a). LLSVPs are regions of anomalously slow (slower than ambient mantle) seismic velocities, close to the core–mantle boundary. Since large-scale mantle structure is intimately related to the supercontinent cycle, LLSVPs (Li and Zhong, 2009) are thought to exist for (at least) a similar time frame as the supercontinent itself (i.e. present-day LLSVPs are thought to have existed at least back to 320 Ma) (Li and Zhong, 2009), but not necessarily maintaining their present-day geometry (Flament et al., 2017; Zhang et al., 2010; Zhong and Rudolph, 2015).

The PGZ method to establish absolute palaeolongitude therefore assumes: (i) the geometric stability of the present-day positions of LLSVPs back to the time of interest, and (ii) that there is a positive statistical correlation with margins of LLSVPs and the extrusion of LIPs and kimberlites at the Earth's surface. Adopting the PGZ method allows one to position continents longitudinally by reconstructing the positions of LIPs and kimberlites to overlie the margins of LLSVPs while simultaneously using TPW-corrected palaeomagnetic data (Torsvik et al., 2014). In this way, models with explicitly defined and reproducible absolute plate motions can be created (Domeier and Torsvik, 2014). However, a number of recent studies have raised questions about the assumptions implicit in the PGZ approach. For example Flament et al. (2017) and correspondence by Torsvik and Domeier (2017), Doucet et al. (2020), Zhong and Rudolph (2015) and Zhong and Liu (2016) on long term LLSVP stability and Austermann et al. (2014), Davies et al. (2015), with response by Doubrovine et al. (2016) on the statistical correlation. Consequently, while using the PGZ method for plate reconstructions in the Palaeozoic is currently an open area of research, the theoretical and practical application for Precambrian times remains untested.

The other proposed method of determining absolute palaeolongitude for deep time reconstructions is known as the 'orthoversion model' and suggests that successive supercontinents coalesce orthogonally (90° longitude) above the downwelling formed by subduction at the margin of the previous supercontinent (Mitchell et al., 2012). Mitchell et al. (2012) test their model by first determining the minimum moment of inertia (I_{min}) during each phase of supercontinent assembly. This is done by rotating the available palaeomagnetic data into a relative reference frame of a fixed continent (Africa for the Phanerozoic, Laurentia for the Neoproterozoic) and then fitting a great circle to the resulting poles. I_{min} is defined as the orthogonal axes (or pole) of the great circle and is taken to approximate the TPW axis. Mitchell et al. (2012) fitted great circles to palaeomagnetic data for a selection of time periods (1165–1015 Ma, 805–790 Ma, 550–490 Ma and 220–90 Ma) and calculated that the angle between each successive I_{min} was ~90°; as expected in the orthoversion model. The initial (palaeolongitudinal) placement of Pangea is constrained from its position at ~90 Ma (centroid of I_{min} at 0°N, 10°E) when the most recent TPW episode finished (Steinberger and Torsvik, 2008). Therefore, during Rodinia and Gondwana, when I_{min} was 90° from present day, Mitchell et al. (2012) proposed that the centre of mass of both was positioned at 100°E.

As with the PGZ, a number of limitations are apparent with the orthoversion model. In particular, the method of Mitchell et al. (2012) does not separate continental motion from true polar wander when calculating I_{min}, thus it assumes that during these times TPW is the primary signal recovered from palaeomagnetic data and not continental motion. Secondly, the orthoversion model is inherently dependent on both the quality and abundance of palaeomagnetic data (e.g. the Rodinia I_{min} in Mitchell et al. (2012) is based on only three poles), as well as the continental configuration of the time (as the continental configurations can determine the relative position of palaeomagnetic data when rotated into a specific reference frame). Torsvik and Cocks (2017) highlight this succinctly by using slightly different palaeomagnetic data, and a slightly different Gondwana configuration to produce an I_{min} between 550 and 490 Ma of 50°S, 64°E (compared to the estimate of Mitchell et al. (2012) of 30°S, 75°E). Finally, the calculation of I_{min} at each time step occurs within a fixed relative reference frame (i.e. Fig. 2c), meaning that the

I_{min} itself cannot be restored to an absolute palaeogeographic position. Thus, the longitudinal centre of Rodinia at 100°E is not explicitly proven by Mitchell et al. (2012). Instead, since the calculated successive I_{min}'s are 90° apart, it is inferred to be in this location.

2.5. Geology

Geology is unfortunately silent on the absolute positioning of continents in time, except in circumstances such as the PGZ method discussed above. However, it contains a wealth of information of relative plate motions in the Mesozoic and Cenozoic (e.g. seafloor spreading), and in deeper time through the temporal evolution of sedimentary basins and facies, and tectonic affinities inferred from geochemistry, zircon arrays, magmatism and metamorphism. However, geology does have an advantage over palaeomagnetic data in that there are many different types of data available, especially from small and minor terranes in the Precambrian that are otherwise unconstrained palaeomagnetically. Given the wealth of geological data, especially in the Neoproterozoic, there is a general hierarchy of use that is a reflection of the scale of the problem. Our approach is to start by building a global framework and work progressively to finer resolution to inform the localised nature of that framework.

The first and most important geological data to gather is evidence of rifts and arcs, as they describe separation (usually leading to seafloor spreading) and convergence, respectively, and can therefore put in place the framework for plate motions and subsequent interpretation of geological data. Secondly, identifying piercing points where geological boundaries can be matched on now separate continents (e.g. Appalachians/Caledonides and the Gondwana-forming orogenies), or ways of fitting two continents together in a stable configuration. These piercing points are important because reconstructing continental configurations with high confidence allows the generation of more rigorous APWPs and they help to constrain the location and orientation of both rifts and arcs on the periphery of continents. Unfortunately, due to deformation and progressive alteration of continental crust (e.g. changes of continent-ocean boundaries (COBs)), in pre-Gondwana times it is difficult to be more precise than matching the margins of large continents and for smaller cratons and terranes it is almost impossible. A pertinent example of this are the four different proposed configurations of Australia and Laurentia during Rodinia (see reviews by Li et al., 2008; Merdith et al., 2017b), which all broadly match the same margins against each other (east coast of Australia with the west coast Laurentia, with or without an intervening continent) but place them in different relative positions.

After arcs and rifts, we can loosely (but not exhaustively) group geological features and data based on their applications. Sedimentary basins, dyke swarms, detrital minerals, geochemical signatures and fossils are typically used to determine provenance or latitudinal band and align once contiguous regions. The time-scales and conditions of metamorphism together with structural data can be used to infer the tectonic setting and polarity of collisional events or help constrain the nature of indeterminate plate margins such as transform boundaries. These types of data assist in increasing the resolution of a plate model by understanding the geology at smaller scales within the framework of a specific tectonic setting, such as an arc or rift. We stress here that the relationship between detailed regional geology and the broader framework of a plate model is not a 'one-way street' but is highly iterative. If, for example, a detailed geological study determines that an interval of magmatism and sedimentation that was originally interpreted as a failed rift, in fact led to seafloor spreading, then the broader scale tectonic framework and plate model must be re-evaluated. Finally, due to the qualitative nature of most geological data, the iteration and implementation of these data into the plate model typically necessitates qualitative decisions that others may disagree with. Iteration over the model continues until we approach tectonic congruency within the model (i.e. data-based iterations in one part of the world do not nullify data in other areas of the world). We stress that this does not mean our model is 'correct' or 'true', just that it is internally consistent with as much data as possible. Consequently, we consider the model presented here a viable, but non-unique interpretation of Neoproterozoic data.

A specific example of the importance of interpreting geology within a full-plate framework is given by recent work on the Stenian–Cryogenian evolution of the East African Orogen. Although arc-related magmatism has been recognised in the northern East African Orogen for a number of decades (e.g. Stern, 1994), the recognition of similar-aged arc magmatism in the higher-grade southern East African Orogen of Madagascar, Southern India and East Antarctica has been more controversial and under-appreciated until recently (Archibald et al., 2018; Archibald et al., 2017; Armistead et al., 2019; Plavsa et al., 2015; Ruppel et al., 2018). In one particular example, work over the last decade on Western Dronning Maud Land in East Antarctica has identified an extensive Stenian–Tonian juvenile arc system (named TOAST; Elburg et al., 2015; Jacobs et al., 2015; Ruppel et al., 2018). This discovery has gone hand-in-hand with the recognition of a similar region in western Madagascar, known as the Dabolava Arc (Archibald et al., 2017; Tucker et al., 2011) (e.g. Fig. 8). These arcs are now separated by a considerable distance, but their reconstructed position in the Neoproterozoic and their similarity has led to us interpreting them as part of one continuous subduction system that was active for the Stenian and Tonian. In this manner, we now include TOAST as another part of Azania and have reworked a number of the plate boundaries in Merdith et al. (2017a) to reflect these new geological data and tectono-geographic interpretations.

2.6. Kinematic considerations

The final line of reasoning used to create full plate models are plate kinematic constraints. These are not defined explicitly through geological or geophysical data of the types outlined above, but rather are developed from the idea that the evolution of plate motions through time must follow the broad principles of plate tectonics in a way that would seem reasonable; for example, by equivalency with more recent and well-constrained plate motions. The most basic requirement is that continental blocks cannot pass through or significantly overlap other continents and we must be able to describe the position and motion of each continental block for as long as the crust within that block is thought to have existed. While this may seem obvious, these considerations present a powerful method for discriminating between competing reconstruction scenarios. Models constructed for deep time that cannot evolve towards more recent and present-day configurations of continents cannot be considered correct. Similarly, models requiring an implausible kinematic evolution in order to meet present-day configurations cannot be correct. A tangible example is Rodinia, for which a range of configurations could be permissible based on available palaeomagnetic and geological data (see reviews in Evans, 2013; Li et al., 2008; Merdith et al., 2017b). However, analysing the sequence of plate motions required to translate each continent to their (better constrained) positions during the Palaeozoic is more plausible in some of these scenarios than others, such as not requiring individual terranes or blocks to cross multiple ocean basins or navigate their way around a stable continent (Merdith et al., 2017b). Further examples where kinematic constraints add useful insights are when constructing models that explicitly trace the evolution of plate boundaries and tectonic plates. An example is expressed in the logic of Domeier (2018) who inferred that the longitudinal position of Tarim, North China and South China during the late Cambrian–Devonian must have remained stable relative to one another, because palaeolatitudes from palaeomagnetic data overlapped and therefore must be consistent with their end position in the more well constrained Devonian–Triassic.

Finally, we take a uniformitarian view of tectonic evolution, in that we assume that plate tectonics and relative plate motions were operating on similar principles in the Neoproterozoic to what we can observe in the Mesozoic and Cenozoic. During more recent times, the motion of

plates remains relatively constant for time lengths on the order of 10–100 Ma, with changes in motion occurring comparatively quickly (< 3 Ma) and tied to an event further afield, such as terrane collision in a subduction zone, subduction onset, rifting onset or ridge subduction (e.g. Austermann et al., 2011; Cawood et al., 2016; Cawood and Buchan, 2007; Knesel et al., 2008). The representation of this within a conceptual framework is that a single continent or plate may move for time lengths on the order of 10–100 Ma around a single Euler pole, before a plate reorganisation event triggers a change in direction and velocity of the plate (Gordon et al., 1984). Within palaeomagnetic data, this approach is exemplified in Torsvik et al. (2008), where filtered compilations of data result in smooth APWP segments punctuated by cusps in motion and velocity, and more recently by Wu et al. (2020). For the Neoproterozoic, which has much more sparse palaeomagnetic data coverage than the Phanerozoic, the logic can be applied by linking changes in plate direction (as suggested or necessitated by palaeomagnetic data) directly to geological evidence of a change in tectonic regime within the region of interest (e.g. Merdith et al., 2017b).

2.7. Synthetic ocean plates

A complete full-plate model, by definition, includes a representation of the evolution of ocean basins through time. This is the most uncertain part of any full-plate model. With a few exceptions (e.g. Granot, 2016), no pre-Jurassic ocean crust is preserved *in situ*, so that even where we can infer the presence of divergent plate boundaries (for example, following continental breakup), the precise geometry and spreading rates at these boundaries are conjectural. Consequently, there are no unique solutions to the definition of these boundaries and the synthetic ocean plates constructed from them. The main aim in the reconstruction of ancient ocean basins is to ensure that the synthetic plates and plate boundaries are at least consistent with sparse observations preserved on the continents.

Firstly, although we have little data on the creation of oceanic lithosphere for pre-Jurassic times, the geological record does preserve data on the consumption of oceanic lithosphere at subduction zones. The most important criteria that therefore must be met are that (i) (sub-) orthogonal divergence occurs at mid-ocean ridges and that (ii) convergence occurs at subduction zones (Domeier and Torsvik, 2014). The former of these two criteria typically occurs between continents during supercontinent breakup or when small terranes rift from a continent (Dalziel, 1997). The latter of these includes subduction along the margins of continents as well as within intra-oceanic arcs. Thus, these two criteria necessitate the extrapolation of known plate boundary positions (e.g. preserved continental arcs, rift zones) into larger areas to ensure the tectonic congruency of the model (in this case, that convergence or divergence at one location doesn't nullify the same criteria in another location). It is this step, in particular, that requires significant iteration when constructing a model. Maintaining tectonic congruency for a model is best achieved when the extrapolation of plate boundaries is done as simply as possible. For example, in reconstructing an ocean basin without any continental crust (e.g. Pacific Ocean, Panthalassa Ocean), a triple junction is usually the simplest expression of a ridge system that ensures divergence in all directions and convergence at its margins (Domeier and Torsvik, 2014). The evolution of such a triple junction could also be seen in the Ediacaran opening of the Iapetus Ocean (e.g. Pisarevsky et al., 2008; Robert et al., 2020),

3. Model selection and justification

3.1. Existing plate models

The selection of which full-plate model to assist in solving a problem is dependent on the nature of the problem, as each published plate model is constructed using a different approach and has a different reconstruction framework. For example, a study looking at absolute plate motions of the Cenozoic has little use for models connected to the Palaeozoic or Neoproterozoic. Instead, such studies typically include a comparison with previously published models as well as a rigorous mantle reference frame. Similarly, a study that traces the latitudinal distribution of continental arcs through the Phanerozoic has no need for a mantle reference frame and a study investigating the changes in net rotation through time would be concerned with small, localised improvements from regional models but more focussed on capturing the large-scale changes that occur when continents breakup. Although newer plate models typically address the shortcomings of previous models or implement more refined updates of regional areas, this does not necessarily make them better for all applications. Older plate models have been more rigorously tested and used by the community and as one travels further back in geological time, the data are more ambiguous and can invite alternative interpretations. For the purpose of this study, the existing plate models we consider are only those that are publicly released with fully self-consistent with coherent plate motions and plate boundaries. Thus, we omit many models that provide only continental motions (Scotese, 2016; Torsvik and Cocks, 2016), alternative or regional Rodinia configurations (Evans, 2013) or regional refinements of global models for the Mesozoic and Cenozoic (e.g. Vaes et al., 2019).

The major step forward for producing full-plate models was the construction of open-source computer software specifically designed to work with full-plate reconstructions (e.g. GPlates; (Gurnis et al., 2012). Following their development, GPlates-compatible global models for the Early Jurassic to present (Seton et al., 2012; Shephard et al., 2013) and a model for the Late Palaeozoic (Domeier and Torsvik, 2014) soon followed (hereafter, SET12 and DT14, respectively). Subsequent work by Matthews et al. (2016) (MAT16) bridged the gap between the Palaeozoic and Jurassic, linking a slightly modified version of DT14 with an updated SET12 model, the Müller et al. (2016) model (MUL16). Further back in time, two models for the Early Palaeozoic (500 to 410 Ma) now exist: Domeier (2016) (DOM16), which encompasses the evolution of the Iapetus and Rheic Oceans, as well as the motion of Gondwana, and Domeier (2018) (DOM18), which models the evolution of the first generations of Tethyan Oceans and Central Asian blocks (Siberia, North and South China, Tarim). For the Neoproterozoic, Merdith et al. (2017a) (MER17) produced a full-plate model from 1000 to 520 Ma, using the models of continental motion presented by Li et al. (2013, 2008) as a base. An alternative reconstruction from the late Palaeozoic to present-day has been presented by Young et al. (2019) (YOU19). YOU19 offers an alternative full-plate model for the Palaeozoic to the DT14 and MAT16 models that does not rely on the PGZ method. Finally, a deforming plate model was produced (Müller et al., 2019) (MUL19) that modelled rift and convergence deformation from 250 to 0 Ma. Table 1 summaries the main features of these models.

3.2. Cenozoic and Mesozoic plate models

We consider three plate models for the Cenozoic and Mesozoic: SET12, MUL16, and MUL19 (Fig. 4). The SET12 model spans from present-day to 200 Ma, with MUL16 and MUL19 extending back to 230 and 240 Ma, respectively. The main geological constraint of these models are the magnetic lineations preserved in oceanic crust that describe the relative movement between the pairs of continents breaking apart during the fragmentation of Pangea. The evolution of the Atlantic, Indian, Southern, Arctic and Cenozoic Pacific oceans are consistent, to the first order, across all three models. Larger differences between the models arise in regions where oceanic crust has been subducted, upon which they then rely on a combination of geometric (e.g. assumption of symmetrical spreading), geological, seismic and palaeomagnetic data to constrain the motion and evolution of terranes that open and close ocean basins (e.g. Liu et al., 2010; Liu et al., 2008; Sigloch and Mihalynuk, 2013). In these regions, the tectonic histories, even for Cenozoic times, remain the subject of ongoing research and the scenarios embedded in the global models used in this study represent one candidate amongst

Table 1
Summary of main reconstruction features of the full-plate reconstructions discussed in text. Italicised models are the models used in construction of the model presented in this study.

Model	Time (Ma)	Scope	Reference Frame			LLSVPs	Hierarchy Structure
			Palaeomagnetic	Mantle	Details		
SET12	200–0	Global	No	Yes	TPW corrected palaeomagnetic data (200–100 Ma). Hotspot motion (100–0 Ma).	No assumption.	Branching.
DT14	410–250	Global	Yes	Yes	TPW corrected mantle reference from 410–250 Ma.	Assumes stable and long-lived.	Flat.
MUL16	230–200	Global	No	Yes	TPW corrected palaeomagnetic data (200–100 Ma). Hotspot motion (100–0 Ma).	No assumption.	Branching.
MAT16	410–0	Global	Yes	Yes	TPW corrected mantle reference from 410–0 Ma.	Assumes stable and long-lived.	Branching.
DOM16	500–410	Gondwana-Laurentia-Baltica	Yes	Yes	TPW corrected mantle reference from 500–410 Ma.	Assumes stable and long-lived.	Flat.
MER17	1000–520	Global	Yes	No		No assumption.	Nodal.
DOM18	500–410	Gondwana-Siberia-China	Yes	Yes	TPW corrected mantle reference from 500–410 Ma.	Assumes stable and long-lived.	Flat.
YOU19	410–0	Global	Yes	Yes	TPW corrected mantle reference frame from 250–0 Ma.	No assumption.	Branching.
MUL19	250–0	Global	No	Yes	Optimisation method after Tetley et al. (2019).	No assumption.	Branching.
This model	1000–0	Global	Yes	No		No assumption.	Nodal from 1000–410 Ma. Branching from 410–0 Ma.

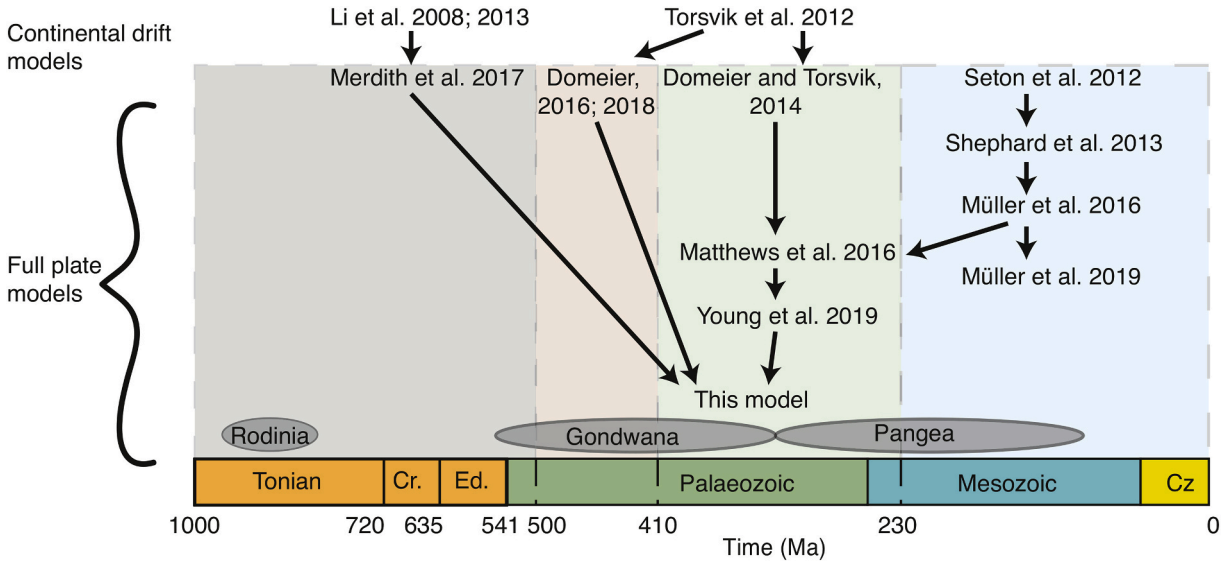


Fig. 4. 'Family-tree' of full-plate models and some of the key underlying continental drift type models leading to their development. We stress that more recent models are not necessarily better nor replace older models, rather typically present some alternative interpretation of key data or are based on different assumptions. See text for more details. The model presented here bridges the MER17, DOM16, DOM18 and YOU19 models into a single continuous plate model. X-axis not to scale. Cr, Cryogenian, Ed, Ediacaran.

many competing models. For example, the extent of subduction systems within the Tethyan domain and the nature of India-Eurasia collision is still hotly debated (Hu et al., 2016; Parsons et al., 2020; van Hinsbergen et al., 2020; van Hinsbergen et al., 2012). Similar combinations of methods have been used to propose alternative interpretations for circum-Pacific regions, especially for the Cretaceous and earlier times in the northwest Pacific (Domeier et al., 2017; Konstantinovskaya, 2002; Shapiro and Solov'ev, 2009; Vaes et al., 2019; Wu et al., 2016), the southwest Pacific (Hochmuth et al., 2015; Matthews et al., 2015; Schellart et al., 2006; Sutherland et al., 2020) and the northeast Pacific (Clennett et al., 2020; Sigloch and Mihalynuk, 2013). All of these regions invite competing models and alterations to existing global models and it is notable that many of the studies mentioned above have benefited from using the resources made available by previous global studies, beginning with SET12, as a starting point for detailed regional analysis.

All three models employ a relative hierarchy (Fig. 2a), in which a fully relative plate motion model is tied to an absolute plate motion model through Africa. The relative hierarchies are similar across the models because of the preserved oceanic crust. These global relative motion hierarchies are then linked to an absolute reference frame tied to the mantle, though the details of these reference frames differ between models. SET12 uses a hybrid reference frame, using a moving hotspot reference frame for 100–0 Ma (O'Neill et al., 2005) and a true-polar wander corrected palaeomagnetic reference frame for 200–100 Ma

(Steinberger and Torsvik, 2008). MUL16 also adopts a hybrid absolute reference frame, but uses the moving hotspot model of Torsvik et al. (2008) instead of that of O'Neill et al. (2005) based on an assessment of the geodynamic plausibility of a range of alternative mantle reference frames by Williams et al. (2015). MUL19 departs from both SET12 and MUL16 in that is uses an absolute reference frame derived by Tetley et al. (2019). The method of Tetley et al. (2019) optimises absolute plate motions through a joint inversion involving trench motion, fitting hotspot motion tracks and net rotation to determine the motion of Africa (at the top of the relative hierarchy) that simultaneously best fits all three criteria. Despite the emphasis on mantle reference frames in these previous global models, the same relative plate motion hierarchies can also be tied to a pure palaeomagnetic reference frame (e.g. Cao et al., 2019; Torsvik et al., 2008).

In this study, we rely on palaeomagnetic data as the main basis for linking absolute plate configurations continuously from the Cenozoic to the early Neoproterozoic. It is far more problematic when we tie plate configurations to the mantle. Nonetheless, some aspects of the more recent plate motions still rely on observations from hotspot trails—specifically, the motion of the Pacific Plate and other oceanic plates that have bordered it. During the Early Cretaceous, these plates lay within the Panthalassa ocean basin that was entirely surrounded by subduction zones, meaning that we cannot tie the motions of the oldest crust of the Pacific Plate to the continents by seafloor spreading anomalies.

Finally, with regard to Mesozoic-Cenozoic global plate models, we note that MUL19, while containing the same relative framework as SET12 and MUL16, also contains deforming plates. In MUL19, deformation of rifts and collisional zones are modelled explicitly, making it the first plate model to step away from the simplification of rigid plates that all other models assume. However, the reconstruction here relies on the simpler, rigid approximation used in SET12, MUL16, and other previous studies.

3.3. Mid-late Palaeozoic plate models

The progression of the three Palaeozoic plate models (all modelling 410–250 Ma) is slightly more nuanced than in the Mesozoic and Cenozoic because of the absence of preserved oceanic crust. DT14 is the original model and both MAT16 and YOU19 used DT14 as the basis of their Palaeozoic models and then connect to MUL16 for the Mesozoic and Cenozoic. In effect, MAT16 is the connection of DT14 (i.e. minimal changes) to MUL16, while YOU19 is an alternate version of DT14 for the Palaeozoic.

DT14 is heavily based on work by Torsvik et al. (2012) and models the amalgamation of Pangea through the collision of Laurussia and Gondwana and the evolution of the Palaeo-Tethys and opening of the Meso-Tethys oceans. The model has a flat hierarchy (Fig. 3a) with APWPs defined for each individual continent and each continent being tied directly to the spin axis. Domeier and Torsvik et al. (2014) also use the PGZ method to constrain absolute palaeolongitude. Therefore, their model assumes the stable, immutable nature of the present-day LLSVPs within the mantle back to 410 Ma. DT14 is presented in both a mantle and a palaeomagnetic reference frame, with the mantle reference frame being corrected for TPW after Torsvik et al. (2014).

MAT16 adopted the DT14 model, with minor amendments required to link it with MUL16 (see Matthews et al. (2016) for details). A key difference between the two models is that MAT16 translated the flat hierarchy of DT14 into a fully relative reference frame (i.e. converted the structure from Fig. 3a into Fig. 2a), where the motion of all plates are tied to Africa, which is then tied to an absolute plate motion model. The absolute plate motion model of MAT16 is the same as in both MUL16 (i.e. a hybrid between hotspots, slabs and palaeomagnetic data) and DT14 (i.e. absolute latitude and longitude, corrected for TPW). Thus, MAT16 also invokes the PGZ method.

YOU19, while starting from MAT16 as a base, differs much more from MAT16 than MAT16 does from DT14. This is because YOU19 uses a different base assumption, leading to notable changes in the actual plate model itself. The most important difference is that YOU19 does not assume that LLSVPs were fixed and stable back to 410 Ma. They abandon the PGZ method for constraining palaeolongitude and thus argue that they can better accommodate geological and kinematic (plate speed and trench migration) criteria more strongly than either DT14 or MAT16. The two key changes that YOU19 implemented (relative to DT14 and MAT16) are shifting Laurussia in latitude and longitude to be closer to its position in Pangea against Gondwana, thus removing a dextral motion between the Patagonian margin of South America and Laurussia (e.g. Fig. 2c), and removing easterly drift of South China during the Carboniferous–Permian. The implementation of both in DT14 (and then in MAT16) is a consequence of the PGZ method, since the longitudinal position of Laurussia and South China is based on fitting preserved eruptions to the edges of LLSVPs (Domeier and Torsvik, 2014). YOU19 argue that the interpretations of DT14 introduce unrealistic kinematic scenarios: 8000 km of relative dextral motion between Laurussia and the Patagonian margin of Gondwana (e.g. Fig 2c) at a relative plate velocity of 30 cm/a and South China moving at plate speeds of 40 cm/a between 260 and 250 Ma in MAT16 (Young et al., 2019). The dextral motion between Gondwana and Laurussia of DT14 and MAT16 that that YOU19 removed is not a transition from the Pangea B to Pangea A configuration, which is explicitly defined as dextral motion after Pangea formed (Domeier et al., 2012). Rather, all three models adopt a Pangea A configuration and include *some* component of dextral motion between Laurussia and Columbian–Mexican margin of Gondwana in the Devonian. Finally, the position of Laurussia in YOU19 is unsupported palaeomagnetically by ~30° (Section 4.2 and 5.1), which is problematic as there is an abundance of data from both Laurentia and Baltica to constrain its position at this time.

Recently, Wu et al. (2020) proposed a new integrated geological and palaeomagnetic model for the amalgamation of Pangea. Their study used a different selection of palaeomagnetic data (all three mid-late Palaeozoic full-plate models discussed here used the compilation of Torsvik et al. (2012) as a base) and a new method of APWP generation that weighted poles based on their quality and uncertainty. The model of Wu et al. (2020) also suggested that the formation of Pangea was originally initiated by collision between Laurussia and a promontory of Gondwana consisting of the Variscan Massifs at ca. 400 Ma. In their model, the promontory formed by the scissor-like opening of the Palaeotethys Ocean off the northern margin of Gondwana. In principle this model would be very compatible with the one we present here, however as the model of Wu et al. (2020) is currently only palaeogeographic, we do not consider it as an option for merging in this study. YOU19, like MAT16, uses a relative plate hierarchy with Africa as the root of the hierarchy. Africa is connected to an absolute plate motion model using the Torsvik and Van der Voo (2002) APWP for the Palaeozoic, before the model transition to the absolute plate motion model of MUL16. Because the model has no absolute palaeolongitude control, YOU19 does not constrain or correct for TPW in the Palaeozoic and is therefore presented in a purely palaeomagnetic reference frame.

3.4. Early Palaeozoic plate models

Two separate models exist for part of the Early Palaeozoic between 500 and 410 Ma. Each of these two models focus on a separate area of the Earth at the time. DOM16 focuses on the evolution of the Iapetus and Rheic oceans and the amalgamation of Laurussia (Baltica, Laurentia and Avalonia). DOM18 models the evolution of Siberia, Gondwana, the terranes that now make up the Central Asian Orogenic Belt and the Chinese cratons (Tarim, North and South China). While each model focuses on a different area, the overarching assumptions and framework of both models are identical. Both models follow the approach of DT14, possessing a flat hierarchy with APWPs being defined for most continents, such that they all move independently from each other. The model adopts the hypotheses of the PGZ method back to 500 Ma, using

the location of LIPs and kimberlites to constrain absolute palaeolongitude. Both models therefore have a TPW correction, and are presented in a mantle and palaeomagnetic reference frame.

3.5. Neoproterozoic

Only one full plate model exists for the Neoproterozoic (MER17, Merdith et al., 2017a). MER17 is based on Li et al. (2013, 2008) and models the evolution of Rodinia; it's breakup and the amalgamation of Gondwana (1000–520 Ma). There are, however, a number of important considerations that differentiate MER17 from Phanerozoic full-plate models. Firstly, MER17 used a hybrid plate rotation hierarchy, defining two separate nodes that move independently from each other using palaeomagnetic data tied directly to the spin axis (India as one and Laurentia, as the centre of Rodinia, as the second) (Fig. 5a, b). In this model, India and Laurentia both act as separate roots that then constrain a series of relative plate rotations that collectively describe the rest of the world. Secondly, the continental drift model of Li et al. (2013) invokes the orthoversion model of determining palaeolongitude, where they fix the I_{min} of Rodinia to be at 100°E. As MER17 adopted these rotations as their base, there is an element of the orthoversion model preserved between models. However, MER17 also drastically changed the configuration of Rodinia, as well as the timing of breakup, compared to Li et al. (2013), relative rotations within the Laurentian (i.e. Rodinian) node and the absolute rotation of Laurentia itself in order to fit geological and kinematic constraints. They did not recalculate TPW and the I_{min} of Rodinia, thus MER17 does not have a strict absolute palaeolongitude control. Finally, there is no correction for TPW in MER17 and no mantle reference frame; the model is presented purely in a palaeomagnetic reference frame.

3.6. Model selection

In order to produce a coherent global model, we must select from the models described above that best align with our goals: (i) open the Neoproterozoic and Cambrian up for quantitative tectonic analysis; (ii) create a framework that can support local or regional studies for the Neoproterozoic and (iii) a foundation for future studies looking at long timescale (> 10–100 Ma) trends in either tectonics or geodynamics.

As our aim is to produce a model back to 1 Ga, three choices are already made for us because they are the only models that exist for those time periods: MER17 for 1000–520 Ma, and DOM16 and DOM18 for 500–410 Ma. For the remaining time period, MAT16 (an extension of DT14) and YOU19 are viable options. Both models link to the MUL16 model and choosing between them requires considering the reconstruction framework (e.g. hierarchy, reference frame) of our model with respect to our intent. To satisfy our goals, we need a model in a palaeomagnetic reference frame. We acknowledge the value and potential in exploring hypotheses for constraining palaeolongitude. However, since tectonic reconstruction models, such as the one we are presenting here, are a required starting point for exploring the long-term evolution of mantle, we have kept the model conservative by not assuming the fixity of LLSVPs or that TPW dictates supercontinent position. Therefore, we elect to leave palaeolongitude unconstrained by either PGZ or orthoversion methods. Thus, we selected the YOU19 model, as it has removed the absolute palaeolongitude controls adopted in MAT16. We stress that our approach is deliberately conservative and requires the fewest *a priori* assumptions, but anticipate that future developments will see improvements in the model presented and that a comparison of several end member models would be useful for evaluating the long-term connection between lithosphere and mantle. One promising way forward could be to optimise tectonic parameters, such as subduction zone migration and plate velocity in the manner of Tetley et al. (2019) to define a mantle reference frame. The model we present is an essential precursor for such techniques. Our model is constructed with a palaeomagnetic reference frame, that is, even at younger times, there is no mantle reference frame. For studies needing such a reference frame, which only exists since the Cretaceous, we suggest people use either SET12, MUL16 or MUL19.

3.6.1. Our approach to plate modelling

Here we outline our approach to merging individual plate models into a coherent global plate model spanning the past 1 Ga. As detailed above, our goal is a geologically constrained model within a palaeomagnetic framework. In addition to reconstructing plate motions, we also model plate boundaries, which requires us to also focus on the relative motion between plates. The evolution of plate boundaries is commonly preserved in the geological record such as passive margins marking divergent boundaries and magmatic arcs recording convergence. Palaeomagnetic data, although providing a quantitative absolute constraint on the position of a craton, have varying uncertainty that allow some manipulation and flexibility. For example, continental drift

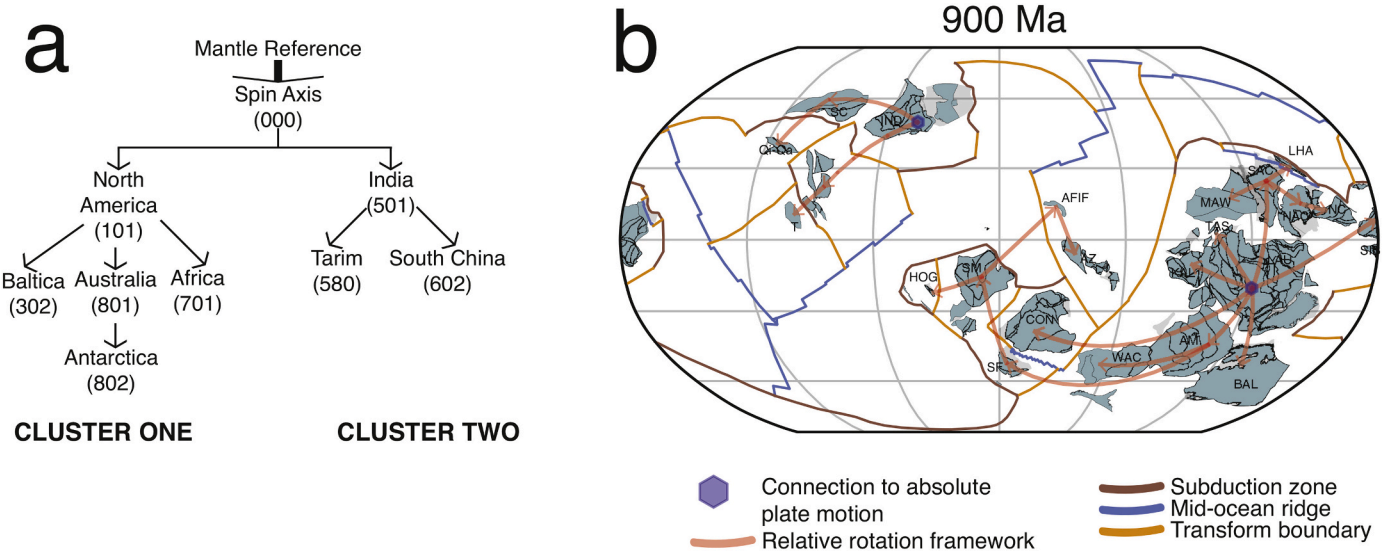


Fig. 5. Overview of the rotational framework of a hybrid plate motion hierarchy. (a) In this case, two different nodes or clusters sit at the top of their respective branches of the hierarchy and ground regional relative plate motions. (b) Map view of the schematic at 900 Ma from this study. Two different plates (India and Laurentia; blue hexagons) sit at the top of the hierarchy and connect to the deep earth, with regional plate motions being defined relative to each.

models (and APWPs) typically fit the data as tightly as possible. However recent studies have analysed the effect of exploring both the temporal (i.e. age constraints) and statistical uncertainty to create alternative APWPs (Tetley et al., 2019; Wu et al., 2020). Given this, we use a hybrid approach that adopts parts of both the flat, palaeomagnetic hierarchy traditionally used for Precambrian reconstructions and the relative framework used in more recent times.

Using this approach, our model has multiple clusters of related cratonic elements moving together (Fig. 5a). Whether a specific cratonic element moves relative to another is dependent on their geological relationship. For example, if they are separated by an incipient ocean basin as indicated by geological data then we suggest that it is easiest for them to be moving relative to each other (within the bounds of whatever available palaeomagnetic data), because the relative relationship of divergence (expressed as a mid-ocean ridge) is preserved. The hierarchy is defined by geological precedence, where terranes move relative to blocks, blocks move relative to cratons and cratons move relative to 'supercontinents'. In this manner, generally (but not necessarily exclusively), crust with more preserved data should always be placed above crust with less preserved data in the hierarchy, because we have more confidence in the geological evolution (and also likely palaeomagnetic constraints) from these continents. Alternatively, if continents are separated by a large ocean basin, we form a new cluster. This cluster-approach has an added benefit in the more uncertain Neoproterozoic, as it means that we can simply introduce a new cluster for Rodinia, which has Laurentia as the root of the relative hierarchy, instead of maintaining Africa or the Congo craton at the top of the cluster (which are the roots of Pangea and Gondwana, respectively) and can also introduce a cluster for India and South China which, in our interpretation, move separately to Rodinia on the other side of the globe.

A full-plate reconstruction models both continents (palaeomagnetic data) and plate boundaries (geological data). Therefore, we use both data simultaneously to iterate towards a solution. Palaeomagnetic data are used initially to build a continental drift framework (e.g. (Li et al., 2013, Li et al., 2008). If palaeomagnetic data are abundant and of high quality, then either an APWP or GAPWaP are constructed, which we do for the Phanerozoic. We then introduce geological data in the form of plate boundaries (e.g. compilation of rifts and arcs (Merdith et al., 2017b)) and use the compilation to manipulate the model in a manner that still fits the palaeomagnetic data, but also accommodates geological data. Structural and metamorphic constraints are used here principally to infer (where possible): (i) polarity of subduction, (ii) collision timing and (iii) orientation of rifting. Once the broader tectonic framework is implemented, we begin introducing smaller blocks and terranes into this framework. This approach allows us to increase the resolution of the model within key areas while maintaining the tectonic coherency of the model as a whole. For example, where the broader tectonic framework models subduction leading to collision, the introduction of terranes and smaller blocks that preserve evidence suggesting a two-stage collision or accretion of an oceanic arc can be used to more finely model the plate boundary network. Other pieces of geological data, such as faunal provinces (e.g. Burrett et al., 1990), isotopic signatures (e.g. Collins et al., 2011) and detrital zircons (e.g Cawood et al., 1999) are used here to assist with connecting disparate terranes to larger blocks that they share affinity with or to infer the presence of a plate boundary not directly preserved in the geological record (such as by a diverging fossil record).

Because our model contains geological data in the form of plate boundaries, we are particularly interested in ensuring the forwards and backwards compatibility of any decision made around geological data, especially for terranes or blocks that have limited palaeomagnetic data. For example, if the data support two or three interpretations in the early Neoproterozoic, but only one of those is consistent with an Ediacaran (or younger position), then we consider that position more reliable than the other two. However, we argue that this logic also works in reverse; if a number of positions are deemed viable in the Ediacaran for a terrane based on the data available, but only one of those also fits what data are available in the early Neoproterozoic, then we will use the older data to force an interpretation of the younger data (e.g. Evans, 2009). This argument is highlighted by the concept of 'world uncertainty' (the percentage of total crust (oceanic and continental) on the earth at any one time that is also preserved at present-day) of Torsvik et al. (2010b). Because time is asymmetrical, this means that the level of confidence we have at present-day is 100%, but decreases linearly back in time to ~70% at 200 Ma (i.e. 70% of all crust at 200 Ma is no longer preserved). At 400 Ma, the world certainty is ~73% (Domeier and Torsvik, 2017), and using estimates of continental crustal volumes, at 600 Ma it is between 75 and 80% (Cawood et al., 2013a). Therefore, for the Mesozoic and Cenozoic, data from younger times are much more compelling to force interpretations of older data because of how much more confident one can be in the last 20 Ma. Comparably, the difference in this measure of uncertainty is much smaller between the Neoproterozoic and Cambrian, thus we suggest that models in this time period should simultaneously use older and younger data to iterate towards a solution.

4. Palaeomagnetic data

A major problem in comparing the Phanerozoic models is that they all use different rotational frameworks, including reference trees (i.e. flat vs hierarchical) and different absolute reference frames. In order to properly synthesise the DOM16, DOM18 and YOU19 models into a single reconstruction, we first need to lay a coherent groundwork in defining an absolute plate motion model for the largest continents during this time in order to merge the individual models. To do this, we first derive a new APWP for Gondwana (540–320 Ma) and GAPWaP for Pangea (320–0 Ma) using the palaeomagnetic compilation of Torsvik et al. (2012) to provide an absolute palaeomagnetic reference frame for 540 to 0 Ma. We also apply the GAPWaP to the MUL16 portion (i.e. the Mesozoic and Cenozoic) of the YOU19 model. We do this to ensure compatibility between the Cenozoic and Palaeozoic, and also because our goals for this model are broad scale (> 10–100 Ma) trends, mostly focussed on the Neoproterozoic. The method we follow to calculate our APWP and GAPWaP is outlined below. For the Neoproterozoic, and non-Gondwana constituents of the Palaeozoic, we use the compilations of palaeomagnetic data as presented in MER17, DOM16 and DOM18, along with some other additions. Palaeomagnetically derived alterations to the models are also discussed below.

4.1. APWP and GAPWaP construction

The absolute reference frames for Gondwana (540–320 Ma) and Pangea (320–0 Ma) used in this study are derived using the method and velocity-optimised global palaeomagnetic data of Tetley (2018). APWPs are routinely constructed using poles assigned averaged or nominal ages, which particularly for older times, where palaeomagnetic constraint becomes increasingly limited, contribute to spurious apparent polar wander behaviours. This method directly evaluate individual palaeomagnetic pole age and associated uncertainty in combination with calculated pole A95 latitude and longitude uncertainties to derive optimised APWPs that minimise predicted plate velocities and plate velocity gradients (instantaneous accelerations). The resulting rate of apparent polar wander in optimised APWPs was reduced globally by an average of 56% by comparison to existing APWPs, resulting in predicted Phanerozoic plate motions displaying greater kinematic consistency with present-day plate motion behaviours.

Optimised APWPs were produced for the 15 major continental blocks of Amazonia, Australia, Colorado, East Antarctica, Greenland, India-Pakistan, Madagascar, Meseta, North America, Northeast Africa, Northwest Africa, Panama, Patagonia, Somalia, and Stable Europe. Applying the method as described in Torsvik et al. (2012, 2008) and the data provided in Torsvik et al. (2012), optimised continental pole data from all 15 continents were rotated from their individual source

coordinate frames into a consistent South African coordinate frame using the rotation model from this study. Now in a consistent coordinate frame, a GAPWaP for Pangea was produced using all poles aged 320–0 Ma (due to the collision of Laurussia and Gondwana during the Late Carboniferous), with a second GAPWaP produced using poles aged 540–320 Ma associated with Gondwana (South America, Africa, India, Antarctica and Australia) only. For both GAPWaP reference frames, the *GMAP* software was used (Torsvik et al., 2012; Torsvik et al., 2008; Torsvik and Smethurst, 1989), applying a running mean method using a window size of 20 Ma and a step size of 10 Ma.

4.2. Palaeomagnetic compilation

A compilation of palaeomagnetic data was used to constrain the position of all continental blocks during the Neoproterozoic and for non-Gondwanan continental blocks during the early and middle Palaeozoic. The Neoproterozoic data are presented in Table 2 and a GPlates compatible file of the data is also presented in the Supplementary Material. Fig. 6a–c shows the great circle misfit of our model to the selected poles. As the majority of the data have already been used in the MER17, DOM16 and DOM18 reconstructions, we point readers to those publications for in-depth discussion of the data. Here, we discuss two alterations to the base models that we implemented based on palaeomagnetic data: Tarim at ca. 700 Ma and Laurussia at ca. 420–400 Ma.

The MER17 model omitted Tarim prior to 700 Ma due to its pre-700 Ma palaeomagnetic data nullifying the position that placed it outboard of Australia. We rectify this and include a geological argument for its position against India-South China during the Tonian (1000–720 Ma) and Cryogenian (720–635 Ma) (Section 5.4.2). The rationale for placing Tarim in this position is to allow for a ~180° rotation required by palaeomagnetic data. Two well-dated and high-quality poles; the 760–720 Ma Qiaoenbrak Formation (Wen et al., 2013) and the 770–717 Ma Baiyisi Volcanics (Huang et al., 2005) are internally consistent and require Tarim to be inverted 180° from its present-day position (i.e. northern margin facing south). A third pole, assumed to be pre 700 Ma, from the Aksu Dykes (Chen et al., 2004) is rejected for poor age constraints and the possibility of remagnetisation (Wen et al., 2017). Comparably, three younger poles: the 635–550 Ma Sugetbrak Formation (Zhan et al., 2007), the ca. 635 Ma Tereeken Cap Carbonate (Zhao et al., 2014) and the 621–609 Ma Zhamoketi Andesite (Zhao et al., 2014) are all consistent with each other and indicate that Tarim was in its present-day orientation. A recent pole by Wen et al. (2017) from the Lower Sugetbrak formation (640–615 Ma) stands in conflict with these three poles, suggesting a ~50° rotational difference in the orientation of Tarim, while maintaining the same palaeolatitude. Wen et al. (2017) dismiss the three earlier poles due to similarity to Silurian–Devonian poles for the Sugetbrak Formation and possible remagnetisation for the latter two poles, respectively.

Successfully fitting the two older poles with either the three younger poles or the single pole of Wen et al. (2017) is not possible in a model in which Tarim is surrounded by continental lithosphere for the Neoproterozoic or in a scenario where Tarim is attached to the northwestern or northern margin of Australia or the northern margin of India (e.g. instead of South China). An accommodation of the data can be obtained by placing Tarim in a 'Missing-Link' position (between Australia and Laurentia) with breakout and rotation of Tarim from ca. 700 Ma; as argued by Wen et al. (2018, 2017). However, beyond the kinematic issues with Missing-Link style models (Merdith et al., 2017b), it is difficult to account for the formation of the 760 Ma Aksu Blueschist if Tarim was located in the centre of an assembled Rodinia (see comment by Song and Li et al. (2019) and reply by Wen et al. (2019)). In the present model, we use the pole of Wen et al. (2017) due to its greater reliability, though our model could easily be adapted to fit the other three poles if necessary (Section 5.4.2.). We also note that although we argue that India-South China were separate from the rest of Rodinia, our preferred Neoproterozoic position for Tarim is also compatible with models in which India-South China formed part of Rodinia (e.g. Cawood et al., 2013b).

In the YOU19 model, Laurussia was moved ~30° further north in latitude relative to its position in DT14 and MAT16 (Section 3.3). The consequence of this decision by YOU19 is that Laurussia is not in a palaeomagnetically constrained position in the late Silurian and early Devonian. For this model, in addition to the compilation of palaeomagnetic data in Torsvik et al. (2012), we also used palaeomagnetic data from mainland Baltica (Table 2) to constrain the late Silurian to early Devonian position of Laurussia. We implement these alterations to produce a coherent motion of Laurentia (later Laurussia) and Gondwana that fits palaeomagnetic data, while also ensuring that the relative motion between Gondwana and Laurussia is convergent, rather than dextral transform (e.g. Fig. 2c).

5. Alterations to models

We describe the alterations made to individual models separately for clarity, however, we stress that no single model was treated in isolation. Each alteration, whether during the Tonian or Devonian, was evaluated both forwards and backwards in time in order to ensure continuity with both older and younger geological and/or palaeomagnetic evidence. We begin our discussion with the alterations made to YOU19, followed by alterations to DOM16, DOM18 and MER17. The alterations to DOM16 and DOM18 are discussed together, as the two models essentially form a single global model between 500 and 410 Ma. The most significant changes, and the focus of much of the discussion, occurred in MER17. This is because, firstly, connecting this model with younger models in order to validate Neoproterozoic tectonic-geography is a primary goal of this study, and secondly, because many of the alterations are completely new and have never been incorporated into a plate model before. Fig. 7a–b displays a latitudinal overview of the major and minor cratons in our model, with a comparison to the DOM-MAT models for the Phanerozoic, and the model of Li et al. (2013, 2008) for the Neoproterozoic. Figs. 8, 9 and 10 show overviews of our reconstruction at 1000 Ma, 500 Ma and present-day with relevant terranes and blocks highlighted.

5.1. YOU19

The primary change we made to YOU19 was the implementation of a new APWP for Gondwana from 540 to 320 Ma and a GAPWaP for 320 to 0 Ma (Tetley, 2018). We also adjusted the position of Laurussia during the Devonian in order to better fit palaeomagnetic data and implemented an alternative position for Lhasa (against northwest Australia) that we consider to be more consistent with geological data in the Neoproterozoic (Section 5.4.1).

In the YOU19 reconstruction, Laurussia is rotated roughly 40° counter-clockwise compared to the DT14 and MAT16 reconstructions (Fig. 11). While these changes improved the global kinematic integrity of the model (Young et al., 2019), the position of Baltica in this configuration conflicts with palaeomagnetic data, which indicates it lay at more southerly latitudes (Torsvik et al., 2012). We used the compilation of Torsvik et al. (2012) as a base, however, as many of the poles in that dataset for the late Silurian to early Devonian were taken from the British Isles (c.f. Jeleńska et al., 2015), we supplement it with some data from cratonic, continental Europe (Table 2, S. Pisarevsky pers. comm.). We modify the position of Laurussia from that used in YOU19 such that it fits the cluster of poles at this time (Fig. 11b). This modification places it in a similar latitudinal position to DT14 and MAT16 (e.g. Fig. 7a), however, we shift it further east relative to DT14, so that it is closer to its final position in Pangea. This position then satisfies the kinematic and structural issues outlined in YOU19, while maintaining Baltica and Laurussia at a palaeolatitude permitted by palaeomagnetic data.

The Lhasa block, currently preserved in the Tibetan Plateau between India and Tarim, is an E–W elongated block consisting of Precambrian

Table 2
Summary of palaeomagnetic data

Key	Rockunit	OldAge	YoungAge	Glat	Glon	Plat	Plon	A95	Reference
Laurentia									
L1	Gunbarrel Intrusions combined	780	776	45	-110	14.6	127	3.2	Harlan et al. (2008).
L2	Uinta Formation	800	750	41	-110	0.8	161.3	4.7	Weil et al. (2006).
L3	Galeros - Carbon Canyon	764	750	35.15	-111.8	-0.5	166	9.7	Weil et al. (2004); Eyster et al. (2019).
L4	Kwagunt Formation	759	743	36.15	-112	14.2	163.8	3.5	Eyster et al. (2019).
L5	Kwagunt Formation 2	748	736	36.15	-112	18.2	166	7	Weil et al. (2004).
L6	Franklin Dykes	727	712	75	-82	8.4	163.8	2.8	Denyszyn et al. (2009).
L7	Long Range Dykes	617	613	53.5	-57.5	-19	175.3	17.4	Murthy et al. (1992); Hodych et al. (2004); Age: Kamo and Gower (1994).
L8	Skinner Cove Formation	554	548	50	-60	15	157	9	McCausland and Hodych (1998).
L9**	Andres Red Beds	423	393	41	-74	13	105	9	Miller and Kent (1988).
L10**	Wabash Reef	423	415	40.85	-85.7	17	125	5.3	McCabe et al. (1985); Torsvik et al. (1996).
L11**	Rose Hill Formation	433	427	39	-79	19.1	128.3	5.8	French and Van der Voo (1979).
L12**	Ringgold Gap Sediments	456	433	34.51	-85.06	24	146.6	7.7	Morrison and Ellwood (1986).
L13**	Tablehead Group Limestone mean	470	456	48.33	-58.43	13.4	149.3	3.9	Hodych (1989); Hall and Evans (1988); Deutsch and Prasad (1987); Torsvik et al. (1996); Torsvik et al. (2012).
L14**	St George Group Limestone	485	456	48.3	-59	17.5	152.4	4.3	Deutsch and Prasad (1987).
L15**	Oneota Dolomite	485	470	43.41	-91.23	10.3	166.5	11.9	Jackson and Van der Voo (1985).
L16**	Moore Hollow sediments	500	490	31	-99	-0.6	163	8.5	Farr and Gose (1991)
L17**	Morgan Creek	497	470	30.25	-98.5	10.6	158	9.7	Loucks and Elmore (1986).
L18**	Point Peak	497	485	30.5	-99	5.2	165.8	6	Van der Voo et al. (1976).
L19**	Taum Sauk Limestone	497	485	37.55	-90.31	-3.4	175.1	7.1	Dunn and Elmore (1985).
L20**	Roywe dolomite	497	485	34.25	-97.11	12.6	157.3	4.3	Nick and Elmore (1990).
L21**	Florida Mountains	497	485	32.05	-107.37	-5.4	168.7	10	Geissman et al. (1991).
L22**	Tapeats Sandstone	520	497	36.11	-113.99	2.3	162.6	3.3	Elston and Bressler (1977).
L23**	Mount Rigaud and Chatham-Grenville	534	530	45.28	24.2	-11.9	184.5	6.2	McCausland et al. (2007).
Baltica									
B1	Southern Sweden Dykes	946	935	59	16	-0.9	240.7	6.7	Elming et al. (2014); Pisarevsky and Bylund (1998).
B2	Branton-Algo Anortthosite	927	905	58.5	6.5	5	249	3.9	Stearn and Piper (1984); Age: Scherstén et al. (2000).
B3	Rogaland Igneous Complex	883	855	58.5	6	-46	238	18.1	Walderhaug et al. (2007).
B4	Hunnedalen Dykes	875	821	59	6.75	-41	222	10	Walderhaug et al. (1999).
B5	Egersund Dykes	619	613	58.5	6	-31.4	224.1	15.6	Walderhaug et al. (2007).
B6	Kurgashlya Formation	570	560	53.3	57.5	-51	135	4.9	Lubnina et al. (2014).
B7	Bakeevo Formation	570	560	54.5	58.2	-42	119	5.3	Lubnina et al. (2014).
B8	Winter coast sediments	558	552	65.5	40	-25.3	132.5	2.8	Popov et al. (2002); Age: Martin et al. (2000).
B9	Zolotitsa sediments I, Russia	560	550	65.5	40	-31.7	112.9	2.4	Popov et al. (2005).
B10	Verkhotina sediments	560	550	65.5	40	-32.2	107.1	2	Popov et al. (2005).
B11	Zolotitsa sediments II	560	550	65.5	40	-28.3	109.9	3.8	Iglesia Llanos et al. (2005).
B12	Zigan Formation	552	544	53.7	56.7	-16	138	3.7	Levashova et al. (2013).
B13	Swedish Limestone (1N)	467	458	58.3	13.9	3	35	13.4	Torsvik and Trench (1991).
B14	Swedish Limestone	480	470	58	13	30	55	9	Torsvik and Trench (1991).
B15	Swedish Limestone (1R)	480	470	59	15	18	46	5.1	Torsvik and Trench (1991).
B16	Narva Limestones	485	470	59	31	18	55	4	Khramov and Iosifidi (2009).
B17	St Petersburg Limestone	480	470	58	30	33	58	3.6	Smethurst et al. (1998).
B18+	Gotland Follingbo Limestone	430	420	57.5	18.5	21	164	6	Claesson (1979).
B19+	Dniestr Silurian Limestone	428	416	48.6	27	14.3	169.3	7.4	Jeleńska et al. (2005).
B20+	Gotland Medby Limestone	427	417	57.5	18.5	23	171	8	Claesson (1979).
B21+	Ringerike Sandst. Norway	426	410	60	10.2	19	164	6.7	Douglass (1988).
B22+	Tiverskaya Series	419	411	48.6	27	0	149	13.3	Jeleńska et al. (2015).
B23+	Ivaniev and Dniestr Sediments	419	393	48.7	26	-1	175	9.6	Lubnina et al. (2007).
B24+	Devonian Seds. Podolia	416	406	48.7	26	-3.7	145.5	6.7	Smethurst and Khramov (1992).
B25+	Dniestrovskaya Series	416	407	48.6	27	2.3	158.4	7.4	Jeleńska et al. (2005).
B26+	Zilair Sediments, Russia	411	375	54	59	-2	161	3.1	Danukalov et al. (1983).
B27+	Eifelian sedimentary rocks, Russia	398	392	50	5	19	173	2.9	Minibaev and Sulutdinov (1991).
B28+	Bashkirea Sediments, Russia	398	385	54	59	-7	162	4.8	Danukalov et al. (1983).
B29+	Kola Dykes, Russia	390	370	68	33	11	147.6	11.1	Veselovskiy and Arzamastsev (2011).
Siberia									
S1	Ust-Kirba Formation	960	930	60	137.2	8.1	2.6	10.4	Popov et al. (2002).
S2	Kitoi Dykes	762	754	52	103	0.4	21.8	6.1	Pisarevsky et al. (2013).
S3	Kesyussa Formation	542	535	71	122.5	-37.6	165	5.2	Pisarevsky et al. (1997).
S4-	Moyero River sediments	459	439	68	104	-14	124	8	Gallet and pavlov (1996).
S5-	Angara River sediments*	460	450	58.5	99.8	-29.5	140.2	6.4	Pavlov et al. (2012).
S6-	Kulumbe section	466	456	68	88.8	-24.1	152.4	3.3	Pavlov et al. (2008).
S7-	Stolobovaya section	466	456	62.1	92.5	-22	158	4	Pavlov et al. (2008).
S8-	Moyero River sediments	468	458	68	104	-23	158	4	Gallet and Pavlov (1996).
S9-	Angara River sediments	473	463	58.5	99.8	-35.2	153.2	3.6	Pavlov et al. (2012).

(*continued on next page*)

Table 2 (*continued*)

Key	Rockunit	OldAge	YoungAge	Glat	Glon	Plat	Plon	A95	Reference
S10-	Moyero River sediments	474	464	68	104	-30	157	4	Gallet and Pavlov (1996).
S11-	Guragir Formation	475	465	68	88.8	-30.9	152.7	3.2	Pavlov and Gallet (1998).
S12-	Angara River sediments	480	470	58.5	99.8	-36.4	158.2	6.5	Pavlov et al. (2012).
S13-	Moyero River sediments	483	473	67.5	104	-33.9	151.7	2.2	Gallet and Pavlov (1996).
S14-	Uigur and Nizhneiltyk Formations	488	478	68	88.8	-35.2	127.2	4.9	Pavlov and Gallet (1998).
S15-	Moyero River sediments	488	478	68	104	-40	138	9	Gallet and Pavlov (1996).
S16-	Kulumbinskaya Formation	505	495	68	88.8	-36.1	130.7	6	Pavlov and Gallet (1998).
S17-	Moyero River sediments	505	495	68	104	-37	138	9	Gallet and Pavlov (1996).
S18	Yunkyulyabit-Yuryakh Formation	512	502	70.9	122.6	-36.4	139.6	4.6	Pisarevsky et al. (1997).
S19-	Kulumbe River section	512	502	68	88.4	-41.9	135.8	2.3	Pavlov and Gallet (1998).
S20-	Khorbusuonka Amgan and Mayan seds.	512	502	71.5	124	-43.7	140.5	2.6	Gallet et al. (2003).
S21-	Nyuya and Lena River sediments	437	427	60.6	116.3	-17.6	102	3.2	Powerman et al. (2013).
S22-	Nyuya and Lena River sediments	438	428	60.7	116.3	-18.6	101.9	4.6	Shatsillo et al. (2007).
S23-	Lena River sediments	454	444	60.5	116.4	-21	109	17.3	Torsvik et al. (1995).
S24-	Nyuya River sediments	456	446	60.6	116.3	-31.3	129.5	3.6	Powerman et al. (2013).
S25-	Kudrino section	466	456	57.7	107.99	-21.1	143.4	5	Pavlov et al. (2008).
S26-	Krivaya Luka Formation	469	459	59.7	118.1	-25.6	117.9	5.1	Iosifidi et al. (1999).
S27-	Krivaya Luka Formation	469	459	59.7	118.1	-28.2	127.1	2.5	Iosifidi et al. (1999).
S28-	Krivolutsky Suite	470	460	57.6	107.8	-32.6	137	8.3	Rodionov et al. (2003).
S29-	Lena River sediments	473	463	59.8	118.1	-32	139	3.1	Torsvik et al. (1995).
S30-	Lena River redbeds	475	465	60	114	-25	137	9	Rodionov (1966).
S31-	Surinsk Formation	485	475	58.3	109.61	-42.2	128.1	5.8	Surkis et al. (1999).
S32-	Verkholensk Formation	506	496	58.5	109.8	-37.69	124	4.5	Rodionov et al. (1998).
S33-	Maya River sediments	515	505	60	132	-45.8	115	5	Pavlov et al. (2008).
West Australia									
WA1	Browne Formation	830	730	-26	126	44.5	141.7	6.8	Pisarevsky et al. (2007).
WA2	Hussar Formation	800	730	-26	126	62.2	85.8	10.3	Pisarevsky et al. (2007).
WA3	Mundine Dykes	758	752	-23	115.8	45.3	135.4	4.1	Wingate and Giddings (2000).
North Australia									
NA1	Johnny's Creek Member	780	660	-24	133	15.8	83	13.5	Swanson-Hysell et al. (2012).
South Australia									
SA1	Angepena Formation	660	640	-32	138	47.1	176.6	5.3	Williams and Schmidt (2015).
SA2	Yaltipena Formation	650	635	-31.5	139	44.2	172.7	8.2	Sohl et al. (1999).
SA3	Elatina Formation, MEAN	645	635	-32	137.5	49.9	164.4	13.5	Embleton and Williams (1986); Schmidt et al. (1991); Schmidt and Williams (1995); Sohl et al. (1999).
SA4	Nuccaleena Formation	635	610	-31	139	32.3	170.8	2.9	Schmidt et al. (2009).
SA5	Brachina Formation	620	590	-32.2	138	46	135.4	3.3	Schmidt and Williams (2010).
SA6	Bunyeroo Formation	590	570	-31.6	138.4	18.1	196.3	8.8	Schmidt and Williams (1996).
SA7	Wonoka Formation	575	555	-31.3	138.6	5.2	210.5	4.9	Schmidt and Williams (2010).
North China									
NC1	Huaibei Sills 890 Ma	913	876	34	117	-52.3	149.3	3.5	Fu et al. (2015).
NC2	Wudaotang and Xinji Fm	541	521	35.6	110.5	18.5	341.9	6.5	Huang et al. (1999a).
NC3	Hebei and Shandong Sediments	541	501	36	118	21.2	335.2	12.4	Zhao et al. (1992).
NC4	NE Sino-Korean Massif	541	485	35.6	110.5	26.8	334.5	8.9	Gao et al. (1983) (recalculated by Zhao et al. (1992)).
NC5-	Zhangxia and Xuzhuang Fms	510	496	35.6	110.5	37	326.7	5.5	Huang et al. (1999b).
NC6-	Zhaogezhuang area carbonates	490	467	39.7	118.5	32.9	294.6	4.7	Yang et al. (2002).
NC7-	Changshan and Gushan Fms	496	485	35.6	110.5	31.7	329.6	5.4	Huang et al. (1999a).
NC8-	Hebei and Shandong Sediments	499	461	36	118	28.8	310.9	12.3	Zhao et al. (1992).
NC9-	Liangjiashan and Lower Majiagou Fm	485	470	35.6	110.5	37.4	324.3	8.5	Huang et al. (1999b).
NC10-	Jinghe	470	456	35.6	110.5	31.5	327.7	7	Huang et al. (1999a).
NC11	Upper Majiagou Formation	470	456	35.6	110.5	27.9	310.4	9.2	Yang et al. (1996).
NC12-	Tianjinshan and Miboshan Formations	480	464	37.2	105.5	31.8	326.5	9.5	Huang et al. (1999b).
South China									
SC1	Yanbian Dykes A	830	818	26.5	101.5	45.1	130.4	19	Niu et al. (2016).
SC2	Xiaofeng Dykes	812	792	31	111	13.5	91	10.9	Li et al. (2004).
SC3*	Yanbian Dykes B	814	798	26.5	101.5	14.1	32.5	20.4	Niu et al. (2016).
SC4	Liantuo Formation	735	705	30.8	111	9.9	160.3	4.6	Jing et al. (2015) and Evans et al. (2000), combined.
SC5	Nantuo Formation	641	631	28.5	110	7.5	161.6	5.9	Zhang et al. (2013b); Zhang and Piper (1997).
SC6	Doushantuo Formation	614	590	30.8	111	25.9	185.5	6.7	Zhang et al. (2015).
SC7-	Douposi Formation (Wangcang)	510	496	32.1	106.2	-39.5	185.1	8.3	Lixin et al. (1998).

(*continued on next page*)

Table 2 (*continued*)

Key	Rockunit	OldAge	YoungAge	Glat	Glon	Plat	Plon	A95	Reference
SC8-	Douposi Formation (Guangyuan)	510	496	32.4	106.3	-51.3	166	8.3	Yang et al. (2004).
SC9-	Shiqian Redbeds	440	425	27.5	108	4.9	194.7	5.6	Opdyke et al. (1987).
SC10-	Shiqian Redbeds	440	425	27.5	108	14.9	196.1	5.1	Huang et al. (2000).
SC11-	Pagoda Formation	458	445	32.4	106.3	-45.8	191.3	3.6	Han et al. (2015).
Congo									
C1	Luakela Volcanics A	770	757	-11.5	24.25	-40.2	122	14.1	Wingate et al. (2010).
C2	Mbozi Complex	773	713	-9.2	32.8	-46	145	6.7	Meert et al. (1995).
Sao Francisco									
SF1	Bahia Dykes (N+R)	928	912	-14	-39	7.3	106.4	6.2	Evans et al. (2016).
Tarim									
T1*	Sugetbrak Formation	635	550	40.9	79.4	19.1	149.7	9.3	Zhan et al. (2007).
T2*	Zhamoketi Andesite	621	609	41.5	87.8	-4.9	146.7	3.9	Zhao et al. (2014).
T3	Lower Sugetbrak Formation	640	615	41	79.5	-21.1	87.4	7	Wen et al. (2017).
T4*	Tereeken Cap Carbonate	640	630	41.5	87.8	27.6	140.4	9.9	Zhao et al. (2014).
T5	Qiaoenbrak Formation, Aksu	760	720	40.8	79.5	-6.3	17.5	9.1	Wen et al. (2013).
T6*	Aksu Dykes	819	795	41.15	80.1	19	128	4.5	Chen et al. (2004).
T7	Baiyisi Volcanics	770	717	41.6	86.54	-17.7	14.2	6	Huang et al. (2005).
T8-	Ordovician Limestones	485	470	41.3	83.4	-20.4	180.6	8.5	Fang et al. (1996).
T9-	Aksu-Kalpin-Bachu area sediments	455	445	40.6	78.9	-40.7	183.3	4.8	Sun and Huang (2009).
T10	Red Sandstone	433	427	40.6	79.4	12.8	159.8	7.3	Zhao et al. (2014), average of three poles from Fang et al. (1996); Li et al. (1990); Fang et al. (1998).
India									
I1	Malani Igneous Suite Grand Mean	770	734	26	72	69.4	75.7	6.5	Meert et al. (2013).
I2	Bhander and Rewa formations	650	530	26	78	47.3	212.7	5.8	McElhinny et al. (1978).
I3*	Jodphur Group	570	520	27	73	1	164	6.7	Davis et al. (2014).
Seychelles									
SE1	Mahe Dykes	753	747	-4.7	55.5	54.8	57.6	12.1	Torsvik et al. (2001).
Rio de la Plata									
RP1	Sierra de las Animas Complex	582	574	-34	-55.3	12.2	78.9	14.9	Rapalini et al. (2015).
RP2	Sierra de los Barrientos Redbeds	600	500	-37.8	-59	15.1	72.6	12.4	Rapalini (2006).
West African Craton									
WAC1	Djebel Boho Volc.	547	526	30.4	-6.7	-27.3	207.1	14.9	Robert et al. (2017).
WAC2	Fajjoud and Tadoughast Volc.	572	551	30.2	-7.8	-21.9	211	15.6	Robert et al. (2017).
WAC3*	Adrar-n-takoucht Volc	577	564	30.4	-7.8	57.6	115.6	15.7	Robert et al. (2017).
East Avalonia									
EAV1#,1	Treffgarne volcanics	482	472	52	-5	-56	126	5.5	Trench et al. (1992).
EAV2#	Stapeley volcanics	471	463	52.6	-3	-26.6	216.1	4.9	McCabe and Channell (1990).
EAV3#	Builth igneous and sediments	468	460	52.1	-3.3	-11	198	10	McCabe et al. (1992).
EAV4#	Tramore volcanics	461	449	52.1	-7.4	-11	198	8.5	Deutsch (1980); Trench and Torsvik (1991).
EAV5#	Borrowdale volcanics	448	438	54.4	-3.2	-8.1	186.2	6.9	Millward and Evans (2003); Channell and McCabe et al. (1992).
EAV6#,2	Midlands Minor Intrusives	442	432	52.5	-1.5	-52.5	181.5	10.4	Vizan et al. (2003).
EAV7#,2	Browgill redbeds	439	433	54.3	-2.5	-13.6	133.9	12.4	Channell et al. (1993).
EAV8#,2	Tortworth volcanics	437	431	51.7	-2.5	7	124	4.7	Torsvik et al. (1994).
EAV9#,2	Mendips volcanics	435	429	51.2	-2.5	-13	91	8.8	Torsvik et al. (1993).
Ganderia									
GAN1#	Bourinot Group	510	496	46.1	-60.4	-21	160	8.1	Johnson and Van der Voo (1985).
West Avalonia									
WAV1#	Nahant intrusives	490	488	42.4	-70.9	-34	140	3.9	Thompson et al. (2010).
WAV2#	Dunn Point volcanics	463	457	45.8	-62.1	2	130	4.1	Johnson and Van Der Voo (1990); Hamilton and Murphy et al. (2004).
WAV3#	Cape St. Mary sills	443	439	46.8	-54	10	140	9	Hodych and Buchan (1998).
Carolinia									
CAR1#,2	Cid Formation metasediments	450	445	35	-80.2	29.6	122.1	5.1	Vick et al. (1987).
CAR2#,2	Uwharrie and Cid Formation metaseds	450	445	35.5	-80	20	80	14.2	Noel et al. (1988).
Cuyania									
CUY1#	Pavon Formation sediments	458	452	-34.6	-68.6	-3.6	166.4	6.6	Rapalini and Cingolani (2004).

* pole not fit by model
from compilation of Domeier (2016)
+ from compilation of S. Pisarevsky (*Pers. Comm.*)
- from compilation of Domeier (2018)
** from compilation of Torsvik et al. (2012)
1 inclination only used
2 no upper age constraint (fits inclination data)
Glat, sample site latitude; Glon, sample site longitude; Plat, pole latitude; Plon, pole longitude; A95, 95% confidence ellipse.

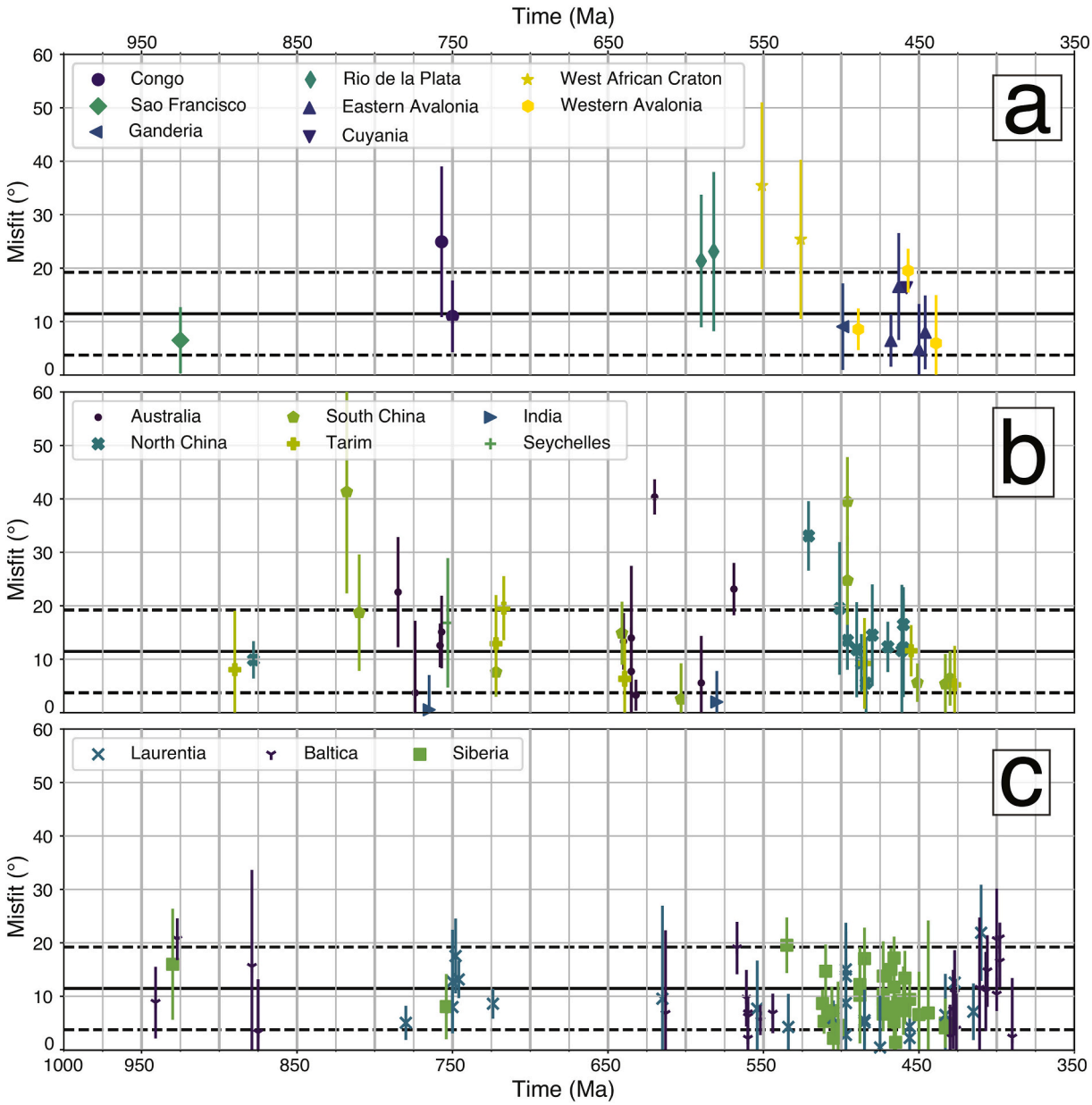


Fig. 6. Summary of the fit of palaeomagnetic data to our model for 1000 to 400 Ma (omitting poles used to construct the Gondwana APWP). Misfit is the minimum great circle distance (in degrees) within the valid time range between the palaeomagnetic pole and the geographic north pole. The error bar on each point is the pole 95% confidence limit (A95). Solid line is the mean misfit of all poles, with the dashed lines representing the standard deviation of the mean. Poles marked as 'not used' or 'inclination only' in Table 2 are not included in this figure. (a) Poles from the constituent cratons of western Gondwana and the Avalonian terranes; (b) poles from the constituent cratons of eastern Gondwana and present-day Asia, and; (c) poles from Laurussia and Siberia.

metamorphic basement, overlain by predominantly Palaeozoic sedimentary rocks and Mesozoic and Cenozoic volcanic assemblages (Yin and Harrison, 2000; Zhu et al., 2013). The Precambrian basement is established only in the southern and central terranes of Lhasa (Zhu et al., 2013) and in the Amdo micro-block that is preserved in the Mesozoic northern Lhasa terrane (e.g. Fig. 10b). Lhasa is typically placed outboard of the Tethyan Himalayan terranes, off the northern margin of India within Gondwana (e.g. Domeier and Torsvik, 2014). However, an alternative position outboard of northwest Australia is also supported; a scenario consistent with tectonic affinities interpreted from zircon age spectra and Hf isotopic signatures (Burrett et al., 2014; Zhu et al., 2011). We find a position off northwest Australia more consistent with the

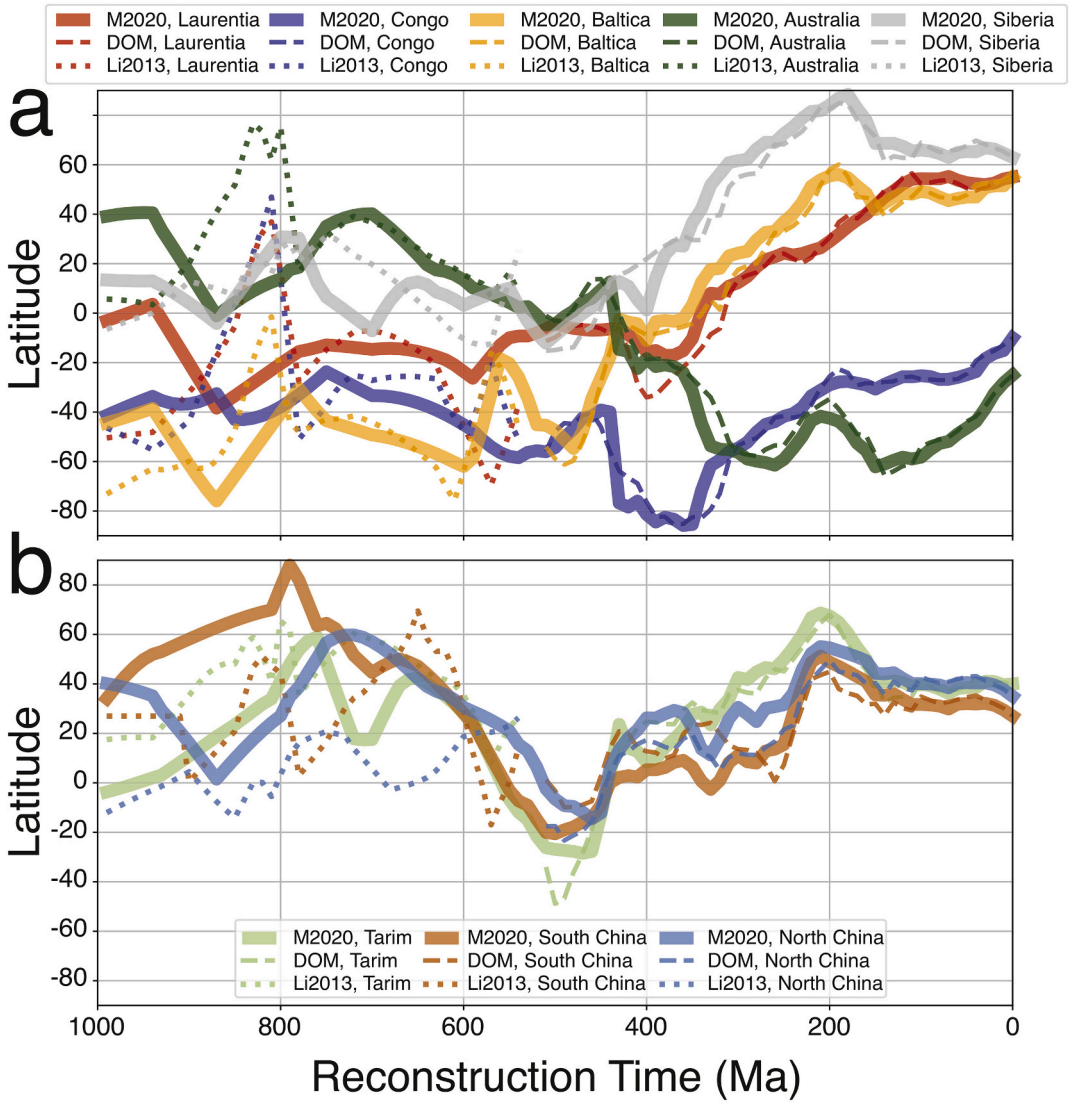


Fig. 7. Comparison of palaeolatitude of major cratons (a) and Chinese cratons (b) from 1000–0 Ma between three models; (i) This model, M2020; (ii) DOM16/18 (500–410 Ma) and MAT16 (410–0 Ma), and; (iii) Li et al. (2013, 2008) (1000–550 Ma). The notable excursion at 800 Ma in the Li et al. (2013, 2008) model is due to their adoption of IITPW at this time (Li et al., 2004).

Neoproterozoic geological record of Lhasa (Section 5.4.1) that preserves magmatism interpreted to represent the existence of a subduction zone and back-arc (Guynn et al., 2012; Hu et al., 2018), which would otherwise be impossible to produce if it was land-locked between India and South China. We therefore alter the position of Lhasa from YOU19 to outboard of NW Australia. For simplicity, we infer Lhasa's motion to follow the drift of the Cimmerian terranes, but recognise that the palaeolatitudes need further refinement in the Jurassic and Cretaceous following syntheses such as Li et al. (2016, 2017) and others.

5.2. DOM16 and DOM18

We sought to preserve, as closely as possible, the palaeolatitudes and the tectonic interpretations (i.e. history of collisions, rifting, subduction and ocean basin evolution) of the DOM16 and DOM18 reconstructions. The position of Gondwana (both in Early Palaeozoic and the older times covered by MER17) has been adjusted to inherit the Gondwana position at 410 Ma from the new Gondwana APWP path described above. Relative rotations of smaller blocks to Gondwana were calculated from DOM16/18 and translated into the new position of Gondwana. Further adjustments to all continental polygons have been implemented to smooth the transition from the late Palaeozoic configurations inherited from the adjusted YOU19 model (adj-YOU19). The following sections detail adjustments to the DOM16/18 models made for the late Cambrian–Devonian.

Fig. 11 shows a direct comparison between the DOM16/18 reconstructions and our adj-YOU19 model at 411/410 Ma. The primary differences between the models are longitudinal, as our adj-YOU19 model shifts Laurussia, Siberia, Kazak, Tairim and North China ~30° longitudinally to the east compared to DOM16/18 (as well as when compared to DT14 and MAT16, which link closely to DOM16/18), in order to better model the amalgamation of Laurussia and Gondwana. This results in a far narrower Rheic Ocean at 410 Ma in our model and a much simpler collision between Laurussia and Gondwana (e.g. Wu et al., 2020; Young et al., 2019). This change is discussed further in context in the following section.

The motions of Baltica, Laurentia, and Siberia are tied directly to the spin axis through their own individual palaeomagnetic reference frame, in contrast to the younger parts of the reconstruction where we retain the hierarchy inherited from YOU19. For minor cratons (Tarim, North China, South China) and smaller blocks (e.g. Tianshan, Kara), we model their motion within a relative hierarchy for the practical reason that this

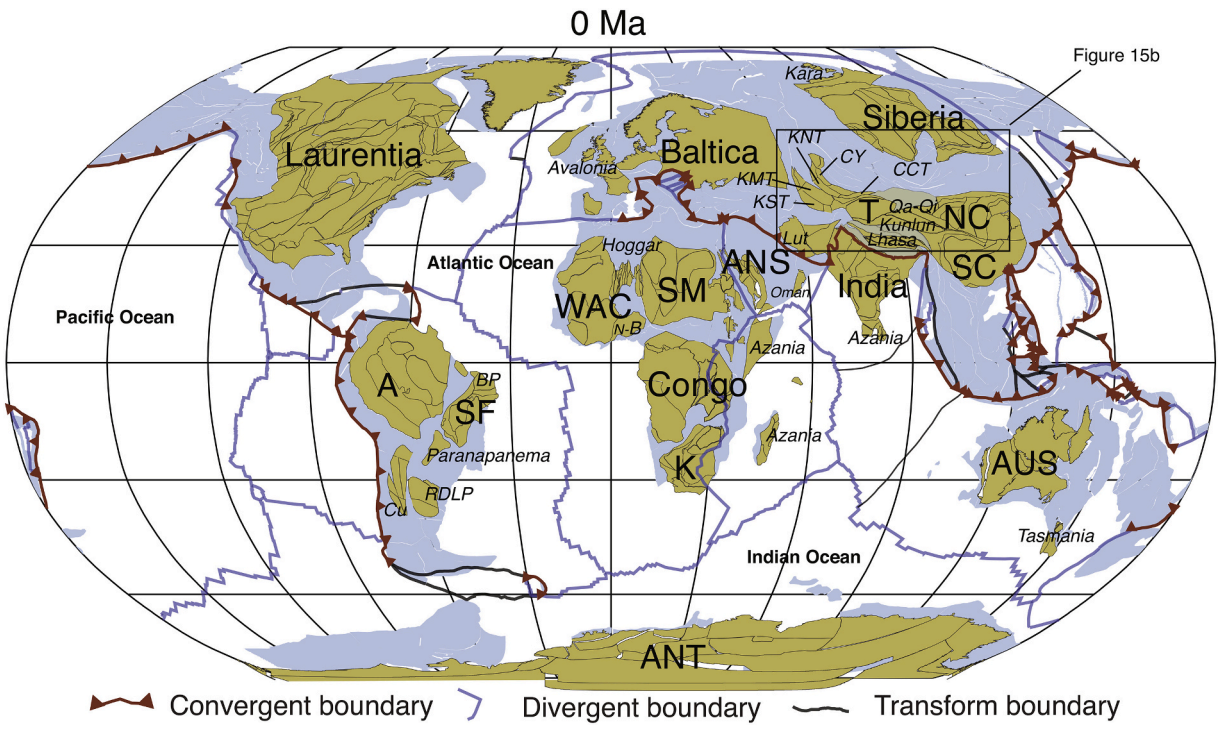


Fig. 8. Distribution of continental crust, ocean basins and plate boundaries in our plate model at 0 Ma, based on MUL16. Tan polygons are areas of continental lithosphere in the Neoproterozoic that we model, blue polygons are areas of present-day continental lithosphere. Abbreviations as Figures 8 and 9. A, Amazonia; Ant, Antarctica; AUS, Australia; BP, Borborema Province; CCT, Chinese Central Tianshan; Cu, Cuyania; CY, Chu Yili; K, Kalahari; KMT, Krygyz Middle Tianshan; KNT, Krygyz North Tianshan; KST, Krygyz South Tianshan; N-B, Nigeria-Benin; NC, North China; P, Paranapanema; ANS, Arabian Nubian Shield; Qa, Qaidam; Qi, Qilian; RDLP, Rio de la Plata; SC, South China; SM, Sahara Metacraton; T, Tarim; WAC, West African Craton.

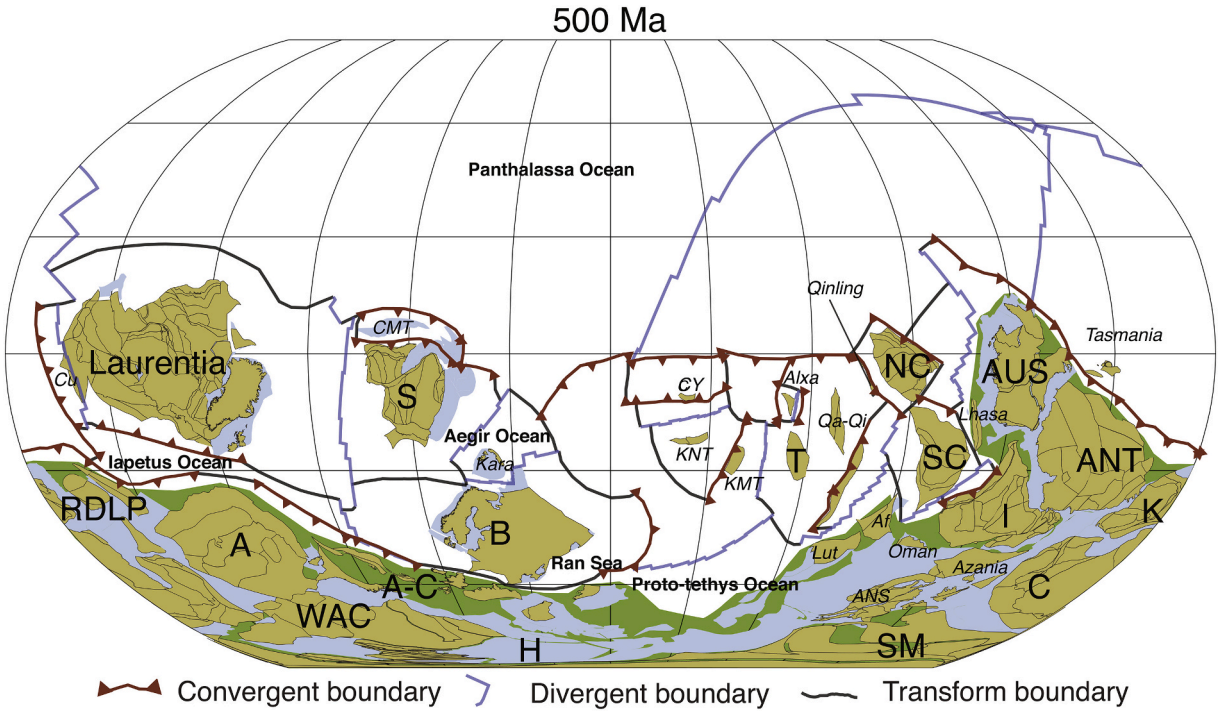


Fig. 9. Distribution of continental crust, ocean basins and plate boundaries in this plate model at 500 Ma, based on DOM16 and DOM18 (e.g. Figs. 12 and 13). Tan polygons are areas of continental lithosphere in the Neoproterozoic that we model, blue polygons are areas of present-day continental lithosphere that are inferred to exist during the Neoproterozoic, but without having firm geological evidence or that have been effected by subsequent deformation (e.g. the distance between a present-day coastline and COB). Green polygons represent a schematic interpretation of congruent continental lithosphere, with intervening crust being subsequently deformed during future tectonic cycles. Abbreviations as Figure 8, in addition to; A-C, Avaloinia-Cadomia; Af, Afghanistan; B, Baltica; C, Congo; CMT, Central Mongolian Terrne; H, Hoggar; I, India; S, Siberia.

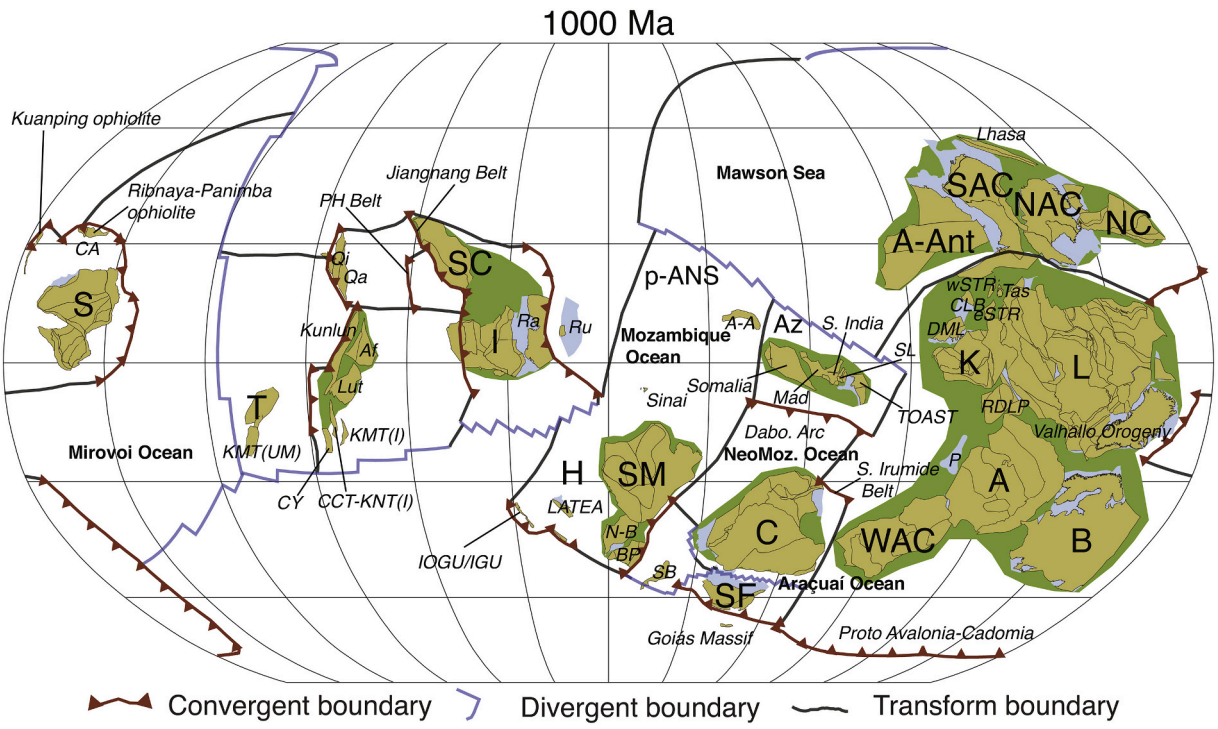


Fig. 10. Distribution of continental crust, ocean basins and plate boundaries in our plate model at 1 Ga. Tan polygons are areas of continental lithosphere in the Neoproterozoic that we model, blue polygons are areas of present-day continental lithosphere that are inferred to exist during the Neoproterozoic, but without having firm geological evidence or that have been affected by subsequent deformation (e.g. the distance between a present-day coastline and COB). Green polygons represent a schematic interpretation of congruent continental lithosphere, with intervening crust being subsequently deformed during future tectonic cycles. A-Ant, Austral-Antarctica; Az, Azania; BP, Borborema Province; CA, Central Angara Terrane; CLB, Coats Land Block; Dabo. Arc, Dabolava Arc; DML, Dronning Maud Land; eSTR, Eastern South Tasman Rise; IOGU, In Ouzzal Granulite Unit; IGU, Iforas Granulite Unit; KMT(I), Krygyz Middle Tianshan (Issedonian); KMT(UM), Krygyz Middle Tianshan (Ulutau-Moyunkum); KNT(I), Krygyz North Tianshan (Issedonian); Mad, Madagascar; NAC, North Australian Craton; NeoMoz. Ocean, Neo-Mozambique Ocean; NC, North China; p-ANS, proto-Arabian Nubian Shield; PH, Panxi-Hannan Belt; Ra, Rayner Province; Ru, Ruker Block; SAC, South Australian Craton; SB, Southern Borborema; SL, Sri Lanka; Tas, Tasmania; wSTR, Western South Tasman Rise.

makes it easier to preserve the consistency of their geological history, as they share multiple plate boundaries with Gondwana. For all these cratons and blocks, we sought to preserve the palaeolatitudes from the parent studies to a reasonable degree allowing for data uncertainties (e.g. Fig. 6). Fig. 7 provides a quantitative comparison between the palaeolatitudes of the DOM16/18 models and our incorporation of them into our adjusted reconstruction.

5.2.1. Deviations from DOM16

The key deviation between DOM16 and our model is a difference in the orientation of Baltica in the late Cambrian (Fig. 12a), where our model has Baltica rotated 90° counter clockwise relative to DOM16. As the DOM16 model only begins at 500 Ma it does not have to explicitly consider the earlier Neoproterozoic history of Baltica. In our opinion the position of Baltica in DOM16 is more congruent with an inverted Baltica (relative to Laurentia) during the Neoproterozoic (Hartz and Torsvik, 2002), where the southern-peri Urals are connected to Greenland. In comparison, MER17 connects Baltica to Rodinia through the Sveconorwegian margin in an upright position relative to the present-day (e.g. Cawood et al., 2003; Dalziel, 1992; Weil et al., 1998). The inverted Neoproterozoic Baltica position of Hartz and Torsvik (2002) results in simpler kinematic motions during the late Ediacaran and Early Palaeozoic, whereas the 'traditional' Neoproterozoic coupling of Baltica-Laurentia requires a more complex motion path in order to fit palaeomagnetic data. However, in our opinion the 'upright' coupling of Baltica and Laurentia is more geologically and palaeomagnetically robust (Cawood and Pisarevsky, 2006; c.f. Slagstad et al., 2019) in the Neoproterozoic than the alternative, and as such we adopt this configuration at ca. 600 Ma (as in MER17) during the opening of the Iapetus Ocean; necessitating a more complex kinematic evolution for Baltica between 600 and 470 Ma (Fig. 12a,b). Our reconstruction of Baltica is therefore quite different to that of DOM16 during the late Cambrian and early Ordovician as we have to implement a ~90° rotation between 520 and 475 Ma of Baltica to fit the same series of palaeomagnetic data at 470 Ma as DOM16.

Baltica palaeomagnetic data compiled by Meert (2014), Torsvik et al. (2012) and Domeier (2016) were used to ensure its latitudinal position remained valid between 550 and 470 Ma (Table 2). Only two poles—one from the Andarum Shale (Torsvik and Rehnström (2001) categorised as C-grade quality by Meert (2014)) and the other from the Narva sediments, (Khramov and Iosifidi, (2009), categorised as B-grade quality by Meert (2014))—are identified for Baltica between 530 and 480 Ma, both with a nominal age of 500 Ma. Despite coeval ages, the poles are ~35° apart from one another and Meert (2014) identified unresolved issues, specifically: few samples constraining the pole and a (possible) effect of inclination shallowing (even after correction for inclination shallowing a ~25° mismatch remains). A strict fitting of the Narva sediments pole would require Baltica to rotate by ~2°/Ma between 550 and 500 Ma; a situation we consider implausible and likely reflecting underlying issues in the palaeomagnetic data. As such, our model does not fit either pole explicitly, though our reconstructed position of Baltica is consistent with the latitude suggested by the inclination data of both poles. By 460–440 Ma, our model closely resembles the DOM16 model, with similar sized Rheic oceans, latitudinal positions and orientations of Gondwana, Baltica and Laurentia (Fig. 12c, d). At 410 Ma, when DOM16 finishes, the only difference is the relative position of Laurasia and Gondwana due to differences in palaeolongitude (Fig. 2c; 11). In our model, Laurussia is much closer to Gondwana resulting in a far narrower Rheic Ocean at 410

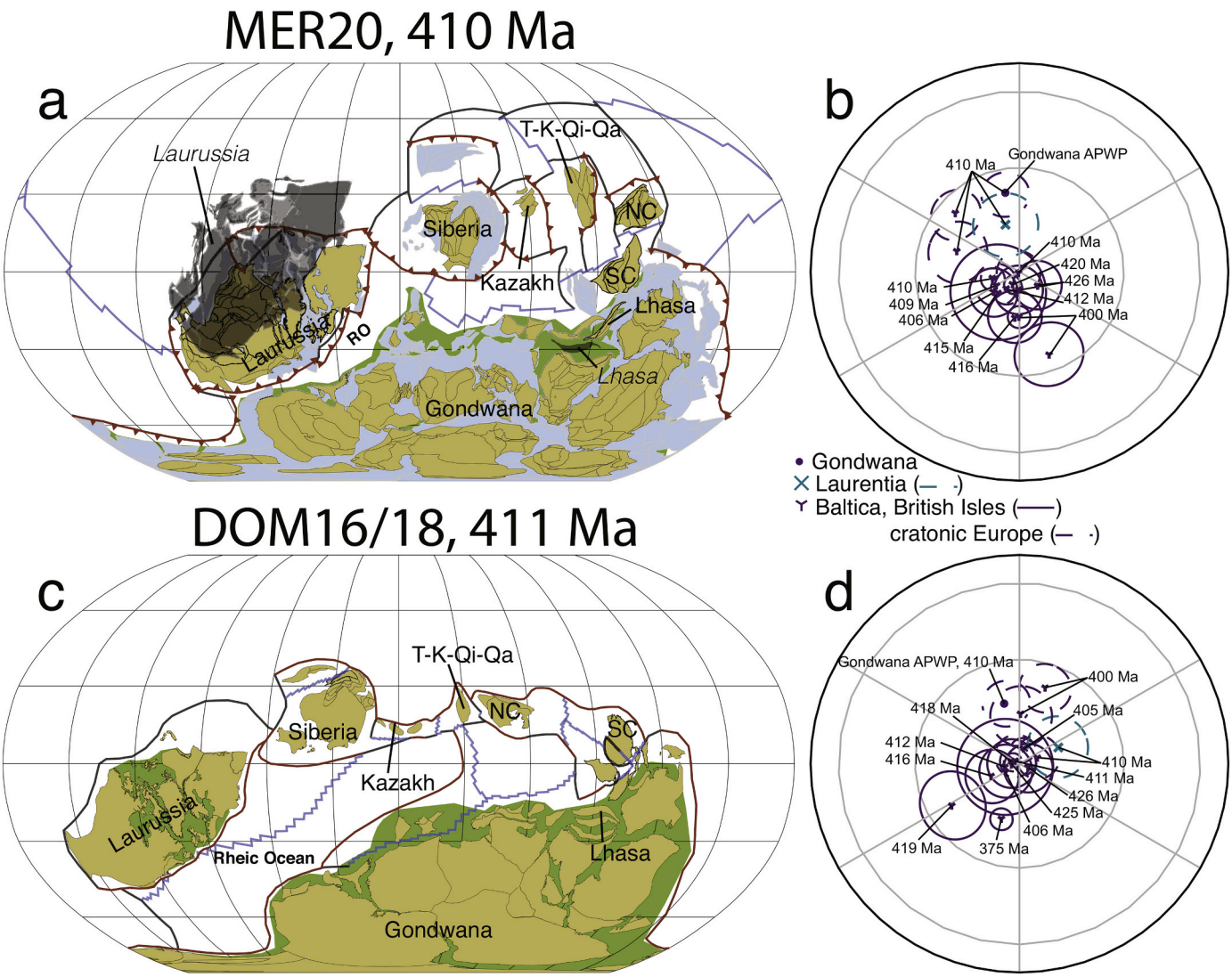


Fig. 11. Comparison of our model (a, b) with Domeier (2018, 2016) (c, d) at 411–410 Ma to highlight the latitudinal changes implemented for Laurussia in our model. Dark outline of Laurussia and Lhasa (italicised labels) in (a) are their original positions in YOU19. Palaeomagnetic data are shown at time of best fit for both models (i.e. map projection view of Fig. 6). Tan polygons are areas of continental lithosphere in the Neoproterozoic that we model, blue polygons are areas of present-day continental lithosphere that are inferred to exist during the Neoproterozoic, but without having firm geological evidence or that have been affected by subsequent deformation (e.g. the distance between a present-day coastline and COB). Green polygons represent a schematic interpretation of congruent continental lithosphere, with intervening crust being subsequently deformed during future tectonic cycles. The DOM16/18 models extend until 410.1 Ma (so we display it at 411 Ma), while YOU19 begins at 410 Ma. NC, North China; SC, South China; T-K-Qi-Qa, Tarim-Kunlun-Qilian-Qaidam.

Ma than in DOM16/18, DT14 and MAT16 (e.g. Fig. 2c, see also Wu et al. (2020)).

The width of the Rheic ocean is poorly constrained (c.f. Dalziel and Dewey, 2019; Domeier, 2018; Wu et al., 2020) especially because of palaeolongitudinal uncertainty. The problem is compounded by the fact that there is only one reliable palaeomagnetic pole constraining our Gondwana APWP between 430 and 400 Ma (Aïr intrusives in Niger, age at 410 Ma, (Hargraves et al., 1987)), meaning the early Devonian portion of the APWP has large uncertainty. Because of this uncertainty, the methods used to create APWPs tend to dampen the effect of this pole (which is true for our APWP). Nonetheless, even with the effect of this pole being dampened, reconstructed palaeomagnetic data (without considering longitudinal constraints) at 410 Ma allow placement of Laurussia and Gondwana to within a few thousand kilometres of one another (e.g. Fig. 11a, see also Wu et al. (2020)). At first glance, this seems problematic, because one might expect that the forces related to subduction zones modelled along the craton margins facing each other would draw the cratons to each other. DOM16, DT14 and MAT16 (along with Torsvik et al. (2014)) solve this problem by changing the palaeolongitude of Laurussia to 90° east relative to Gondwana, allowing for a much wider ocean basin. This position is justified and necessitated in these models by their use of the PGZ method, where Laurussia is reconstructed over the eastern arm of the present-day position of the Pacific LLSVP. However, this position then requires > 8000 km of dextral motion between Laurussia and the Patagonian margin of Gondwana from 400 and 340 Ma (e.g. Fig. 3c). As we do not adopt the PGZ method, our position of Laurussia at 410 Ma relative to Gondwana is much closer to its final collision place and the resulting relative motion between Laurussia and Gondwana between 410 and 340 Ma is of sub-orthogonal–orthogonal collision along the southern Appalachian zone (Hopper et al., 2017), with some dextral transform motion between north-east Laurentia and the northwest margin of Gondwana (e.g. Murphy et al., 2011) and between southern Baltica and north Gondwana (e.g. Arthaud and Matte, 1977). From 340 to 320 Ma YOU19, MAT16 and DT14 have a similar configuration between Laurussia and Gondwana. We stress that while our model this differs from the adopted

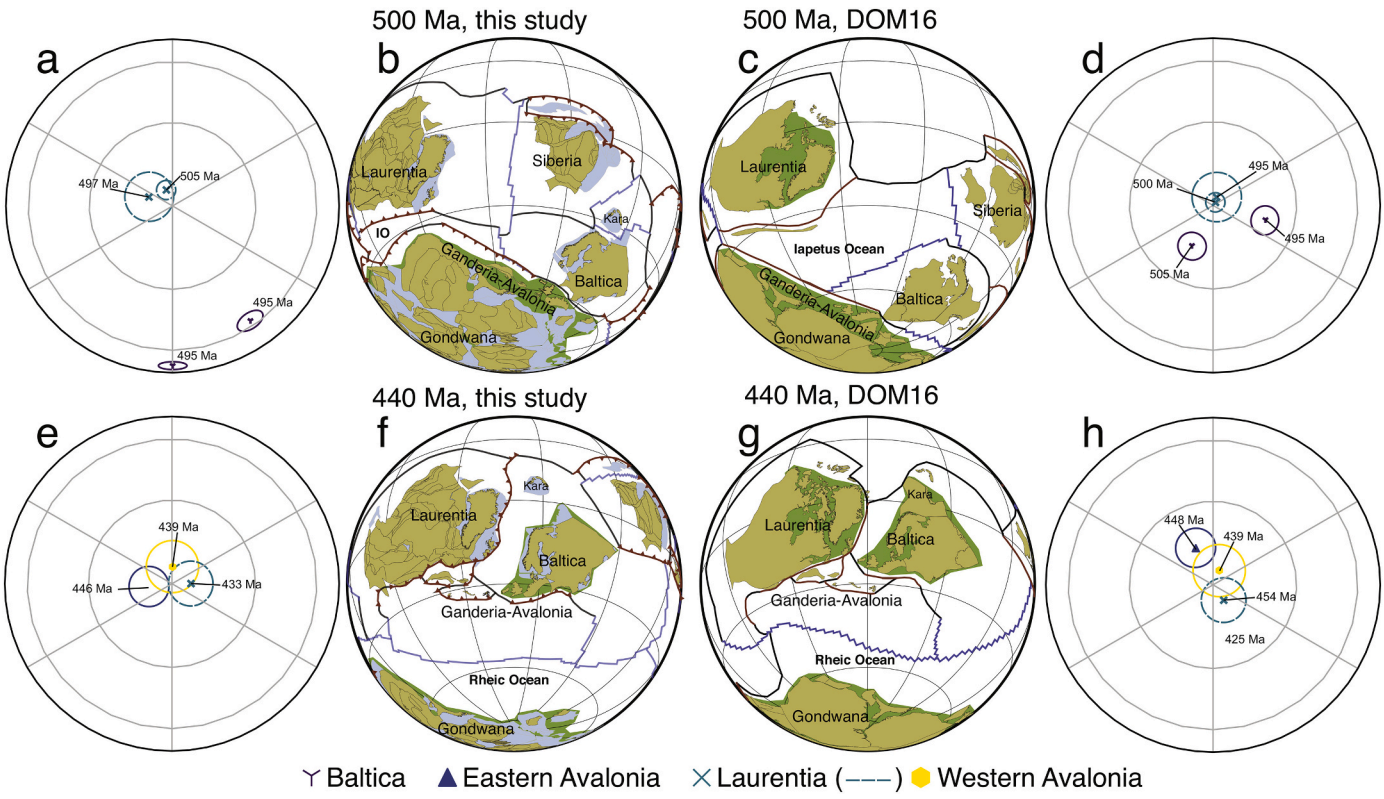


Fig. 12. Comparison of the evolution of the Rheic Ocean between our model (a, 500 Ma; c, 440 Ma) and DOM16 (b, 500 Ma; d, 440 Ma) during the early Palaeozoic. We point out the rotational difference (but similar latitude) in Baltica at 500 Ma in our model relative to DOM16, discussed in text. Palaeolongitude is constrained absolutely in DOM16 but not in our model. Subduction polarities are not provided in the GPlates files of DOM16. Tan polygons are areas of continental lithosphere in the Neoproterozoic that we model, blue polygons are areas of present-day continental lithosphere that are inferred to exist during the Neoproterozoic, but without having firm geological evidence or that have been affected by subsequent deformation (e.g. the distance between a present-day coastline and COB). Green polygons represent a schematic interpretation of congruent continental lithosphere, with intervening crust being subsequently deformed during future tectonic cycles. IO, Iapetus Ocean.

DOM16 model, it is not a particularly novel interpretation and many continental reconstructions show a similar scenario (e.g. McKerrow et al., 2000; Scotese, 2004; Stampfli and Borel, 2002). A more detailed geological and kinematic justification of this interpretation is presented in Young et al. (2019) and a discussion of the palaeomagnetic challenges in amalgamating Pangea are presented in Domeier et al. (2020, 2012), which we direct interested readers to.

5.2.2. *Deviations from DOM18*

Two salient points made by Domeier (2018), pertaining to relative longitude and his model, are also of interest here, and worth reiterating when merging DOM18 into the adj-YOU19 model and then extending the adj-YOU19 model into the Neoproterozoic. Firstly, a long lived south-dipping subduction zone, preserved in the northern Kazakhstan terranes of Urumbai, Selety and Erementau (Degtyarev, 2011; Domeier, 2018; Windley et al., 2007) was longitudinally distributed from Siberia through to the northernmost margin of Gondwana (i.e. North Australia, Papua New Guinea) and secondly, the broader framework of Baltica-Siberia-Gondwana provides geological, spatial and temporal limits on the evolution of this area. These two aspects of the model allowed DOM18 to infer with some certainty the relative palaeolongitude of many of the smaller terranes within the broader absolute palaeolongitudinal constraints imposed by (principally) Siberia, Baltica, Laurentia and Gondwana. Likewise, even though we do not adopt the absolute longitudinal framework of DOM18, we can use the positions of the major cratons to provide a relative control on the possible kinematic evolution of the Chinese cratons and terranes. We follow DOM18 by reconstructing a quasi-stable south-dipping subduction zone to delimit the northerly extent of the Palaeo-Tethys Ocean and this, coupled with the palaeomagnetic data from these cratons and terranes between 500 and 410 Ma, make longitudinal re-ordering of these blocks unlikely. The unlikeliness of longitudinal re-ordering is one of the main constraints and pieces of evidence that lead to significant revision of the positions of Tarim and North China in MER17 that are discussed in the following section (5.4).

The relative positions of terranes (Tianshan, Qaidam-Qilian, Kunlun etc.) can also be considered in a similar manner to how we conceive of the relative ordering of the Chinese cratons during the Early Palaeozoic. In particular, the ca. 470 Ma suturing of Tianshan-Chu Yili (Alexeiev et al., 2019) and the 440–430 Ma suturing of Kunlun, Qaidam, Qilian and Alxa to Tarim (Xiao et al., 2009). Both necessitate an internally consistent relative position between these terranes and Tarim and Siberia in order to be consistent with the geological record. That is, relative to present-day Tarim, Tianshan, Chu-Yili and other Kazakh terranes should be reconstructed somewhere north of the *northern* margin of Tarim during the Ediacaran–Ordovician, but south of Siberia. Similarly, Kunlun, Qaidam, Qilian and Alxa need to be reconstructed to the *south* and *east* of Tarim in the same time period. In a plate model framework, this means that the longitudinal structure of the Proto-Tethyan ocean basin should reconstruct (from west to east): Siberia—Chu-Yili-Kazak-Tianshan—Tarim—Alxa-Qaidam-Qilian-Kunlun—North China—South China (e.g. Fig. 13f, g). Further back in time, we also maintain this same configuration to minimise any terrane reorganising, such that their relative positioning is broadly reminiscent of present-day (e.g. Figs. 9; 16). In this manner, we use these relative longitudinal constraints to infer a configuration for the nuclei of these terranes in the Neoproterozoic, thereby connecting the present-day with their Precambrian history.

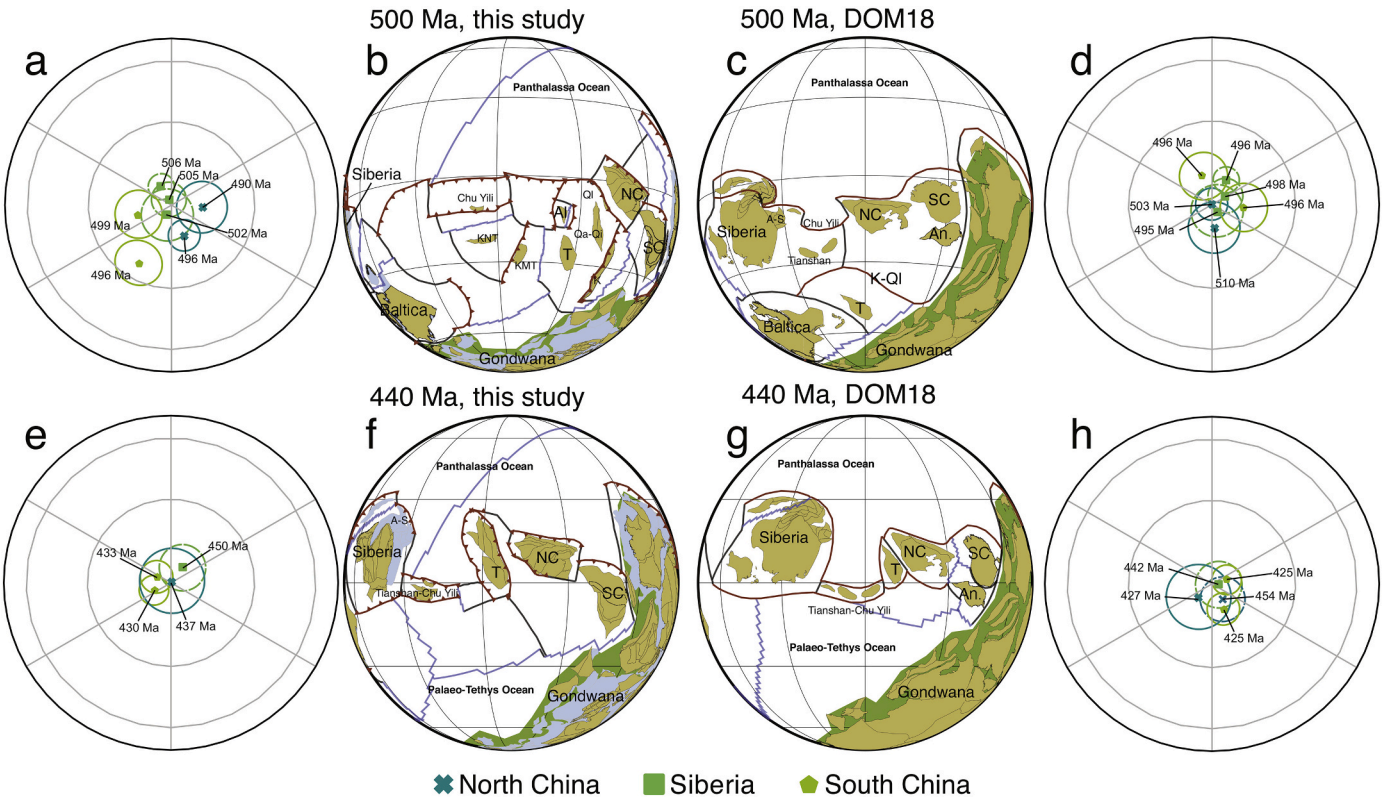


Fig. 13. Comparison of our model (a, c) with DOM18 (b, d) to highlight changes made. Annamia (Indochina, Sibumasu) is not explicitly modelled in our reconstruction. L, Lut (Iran); F, Farah (Afghanistan); T, Tarim. Tan polygons are areas of continental lithosphere in the Neoproterozoic that we model, blue polygons are areas of present-day continental lithosphere that are inferred to exist during the Neoproterozoic, but without having firm geological evidence or that have been affected by subsequent deformation (e.g. the distance between a present-day coastline and COB). Green polygons represent a schematic interpretation of congruent continental lithosphere, with intervening crust being subsequently deformed during future tectonic cycles. Al, Alxa; An, Annamia; A-S, Altai-Sinai; SC, South China; K, Kunlun; KMT, Krygyz Middle Tianshan; KNT, Krygyz North Tianshan; NC, North China; Qa-Qi, Qaidam-Qilian; Ql, Qinling; T, Tarim.

The fundamental difference between DOM18 and our implementation of the model is the longitudinal width of the Proto-Tethyan ocean basin, bounded by Siberia in the west, Gondwana in the east and south and the aforementioned south-dipping subduction zone in the north (e.g. Fig. 13b, c, f, g). The latitudinal extent of the ocean basin remains similar in both models (30–50°), constrained by palaeomagnetic data from Gondwana, Siberia and the Chinese cratons (e.g. Table 2, Fig. 13a, d, e, h). In our model, this ocean basin is much wider (longitudinally) in the late Cambrian and Ordovician than in DOM18, narrowing in size as it evolves due to our implemented easterly drift of Siberia from the Cambrian through to the Devonian. The size of the ocean basin is then similar at 410 Ma (Fig. 11), due to the adopted similarity of the YOU19 from the DT14 reconstruction (Young et al., 2019). The key reason for the difference in width at 500 Ma is because DOM18 places Laurussia further east at 500 Ma than we do (Section 5.2.1). This then forces a narrower ocean basin between 500 and 410 Ma in DOM18 than in our model. The following paragraphs will discuss the regional longitudinal constraints of this ocean basin by considering the position of Gondwana and Siberia.

The Early Palaeozoic position of Siberia in our model is a function of palaeomagnetic data and its position in, and breakout from, Rodinia. In isolation, the simplest explanation of Siberia's journey is that sometime during the late Tonian–Cryogenian (750–700 Ma) Siberia rifted off the northern margin of Laurentia (somewhere near Greenland, see Pisarevsky and Natapov (2003) and Pisarevsky et al. (2013)). At this time Siberia was located equatorially and rotated 60° clockwise from its present-day orientation (Pisarevsky et al., 2013). Palaeomagnetic data are sparse for the remainder of the Neoproterozoic, with the few calculated poles having either poor age constraints or unresolved tectonic coherence with the Siberian craton (Pavlov et al., 2015), and are therefore typically omitted from syntheses (Cocks and Torsvik, 2007; Li et al., 2008; Merdith et al., 2017a). However, from the mid-Cambrian the palaeomagnetic record of Siberia is reasonable (Cocks and Torsvik, 2007) and broadly congruent with the palaeolatitude of the 750 Ma pole (that is, equatorial–sub-equatorial). From the mid-Cambrian, the data suggest a slow northward drift and counter-clockwise rotation (Cocks and Torsvik, 2007), with the orientation of Siberia at ca. 530 Ma inverted relative to present-day. This then requires a ~120° clockwise rotation between 720 and 530 Ma in order to fit its Neoproterozoic position (Metelkin et al., 2012). For the Cryogenian and Cambrian, Siberia's motion can be inferred indirectly using data from Baltica, as outlined in the next paragraph.

The position of Baltica is constrained by clusters of palaeomagnetic data during the Ediacaran and early Cambrian. Furthermore, its latitudinal position places limits on the possible position of Siberia. The equatorial excursion of Baltica in the latest Ediacaran places Baltica at a latitude similar to Siberia. As they cannot be positioned on the same longitude (Merdith et al., 2017a), Siberia must be lcoated either longitudinally east or west of Baltica between 600 and 500 Ma (with Laurentia also occurring on a similar palaeolatitude but further east than either Siberia or Baltica). Domeier (2018) presented similar arguments for the second latitudinal excursion of Baltica (it returns to a high latitude during the Ordovician–Silurian) when it collided with Laurentia to form Laurussia at ca. 440–430 Ma. He argued that the overlapping palaeolatitudes of Siberia and Baltica at this time then requires Siberia to be located more easterly than Baltica by ca. 470 Ma (Domeier, 2018). We also adopt this logic, thus providing a rough relative longitudinal framework for Laurentia-Baltica-Siberia relations from 700 to 450 Ma.

Our model requires the motion of Siberia to be predominantly longitudinal between 700 and 450 Ma (the available palaeomagnetic data

do not suggest more than 30° latitudinal movement). We constrain this to two broad phases of movement, defined by Baltica's two latitudinal excursions (at ca. 560 Ma and 450 Ma). In the first excursion (750–550 Ma), we keep Siberia longitudinally between Laurentia and Baltica, because to move it further east than Baltica at 550 Ma would require relative plate motion greater than 30 cm/a, which we deem unlikely. By 470 Ma, palaeomagnetic data from Baltica suggest it has started drifting north again, so we therefore reconstruct Siberia to also be moving east longitudinally between 550 and 470 Ma, such that by 470 Ma it is located along the same longitude as Baltica; by 450 Ma it is further east than Baltica, such that Laurussia can form by 430 Ma. Our model is therefore similar to that of DOM18 in concept and adherence to available observations, however the different absolute longitudinal positions create a notably different ocean basin in the late Cambrian and Ordovician, within which the Chinese cratons and terranes are then arranged.

Domeier (2018) does not explicitly consider the Neoproterozoic or Early Palaeozoic evolution of the Chinese cratons in his model. At 500 Ma, the DOM18 model places North China off the northern margin of India, and South China off northern Australia. However, retaining these pairwise relationships in the Neoproterozoic is invalidated by what Neoproterozoic palaeomagnetic data exist for each craton (e.g. Fu et al., 2015; Li et al., 2004), and also conflicts with interpreted geological histories (Cawood et al., 2018b; Cawood et al., 2013b). Consequently, our model, which balances both older and younger times, alters the kinematic evolution in order to fit older constraints (Fig. 13, Sections 5.4.1 and 5.4.2).

5.3. MER17

5.3.1. Australia, North China, Lhasa and Tasmania

Significant alterations to MER17 were made between 1000 and 900 Ma along the north-western, western and south-western margins of Laurentia, affecting the motions and positions of Australia, North China, Siberia, Tasmania and Lhasa. We adopt the model of Wen et al. (2018) in having a dextral shear zone between Australia-Antarctica (A-A) and Laurentia during the early Tonian. Wen et al. (2018) argued for placing Tarim against the eastern margin of Laurentia, separating Laurentia from Australia in a 'Missing Link' position (cf. Li et al., 2008, Li et al., 1995), with the dextral shear zone transecting Tarim. However, we consider this position for Tarim is incompatible both with geological data (the 760 Ma Aksu Blueschist (C.-L. Zhang et al., 2013a)) and with the kinematic constraints that would be necessary to move Tarim from this position to its Palaeozoic position (e.g. Merdith et al., 2017b). We therefore use the alteration of Wen et al.'s (2018) model presented in Mulder et al. (2018b), who place a dextral boundary separating the Antarctic crust of Australian affinity exposed in Terre Adélie Land from the Antarctic crust of Laurentian affinity in the Nimrod Igneous Province (Fig. 14a, see also Goodge et al. (2017)).

North China and northern Australia share a similar Mesoproterozoic and early Tonian sedimentary record and both preserve contemporaneous ca. 1.33–1.31 Ga magmatism (Bodorkos et al., 2020; Yang et al., 2020; Zhang et al., 2017) that is interpreted as a large igneous province. Yang et al. (2019) also demonstrated the similarity in detrital zircon ages and hafnium isotope compositions between the Tonian strata of both areas. We find that this position of North China in the latest Mesoproterozoic is compatible with the few reliable palaeomagnetic data for North China in the Neoproterozoic (e.g. Fig. 6, Fu et al., 2015) and places North China in a position readily compatible with its Palaeozoic constraints where the same species of distinctive tommotiid fossils have recently been reported (Pan et al., 2018). A distinct Sino-Australian Cambro–Ordovician faunal province was identified by Burrett et al. (1990) that suggests some proximity in the early Palaeozoic. Cambrian–Ordovician rifting in the Arafura Basin north of northern Australia may represent the initial separation of North China from this margin of Gondwana (Ahmad and Munson, 2013). Palaeomagnetic data necessitate some relative motion between Australia and North China in the Early Palaeozoic from its inferred Mesoproterozoic–Neoproterozoic position (e.g. Domeier, 2018). Given there is no evidence of orogenesis between North China and northern Australia in the Phanerozoic, we infer that North China slowly drifts off this margin from the Cambrian, remaining in close enough proximity to share the identified Cambro–Ordovician faunal provinces (e.g. Fig. 13).

Dong and Santosh (2016) and Dong et al. (2014) describe a 1000 to 900 Ma suture between the Qinling Terrane and North China, preserved as the Kuanping Ophiolite (Fig. 14a–c). As Siberia and Australia are reconstructed adjacent to each other in Rodinia (Pisarevsky et al., 2013), the position of North China along the northern margin of Australia suggests that the Qinling terrane could feasibly be an extension of the Central Angara terrane, where there is a similarly aged (but sparsely described) ophiolite, the Ribnaya-Panimba ophiolite (Vernikovsky et al., 2004; Vernikovsky et al., 2003). In our model, the subduction zones represented by these two ophiolites consume the oceanic lithosphere between Australia, Siberia and Laurentia (the Kuanping Ocean) during the early Tonian. Mulder et al. (2018b) ceased motion at 900 Ma in their model but, we adjust this cessation to 930 Ma wherein the Qinling Terrane rotates to fit against the North China block. This is because we also reconstruct the Lhasa block along the western margin of Australia ((Zhu et al., 2011), see Section 5.1) and here magmatism is preserved from ca. 925 Ma (Guynn et al., 2012; Guynn et al., 2006; Hu et al., 2018; Zeng et al., 2018) (Fig. 14d,e). Consequently, we suggest that this subduction initiated after the closure of the interior Kuanping Ocean and collision of North China-Australia-Antarctica with Siberia-Laurentia along the Qinling-Central Angaran Terrane. The subduction zone then connects northwards through to subduction preserved in Taimyr outboard of Siberia (Vernikovsky et al., 2004; Vernikovsky and Vernikovskaya, 2001) and southward into an oceanic arc outboard of the Mawson Craton of Antarctica, possibly preserved in the southernmost Tonian Oceanic Arc Super Terrane (TOAST) or between Indo-Antarctica and Australia-Antarctica). In our model, Australia sits in a typical SWEAT (South West United States, East Antarctica) configuration (Moores, 1991). We made this change to better fit the arguments put forward by Mulder et al. (2018b), while still maintaining integrity of relative plate kinematics following the reasoning of Merdith et al. (2017b).

Our revised model also incorporates recent refinements to the Proterozoic and early Palaeozoic palaeogeography of the Western Tasmania Terrane. The Western Tasmania Terrane, comprising the Proterozoic geology of Tasmania and the East and West South Tasman Rises (Berry et al., 2008), occupies an important position in deciphering the geological relationship between Laurentia and Australia-Antarctica in Rodinia, and also in understanding the transition between Rodinia to Gondwana. The Western Tasmania Terrane represents an exotic Proterozoic microcontinent that was accreted onto the Pacific margin of eastern Gondwana in the late Cambrian during the Ross-Delamerian orogenic cycle (Berry et al., 2008; Cayley, 2011). The terrane has geological affinities with the central Transantarctic Mountains of East Antarctica and the western margin of Laurentia, including overlapping Palaeoproterozoic basement ages, contemporaneous Mesoproterozoic magmatic and fluid-flow events, and correlated Mesoproterozoic sedimentary strata (Berry et al., 2008; Fioretti et al., 2005; Halpin et al., 2014; Mulder et al., 2015, 2018b). Based on these geological connections, the Western Tasmania Terrane was likely located between East Antarctica and western Laurentia within an assembled Rodinia. The breakout of the Western Tasmania Terrane from its central position within Rodinia is recorded by widespread Tonian–Ediacaran sedimentation and rift-related magmatism (Mulder et al., 2020). The onset of Neoproterozoic rifting of the Western Tasmania Terrane is marked by 780–750 Ma intraplate magmatism (Black et al., 1997; Calver et al., 2013) and latest Tonian (750–730 Ma) siliciclastic and carbonate sedimentation (Calver et al., 2014; Mulder et al., 2018a). Following deposition of Cryogenian rift-related strata and glaciogenic intervals (Calver, 2011; Calver et al., 2014) a final pulse of Neoproterozoic rifting is

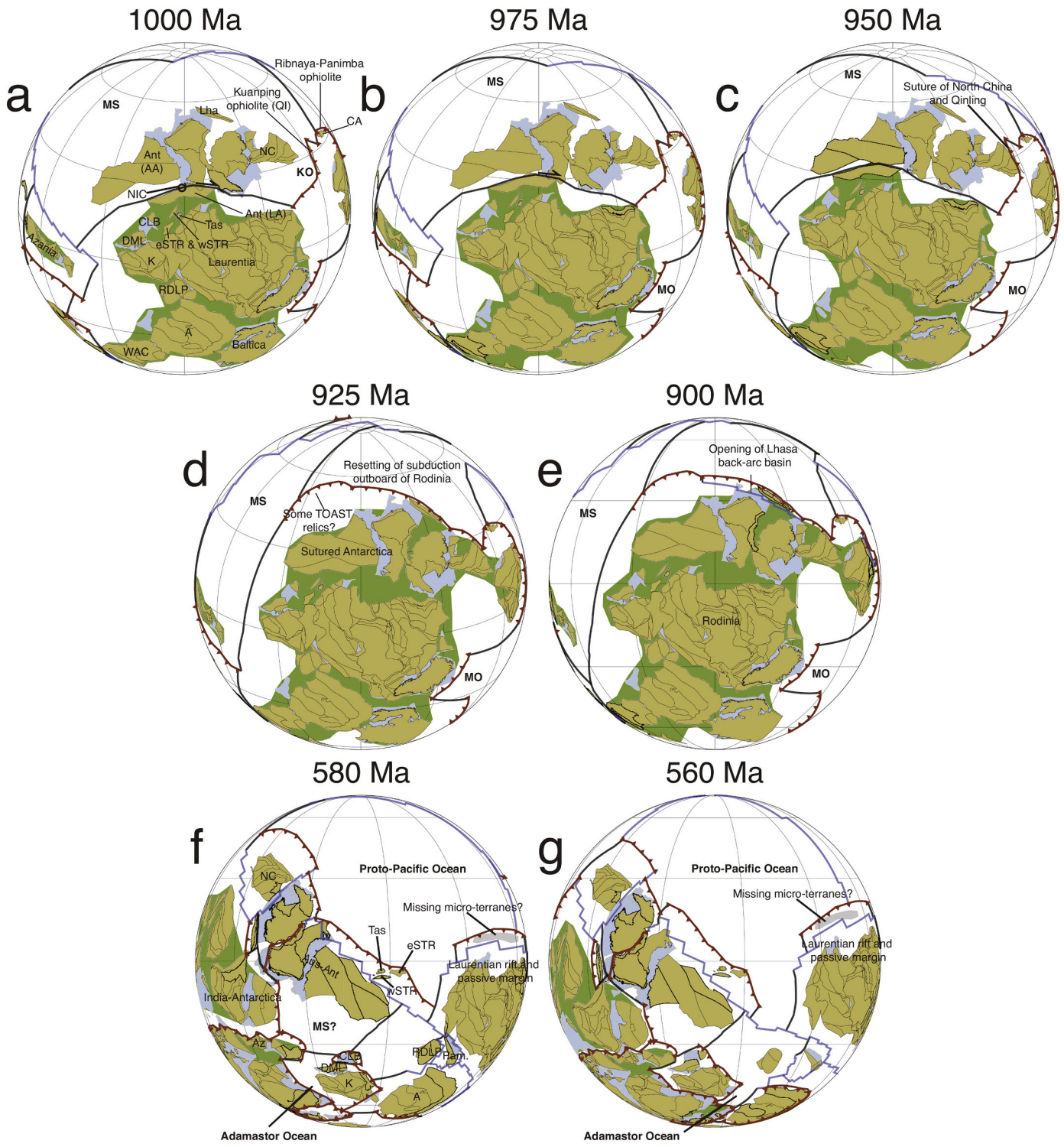


Fig. 14. Snapshots of plate reconstructions showing our updated model for Australia-Laurentia at key time intervals, along with palaeomagnetic data. (a) 1000 Ma; (b) 975 Ma; (c) 950 Ma; (e) 925 Ma; (f) 900 Ma; (h) 580 Ma and (i) 560 Ma. The Tonian model (a–f) follows arguments laid out in Mulder et al. (2018b), while the Ediacaran–Cambrian evolution is after Mulder et al. (2020). Times in these panels reflex the nominal time of best fit for each pole. Tan polygons are areas of continental lithosphere in the Neoproterozoic that we model, blue polygons are areas of present-day continental lithosphere that are inferred to exist during the Neoproterozoic, but without having firm geological evidence or that have been affected by subsequent deformation (e.g. the distance between a present-day coastline and COB). Green polygons represent a schematic interpretation of congruent continental lithosphere, with intervening crust being subsequently deformed during future tectonic cycles. CLB: Coats Land Block; DML, Dronning Maud Land; eSTR: Eastern South Tasman Rise; MO, Mirovoi Ocean; MS, Mawson Sea; Tas: Tasmania; wSTR: Western South Tasman Rise; RDLP: Río de la Plata; WAC, West African Craton.

recorded by voluminous ca. 580 Ma rift-related basalts in northwest Tasmania (Direen and Crawford, 2003; Meffre et al., 2004). Geological correlations permit the Western Tasmania Terrane to have remained attached to either the western margin of Laurentia or the eastern margin of Australia-Antarctica following the opening of the Pacific Ocean (Fig. 10f), prior to being isolated as a microcontinent during ca. 580 Ma rifting and accretion onto its present-day position along the margin of Gondwana by the late Cambrian (Fig. 10g; Berry et al., 2008; Mulder et al., 2020). We follow Mulder et al. (2020) in having Tasmania rift from the Antarctic margin (rather than the alternative scenario of Laurentia), thus implying that some further unknown micro-continents rifted from the western margin of Laurentia at the same time in order to account for that passive margin (e.g. Fig. 14f, g Macdonald et al., 2013) (see also Colpron et al., 2002; Cox et al., 2018; Eyster et al., 2019).

5.3.2. India-South China Accretionary Belt

We preserve the MER17 interpretation of a tight India-South China connection (after Cawood et al., 2013b). This possible connection was suggested previously by Jiang et al. (2003) who noted the similarity between sequence stratigraphy in rift basins preserved in both South China and the Indian Lesser Himalaya (Fig. 15a), as well as by Hofmann et al. (2011) who suggested a geological similarity based on detrital zircon analysis. Arguments for this connection are succinctly summarised in Cawood et al. (2018b) and are not repeated here—instead we focus our discussion of this margin on the relative position of outboard terranes during the Neoproterozoic (Fig. 15), which are based predominantly on their Palaeozoic positions (Domeier, 2018). Here we have sought to preserve their relative internal positions in order to minimise reshuffling of terranes during the Neoproterozoic (e.g. Fig. 16). For example, Kunlun, which is currently preserved south of Tarim and west of Qaidam-Qilian, is always reconstructed with the same internal consistency. Although this may not be an accurate reflection of the ordering and positioning of the terranes, it ensures consistency within the model and minimises terrane shuffling that can preclude unrealistic scenarios, where terranes have to kinematically skirt one another precariously. Fig. 16 gives a schematic overview of our conceptualisation and implementation of this model.

Following Alessio et al. (2018) and Armistead et al. (2019), the northwest margin of India is here interpreted as an extensive Stenian–Tonian accretionary margin that extends as far as the Omani basement and northernmost Madagascar. The pre-Ediacaran basement rocks in Rajasthan and Pakistan share similarities with those of Oman. Granitoids have been dated from Rajasthan and from Nagar Parkar in eastern Sind (Pakistan) at ca. 1.1 Ga (Meert et al., 2013; Raza et al., 2012). There is no evidence of older crust occurs west of the Western Margin Fault of the Aravalli-Delhi Orogen, where the Marwar terrane accreted to India in the latest Mesoproterozoic (Meert et al., 2010) (Fig. 15b). Tonian granitoids and rhyolites occur in inliers through northwest India and Pakistan, where they cluster into crystallisation ages of ca. 990–970 Ma (Haldar and Deb, 2001; Pandit et al., 2003), ca. 860–820 Ma (Davies and Crawford, 1971; Deb et al., 2001; Just et al., 2011; Van Lente et al., 2009) and ca. 775–760 Ma (Ashwal et al., 2013; Gregory et al., 2009; Meert et al., 2013; Van Lente et al., 2009). The latter magmatic and extrusive phase forms one of the largest felsic igneous provinces on the planet—the Malani Igneous Suite—which is also traced to the Seychelles (Fig. 15c–e) (Torsvik et al., 2001; Tucker et al., 2001). Arc accretion continued outboard to Oman where two main phases of subduction and arc magmatism occur, at ca. 850 Ma and ca. 770 Ma (Blades et al., 2020). The latter phase focussed in the southern Mirbat area and interpreted here as the arc that formed ocean-ward of the more back-arc Malani Igneous Suite. Further outboard still, and later accreting onto the Indian margin, the Bobakindro Terrane of northern Madagascar (Armistead et al., 2019) consists of juvenile magmatism that dates from ca. 750–705 Ma (Armistead et al., 2019; Collins, 2006; Thomas et al., 2009).

Many terranes currently preserved north of South China and south of Siberia have Neoproterozoic or older cores. They have not been previously considered in global models (Li et al., 2008; Merdith et al., 2017a) due to the sparsity of data and small size of terranes, which invites many competing and conflicting interpretations of their history. However, in the construction of this continuous plate model, where spatial and temporal continuity is vital, the most compatible Tonian position for these terranes was outboard of the previously discussed large accretionary subduction zone of South China and India. This position places them in the most favourable kinematic, palaeomagnetic and geologically plausible positions for their (more well constrained) Palaeozoic journeys (e.g. Charvet et al., 2011; Domeier, 2018; Xiao et al., 2013). Below we summarise some geological evidence for this, with particular reference to the Tarim Craton, as it is the only block that has multiple reliable palaeomagnetic data from the Neoproterozoic that act as a another line of evidence. We also note that Huang et al. (2019) recently proposed a location outboard of Greenland for the Yili-Tianshan Block on the basis of similar detrital zircon age spectra. However, more work would have to be done to determine whether this Tonian position is consistent with the kinematic evolution necessary for these blocks to fit their Palaeozoic constraints.

Early Tonian age (1000–900 Ma) magmatism and high-pressure metamorphism is preserved in the basements of the Qilian-Qaidam (Qi-Qa), Kunlun and Tianshan-Chu Yili terranes (Song et al., 2012; Tung et al., 2007; Wu et al., 2017). Importantly Song et al. (2012) identified an early Tonian event preserved in a high-pressure metamorphic belt in Qi-Qa. Here, a ~200 km linear belt of granitic gneisses, metamorphosed in the Palaeozoic, have crystallisation ages between ca. 1000 and 900 Ma (Song et al., 2012). Zircons recovered from pelitic and psammitic gneisses from the same belt possess multiple generations of growth, as suggested through cathodoluminescence imaging, and return ages of the (first generation) to between ca. 940 and 900 Ma (Song et al., 2012). These are interpreted to represent a period of granulite facies metamorphism from a continental arc indicating that subduction was active during the Early Tonian (Song et al., 2012). Song et al. (2012) and others (e.g. Zhang et al., 2008) suggested a link between these two blocks and South China on the basis of similar-aged magmatism and metamorphism. However, as the Qi-Qa preserves a different Palaeozoic tectonic history to South China, as opposed to fragments of older lithosphere preserved in the Panxi-Hannan Belt of the Yangtze Craton, we suggest that a subduction zone was located outboard of Qi-Qa while a secondary, smaller ocean was closing between Qi-Qa and the accretionary orogen of the Panxi-Hannan Belt (Fig. 11a–c). Upon the suturing of Yangtze with Cathaysia (ca. 900 Ma, Fig. 11b), subduction relocated outboard of South China and began to close the ocean between Qa-Qi and South China. Similar to the Qi-Qa, the Kunlun terrane preserves scattered magmatic ages of S-type granites and protoliths of orthogneiss and amphibolites ranging between ca. 1000 and 900 Ma (Chen et al., 2004; He et al., 2019; and Chen et al., 2006a; b—both cited in Chen et al., 2008; He et al., 2019). We interpret these rocks and ages as an extension of the same subduction zones outboard of Qi-Qa, and extend it further to the south where (again) similar-aged magmatism is also preserved in the North Tianshan and Chu-Yili (Degtyarev et al., 2017).

The Kazakh terranes (including Krygyz Tianshan and Chu-Yili, Fig. 15a) have poorly constrained Neoproterozoic histories, with only a handful of ages from outcropping magmatic rocks and sedimentary successions. We predominantly follow the summary of Degtyarev et al. (2017) in offering a possible tectonic interpretation of their Neoproterozoic geological history that is linked to the wider globe. Degtyarev et al. (2017) note that there are two broad categories of Precambrian terranes preserved in the Kyrgyz-Tianshan-Yuli area; the Issedonian and Ulutau-Moyunkum terranes. The Issedonian terranes, preserved in the northeast of the western Central Asian Orogenic Belt, include Chu-Yili and the Chinese Central Tianshan and are characterised by late Mesoproterozoic magmatism (e.g. Degtyarev et al., 2011), thick (> 1000 m) 1050–950 Ma quartzite-schist successions followed by ongoing magmatism from ca. 960–890 Ma (e.g. Degtyarev et al., 2008;

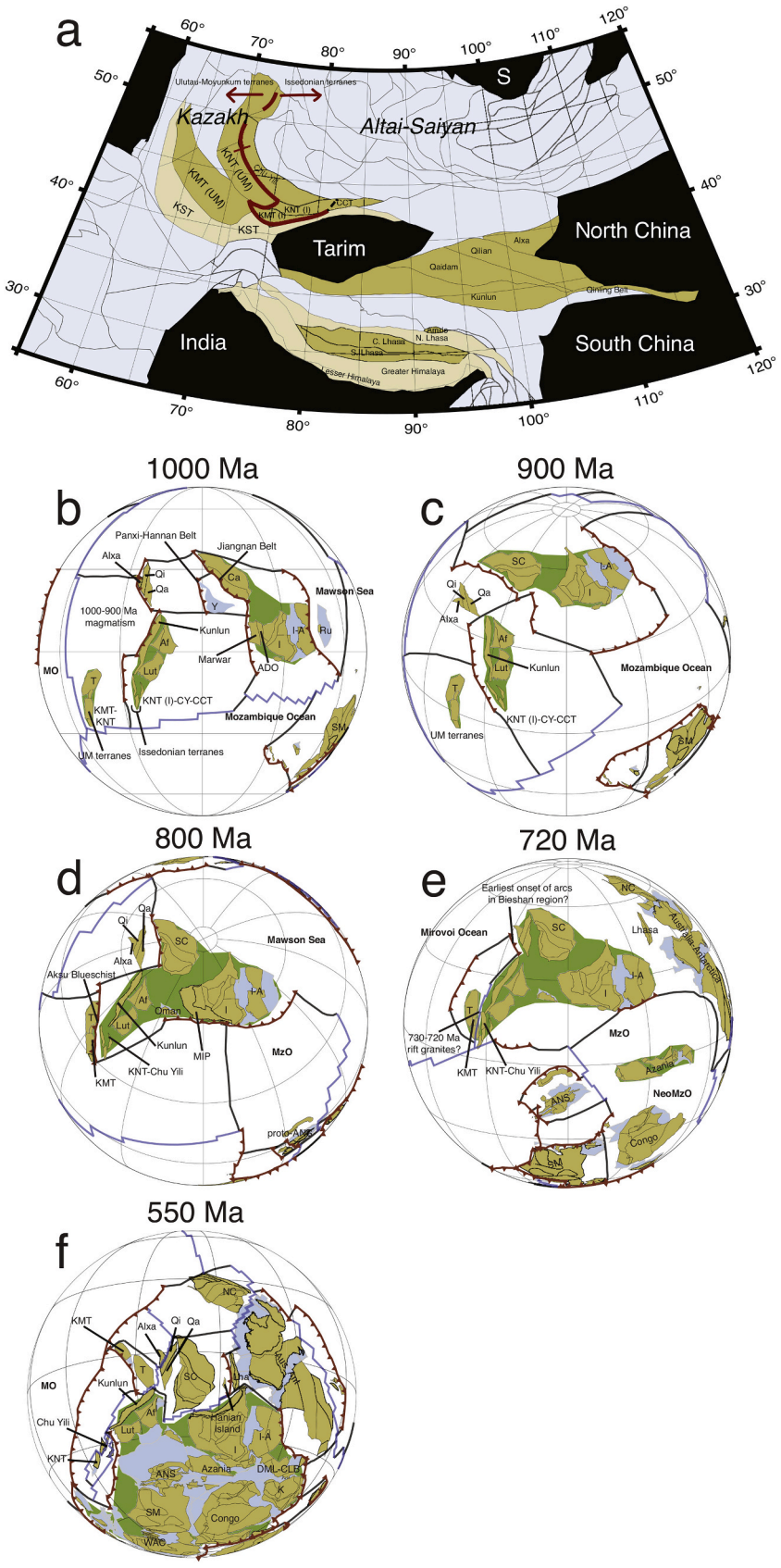


Fig. 15. (a) Regional map at present day of Central Asian Orogenic Belt with modelled terranes highlighted in tan. Light tan terranes are not explicitly modelled but are referred to in the main text. Black areas represent the cratonic components. For the Kazakh area, we use polygons consistent with their Palaeozoic structure. The size, orientation and distribution of crust in these terranes in the Neoproterozoic is unknown due to the subsequent reworking of the terranes. Therefore, the precise position (along a margin), orientation, size and shape of these terrane polygons in the reconstruction figures are speculative and should be treated cautiously. (b–f) Evolution of the India-South China system during the Tonian–Cryogenian at key times. Tan polygons are areas of continental lithosphere in the Neoproterozoic that we model, blue polygons are areas of present-day continental lithosphere that are inferred to exist during the Neoproterozoic, but without having firm geological evidence or that have been affected by subsequent deformation (e.g. the distance between a present-day coastline and COB). Green polygons represent a schematic interpretation of congruent continental lithosphere, with intervening crust being subsequently deformed during future tectonic cycles. ADO = Aravalli-Delhi Orogen; Af, Afghanistan; Aus-Ant, Australia-Antarctica; Ca, Cathaysia; DML-CLN, Dronning Maud Land-Coats Land Block; I, India; I-A, Indo-Antarctica; KNT (I/UM), Krygyz North Tianshan (Issendonian/Ulutau-Moyunkum); KMT (I/UM), Krygyz Middle Tianshan (Issendonian/Ulutau-Moyunkum); MIP, Malani Igneous Province; MO, Mirovoi Ocean; MzO, Mozambique Ocean; NC, North China; NeoMzO, Neomozambique Ocean; Qa, Qaidam; Qi, Qilian; Ru, Ruker; SC, South China; SM, Sahara Metacraton; T, Tarim; WAC, West African Craton; Y, Yangtze.

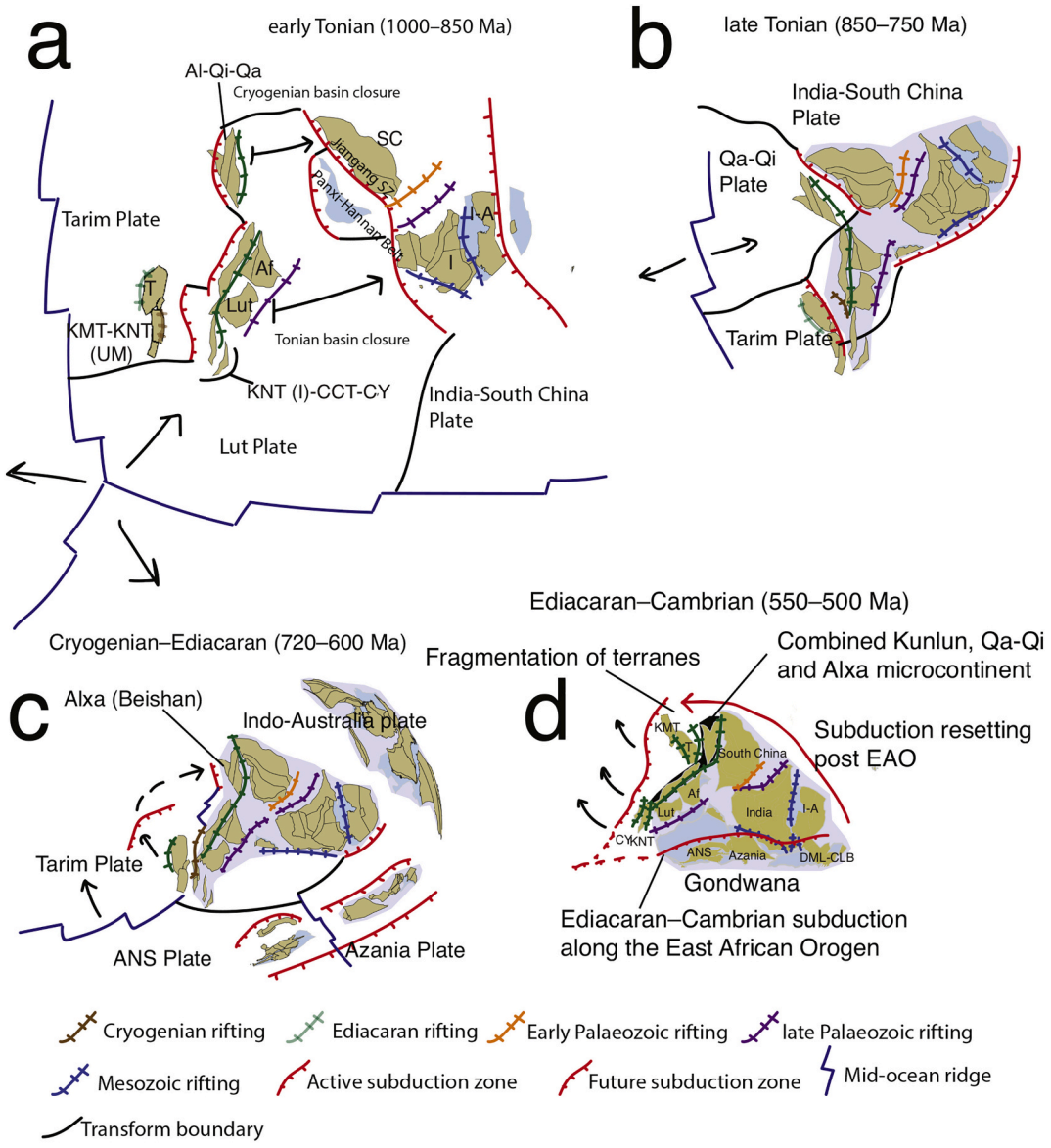


Fig. 16. Schematic of our model for India-South China at key time steps, showing accretion of the Yangtze Craton and numerous smaller terranes and blocks to a large, Tonian subduction zone outboard of the north-western India and the northern margin of South China and their subsequent fragmentation and rifting off during the Ediacaran–Early Cambrian. (a) early Tonian; (b) late Tonian; (c) Cryogenian–Ediacaran, note if the model were adopted to fit the cluster of three palaeomagnetic poles from Tarim then collision would be at ca. 650 Ma, and; (d) Ediacaran–Cambrian. Af, Afghanistan; Al-Qi-Qa, Alxa, Qilian, Qaidam; ANS, Arabian Nubian Shield; CY, Chu Yili; DML-CLB, Dronning Maud Land-Coats Land Block; EAO, East African Orogen; I, India; I-A, Indo-Antarctica; KMT (I/UM), Krygyz Middle Tianshan (Issendonian/Ulutau-Moyunkum); KNT (I/UM), Krygyz North Tianshan (Issendonian/Ulutau-Moyunkum); SC, South China; T, Tarim.

Gao et al., 2015; Huang et al., 2015). Comparably, the Ulutau-Moyunkum terranes are preserved only in the west (in Krygyz) within Kyrgyz Middle Tianshan and Krygyz North Tianshan (e.g. Fig. 10b), and consist of a Palaeoproterozoic basement, with predominantly sedimentary Mesoproterozoic and early Neoproterozoic rocks (Degtyarev et al., 2017). Magmatism, between 840 and 760 Ma (Kröner et al., 2012) and granulite facies metamorphism from 800–760 Ma (Degtyarev et al., 2017; Tretyakov et al., 2016) are recorded only in the late Tonian. Both sets of terranes preserve distinct differences in their Mesoproterozoic histories, minor differences in the Early Neoproterozoic histories but similar histories from the mid-Neoproterozoic (ca. 700 Ma) onwards, suggesting proximity sometime during the late Tonian (800 to 700 Ma?) (Degtyarev et al., 2017). We interpret the Issedonian terranes to be the southernmost extent of the subduction zone spanning Qi-Qa and Eastern Kunlun, as the magmatism preserved in the Issedonian terranes has a continental arc signature (Huang et al., 2014) and is broadly coeval. Comparably, the Ulutau-Moyunkum terranes, which share Mesoproterozoic similarities to Tarim and record no magmatism in the early Neoproterozoic, are located on the opposite side (lower plate) of a closing ocean basin. This culminates with the collision of Tarim (with the Ulutau-Moyunkum terranes) and the combined India-South China continent at ca. 800–760 Ma along the Issendonian margin (Fig. 11d, e). The sparse data and age constraints from these terranes means much of their Neoproterozoic history is conjectural. Although the specific orientation and positioning of the terranes along the margin is speculative our interpretation is that it places the Kazakh terranes in a favourable position for their Palaeozoic evolution which is, comparably, much better constrained.

Two clusters of Neoproterozoic-aged palaeomagnetic data from Tarim make it difficult to elucidate a consistent position with other palaeomagnetic data from Rodinian constituents. Three poles from the Tonian and Cryogenian require a 90° rotation of Tarim in order to fit the

younger pole of Wen et al. (2017), or a 180° rotation to fit the cluster of three poles in the Ediacaran to Cambrian (see Merdith et al. (2017a) and Section 4.2 for a discussion). Within a self-consistent kinematic plate boundary framework, this motion is not permissible if Tarim is positioned either against north-western Australia (e.g. Zhang et al., 2012) or as an extension of the 'Missing-Link' model (Li et al., 2004 for the original proposal of the "Missing-Link" model; Wen et al., 2018, Wen et al., 2017). A plausible position where these palaeomagnetic criteria are met, along with satisfying key geological evidence, such as the 800–760 Ma Aksu Blueschist preserved on the northern margin of Tarim (C.-L. Zhang et al., 2013b), is outboard of the India-South China accretionary belt, where it acts as the final piece of continental lithosphere accreted to the margin. In our model, we suggest the metamorphism recorded by the Aksu Blueschist marks the accretion of Tarim to Chu-Yili and the Tianshan (see Xia et al. (2017) for the most recent discussion, but see also data and discussion from Zhang et al. (2012, 2009). To accommodate the change in position suggested by the palaeomagnetic data, we introduce a ~120° rotation of Tarim and Southern Tianshan away from this margin, such that Tarim's southern margin collides with the outboard margin of Alxa-Qaidam-Qilian, so its northern margin faces an open ocean basin, allowing it to rift northward facing as Gondwana forms towards its more well constrained Palaeozoic position (Fig. 16).

We present the following geological observations in support of this model for Tarim's evolution. Firstly, there is an absence of extensive magmatism on either the northern or southern margin of the Tarim craton between 1000 and 850 Ma, which makes it difficult to include as a part of the upper-plate circum-Rodinian subduction girdle (Cawood et al., 2016). Previous studies, including MER17, place Tarim on the margin of Rodinia typically also include the Chu Yili and Tianshan crust attached in a quasi-present-day configuration to the northern margin of Tarim. In such cases their record of Tonian magmatism supports the interpretation that they formed part of the circum-Rodinian subduction girdle (Ge et al., 2014). However, this location is inconsistent with available palaeomagnetic data (e.g. (Wen et al., 2018). Secondly, rift related granitoids preserved in the Southern Tianshan (Degtyarev et al., 2017; Gao et al., 2015) are here interpreted as evidence of the re-adjustment of Tarim between 730 and 680 Ma to account for the change in palaeolatitude and orientation inferred from palaeomagnetic data (Fig. 11e). In addition, extensive rifting in the southwest of Tarim (Wang et al., 2015) is interpreted to reflect the rearrangement of subduction after Tarim/India-South China amalgamation. This motion is similar to the adjustment of Baltica relative to Laurentia in the latest Mesoproterozoic proposed by Cawood et al. (2010) to account for the Valhalla Orogeny. Xiao et al. (2010) summarise the geology and geochronology of rocks found in the Beishan area of China which record a protracted and complex history of multiple arc development and accretion through the late Neoproterozoic and Early Palaeozoic. Rocks in the Beishan area (Alxa, Figs. 15, 16) range from low-grade sedimentary metamorphic assemblages to gneiss and eclogite complexes and intrusive granitic bodies that have late Neoproterozoic–Cambrian ages (Xiao et al., 2010). These rocks, inferred to represent an active subduction zone and accretionary complex, are unconformably overlain by Cambrian–Ordovician sediments. The earliest record of metamorphism in the area are from a series of SHRIMP U-Pb ages taken from the metamorphic rims of zircons of an eclogite unit at ca. 830–800 Ma (Yang et al., 2006).

With respect to the palaeomagnetic issues of Tarim we raised earlier (Section 4.2), we find that our conceptual model of this rotation of Tarim (e.g. Fig. 16) can fit either set of palaeomagnetic data equally as well, with the key factor being the time of subduction in the Beishan area. Under the cluster of three poles, the motion of Tarim occurs more quickly and peak subduction (possibly resulting in a collision?) would be earlier (ca. 650 Ma), while to fit the pole of Wen et al. (2017) it would occur later at between 600 and 550 Ma. Based on the review of Xiao et al. (2010), we infer that the geological data support the later interpretation more strongly. However, given the novelty of this scenario and the absence of identifiable piercing points, it could be revised in the future to fit the alternative scenario.

Late Neoproterozoic–Early Cambrian rifting events are inferred to have occurred within all the terranes (Kunlun, Qa-Qi, Chu Yili and Tianshan) that we have placed on this Indian-South Chinese accretionary margin, however, the high degree of reworking and suturing of crust from the terranes, coupled with the small size of these terranes makes it difficult to pin down precise rift times. We stress that our interpretation here is preliminary, especially when compared to specialised reviews of the tectonics of this area (Kröner et al., 2007; Wilhem et al., 2012; Windley et al., 2007; Xiao et al., 2013; Yakubchuk, 2017). We reiterate that our intention here is to provide a possible framework that connects and contextualises these terranes within a consistent kinematic and tectonic evolution between the Neoproterozoic and Palaeozoic (Fig. 16), which can be more tightly refined in the future. Ordovician–Silurian sutures between Qa-Qi-Kunlun and surrounding cratons preserve late Neoproterozoic–Cambrian ophiolites (Jian et al., 2014; Shi et al., 2018; Song et al., 2013; Song et al., 2009) thus necessitating the existence of ocean basins, but there are few dates of ocean basin initiation. Xu et al. (2015) date Qilian-Qaidam continental rift basalts to 600–580 Ma, constraining ocean basin formation to the latest Ediacaran–earliest Cambrian, with the oldest ophiolite (the Yushigou Ophiolite) preserved in these terranes is dated to 550 Ma (Shi et al., 2004). Evidence of rifting is more sparse in Kunlun, however, similar stratigraphy, ages and geochemistry of metavolcanic deposits between Kunlun and Qaidam-Qilian (Yuan et al., 2004) suggest coeval rifting is reasonable, though not definite. We follow some recent work (Peng et al., 2019; Zhao et al., 2018) in having separation of Tarim and these terranes in the late Ediacaran (550 Ma here, as a response to the closure of the Mozambique Ocean between India and Congo). Our model closely resembles the schematic framework outlined by Qiantao et al. (2001), while also following Domeier (2018) in maintaining a very close affinity between Kunlun, Qa-Qi and Alxa for the Early Palaeozoic, such that they conceptually form a single elongated terrane that rifts off Gondwana at ca. 550 Ma and collides along the southern margin of Tarim by 440 Ma.

Comparably, rifting on the northern margin of Tarim is easier to constrain. Thick, late Neoproterozoic sedimentary sequences capped with carbonate and an unconformity on the Ediacaran–Early Cambrian imply a prolonged rift phase with breakup at ca. 550–540 Ma (Zhao et al., 2014; Zhu et al., 2017). Similarly, sedimentary assemblages preserved in the South Tianshan orogen are dated from 540–520 Ma (Alexeiev et al., 2020; Safonova et al., 2016), suggesting that ocean basin formation between Tarim and Krygyz Middle Tianshan begins in the Early–Middle Cambrian. Further north, the relationship between the Kryguz North Tianshan and Chu-Yili is also reasonably well established (e.g. Windley et al., 2007; Xiao et al., 2013). Late Ediacaran–Early Cambrian magmatism preserved in Chu-Yili and North Tianshan (Alexeiev et al., 2011; Degtyarev et al., 2017; Kröner et al., 2007) is interpreted to represent development of multiple contemporaneous arcs (e.g. Alexeiev et al., 2020). The Ordovician-aged sutures between Chu-Yili and North and Central Tianshan (Windley et al., 2007) are defined by ophiolitic slithers, implying an ocean basin (or a back-arc) existed between these terranes. We infer that in the late Neoproterozoic to Early Cambrian, the Kazakh and Tianshan terranes that accreted outboard of India-South China were fragmented and rifted off this margin forming a collage (not dissimilar to modern southeast Asia, or the NE Pacific in the Mesozoic, e.g. Sigloch and Mihalynuk (2013) that eventually re-assembled in the Ordovician. We model the time of fragmentation at 550 Ma, because this is the time of collision between India and Congo along the East African Orogen, so we infer that subduction relocated outboard of the northern margin.

Palaeomagnetic data from South China do not permit a fixed fit between South China and Gondwana for the early Palaeozoic. The data do, however, permit a close spatial relationship between them (< 1000 km). Palaeomagnetic data from South China suggest it moved from mid to

lower latitudes between the Cambrian and Devonian (Domeier, 2018; Han et al., 2015). Furthermore, shallow marine faunal data and detrital zircon arrays suggest that between the Cambrian and Devonian, South China shifted from an Indian-Himalayan-Iran affinity (Burrett et al., 1990) to Sibumasu-Australian affinity (Cocks and Fortey, 1997; Metcalfe, 2013; Metcalfe, 2011), broadly consistent of the positions necessary to fit the palaeomagnetic data. Rift sequences in South China and in northern India (Himalayan terranes) are similar, but diverge strongly after the early Cambrian (Jiang et al., 2003), providing some kinematic support for invoking for relative motion between South China and Gondwana. The Sanya Block of Hainan Island (Fig. 15f) is linked through detrital zircon provenance and middle Cambrian trilobites to western Australia and Antarctica rather than South China in the Neoproterozoic (Cawood et al., 2018b; Xu et al., 2014). The presence of Early Ordovician trilobites in the Sanya block also common to South China and Australia (Torsvik and Cocks, 2009) support a close relationship between the three domains by this time (Cawood et al., 2018b). A late Cambrian–Ordovician (520–450 Ma) metabasaltic arc assemblage in Hainan Island (Xu et al., 2008; Xu et al., 2007) is interpreted to be the northerly extension of the Kungaan Orogen that sutured Australia-Antarctica and India (e.g. Xu et al., 2014). We introduce divergent motion between Gondwana and South China at 550 Ma, coinciding with the rift-to-drift sequences of Jiang et al. (2003). This divergent motion moves South China from a position outboard of Northern India at 550 Ma to one that is slightly further east and adjacent to western Australia at 500 Ma, accounting for the arc assemblage in Hainan as well as similar faunal patterns.

5.3.3. ANS-Azania-TOAST

We suggest that, to a first order, the central Arabian-Nubian Shield (ANS) accreted on the kernel of Azania and formed a semi-continuous archipelago outboard of the eastern margins of the Congo Craton and Sahara Metacraton (SM) (Fig. 17; Collins and Pisarevsky, 2005; Merdith et al., 2017a). Geological details and a regional plate model of the accretion of the ANS and Azania are adopted from Collins et al. (n.d.), Blades et al. (2020) and Johnson et al. (2011), though here we extend Azania to the south by attaching portions of the Tonian Aged Ocean Arc Super Terrane (TOAST—Jacobs et al. (2017, 2015)). The similarity in ages, petrology of rocks and $\delta^{18}O$ from zircons between the Dabolava Suite in Madagascar (Archibald et al., 2018) and TOAST (Jacobs et al., 2017; Jacobs et al., 2015; Wang et al., 2020) suggest a similar tectonic environment. As the southern tip of Azania is reconstructed to be adjacent to the location of the TOAST terrane in Gondwana, at the nexus between the East African Orogen and the Pinjarra/Kuunga Orogen, there is also a strong palaeogeographic argument for attaching TOAST to Azania, as their Rodinian reconstructed position requires no alteration for their position in Gondwana (Fig. 17b).

5.3.4. Hoggar, Borborema, Avalonia and Ganderia

The Hoggar Block is preserved between the Sahara Metacraton (SM) and the West African Craton (WAC) in northwest Africa and records a long Neoproterozoic history of accretion of island arcs and continental ribbons. The model incorporated here is based on work by Caby et al. (1989), Black et al. (1994) and Liégeois et al. (1994) and involves three main constituents of present-day Hoggar (from west to east): IOGU-IGU, LATEA and the Aïr Block (Fig. 18a, b).

The broad tectonic framework of the Hoggar block is an accretionary margin consisting of at least 23 individual terranes that were slowly compressed between two large tectonic units—the WAC and the SM—as Gondwana amalgamated. The Aïr block, preserved in the east, is an amalgamation of three closely related terranes: the Aouzegueur, Barghot and Assodé-Issalane terranes. The first two terranes accreted onto the margin of the SM by 650 Ma, with the Aouzegueur terrane preserving a tonalite-trondhjemite-granodiorite (TTG) suite dated at ca. 730 Ma and the Barghot terrane recording calc-alkaline granitoids from ca. 730 to 660 Ma, with a post nappe pluton preserving a U–Pb zircon age of 664 ± 8 Ma, interpreted to provide a minimum age for deformation (Liégeois et al., 1994). Both these terranes were metamorphosed to greenschist or amphibolite facies and were cut by east-verging thrusts. In contrast, the Assodé-Issalane terranes exhibit younger magmatism (ca. 640–580 Ma) and amphibolite-facies metamorphism. They are thrust east over the Barghot terrane. Both Black et al. (1994) and Liégeois et al. (1994) suggest that the Aouzegueur terrane collided first with the SM, followed by the Barghot terrane, which is positioned slightly further south than the former, through an east-dipping subduction zone underneath the two terranes (Fig. 18). Following collision, the Assodé-Issalane terrane (which until this time we position slightly west of the former terranes) was thrust above of the Barghot terrane in response to the closure of the ocean between the WAC and the SM. Our reconstruction implies that this motion was predominantly transpressive, along the dextral Raghane shear zone with plutons dating from ca. 630 to 580 Ma (Liégeois et al., 1994).

Further west from the Aïr block in central Hoggar, the LATEA terranes (Laouni, Azrou-n-Fad, Tefedest and Egéré-Aleksod) all consist of

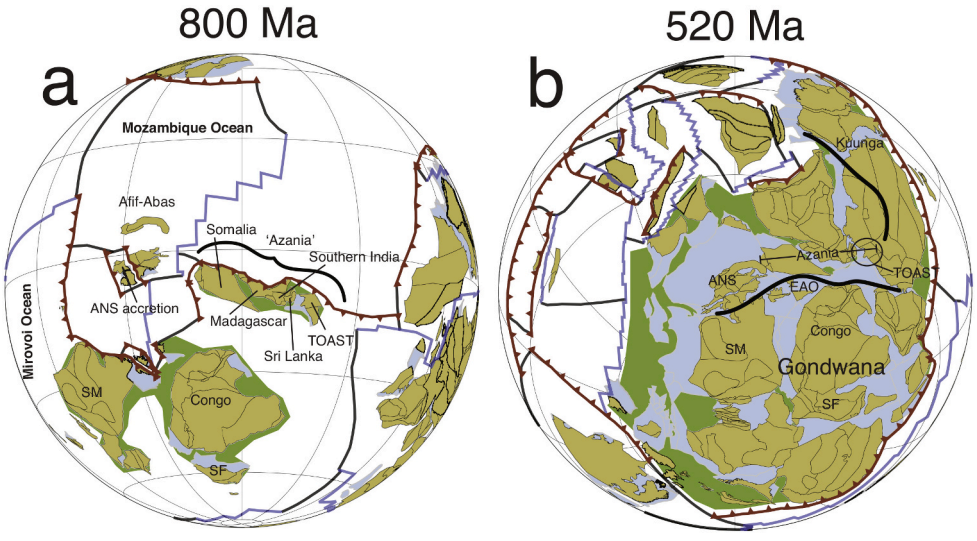


Fig. 17. Amalgamation of the Arabian-Nubian Shield (ANS) after Blades et al. (2015, 2019), Armistead et al. (2019) and Collins et al. (in revision) and the incorporation of the ANS, Azania and TOAST into Gondwana along the East African Orogen at: (a) 800 Ma and (b) 520 Ma. Tan polygons are areas of continental lithosphere in the Neoproterozoic that we model, blue polygons are areas of present-day continental lithosphere that are inferred to exist during the Neoproterozoic, but without having firm geological evidence or that have been affected by subsequent deformation (e.g. the distance between a present-day coastline and COB). Green polygons represent a schematic interpretation of congruent continental lithosphere, with intervening crust being subsequently deformed during future tectonic cycles. Thick black lines follow the suture of the East African Orogen and Kuunga Orogen. ANS, Arabian-Nubian Shield; EAO, East African Orogen; SF, São Francisco; SM, Sahara Metacraton.

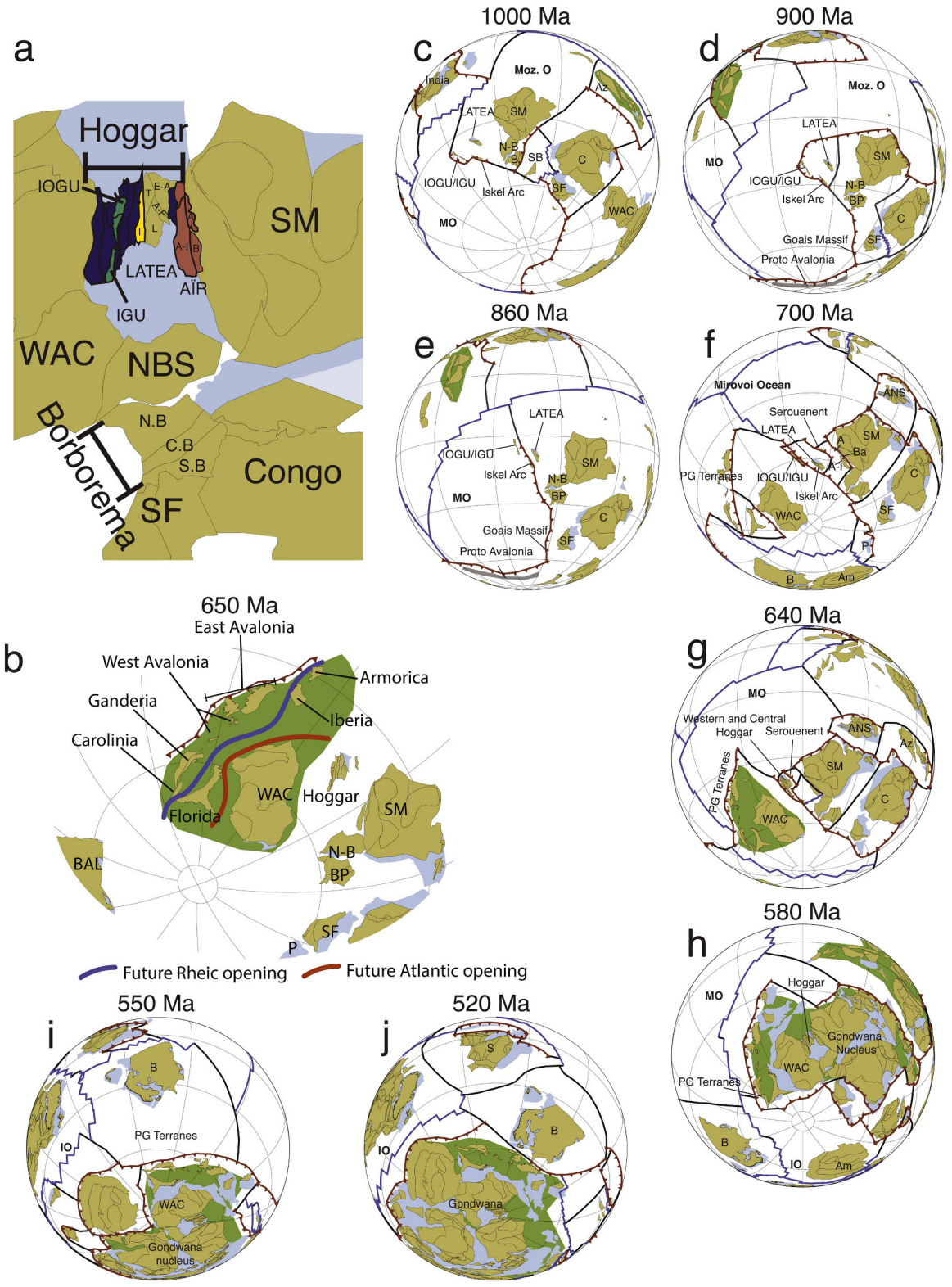


Fig. 18. Amalgamation of Hoggar after Caby et al. (1989), Black et al. (1994) and Liégeois et al. (1994), Borborema and Peri-Gondwanan terranes after Nance et al. (2008) at key time slices. (a) map of key terranes in a reconstructed Gondwana (dark blue terranes are oceanic terranes); (b) map of reconstructed Peri-Gondwanan terranes at 650 Ma; (c) 1000 Ma; (d) 900 Ma; (e) 860 Ma; (f) 700 Ma; (g) 640 Ma; (h) 580 Ma; (i) 550 Ma and (j) 520 Ma. Tan polygons are areas of continental lithosphere in the Neoproterozoic that we model, blue polygons are areas of present-day continental lithosphere that are inferred to exist during the Neoproterozoic, but without having firm geological evidence or that have been affected by subsequent deformation (e.g. the distance between a present-day coastline and COB). Green polygons represent a schematic interpretation of congruent continental lithosphere, with intervening crust being subsequently deformed during future tectonic cycles A, Aouzegueur; A-I, Assodé-Issalane; Am, Amazonia; ANS, Arabian-Nubian Shield; B, Baltica; BP, Borborema Province; C, Congo; C-B, Central Borborema; IGU, Iforas granulite unit; IOGU, In Ouzzal granulite unit; IO, Iapetus Ocean; LATEA, Laouni, Azrou-n-Fad, Tefedest and Egéré-Aleksod terranes; MO, Mirovoi Ocean; Moz. O, Mozambique ocean; N-B, Niger-Benin Block; P, Paranapanema; PG, Peri-Gondwanan terranes; S-B, Southern Borborema; SF, São Francisco; SM, Sahara Metacraton; WAC, West African Craton.

Archaean to Palaeoproterozoic basement, but preserve no Mesoproterozoic or early Neoproterozoic rocks. LATEA was a passive cratonic unit for most of the Neoproterozoic and acted as a nucleus for the accretion of juvenile terranes. The earliest Neoproterozoic activity is the accretion of the ca. 900 Ma juvenile Iskel island arc to the western margin of LATEA, with subduction inferred to be west dipping away from LATEA (Liégeois et al., 2003). The protolith of an eclogitic unit, currently preserved along the shear zone delineating the Iskel arc and LATEA, is dated to ca. 870 to 850 Ma by U–Pb dating from zircons extracted from syn-to-late kinematic plutons (Caby et al., 1982). The combined In-Ouzzal and Iforas granulite units (IOGU/UGI), which are Palaeoproterozoic continental ribbons, preserve few Tonian rocks. From ca. 700 to 640 Ma magmatism is recorded throughout the entire region, suggesting that subduction occurred along both margins of the terranes (Caby, 2003) (Fig. 18d, e). At 630 Ma, collision between the IOGU/UGI terranes and the LATEA block occurred, forming the combined present-day central-western Hoggar region.

The final tectonic events of this area involve a two-step amalgamation process of Western and Central Hoggar (i.e. IOGU/UGI and LATEA) to the Aïr Shield and SM, and the collision between this landmass (Hoggar and the SM) and the WAC, where collisional deformation is preserved in the Pharusian and Dahoymede belts (Merdith et al., 2017a) (Fig. 18f, g). Here, subduction is inferred to have occurred away from the WAC (i.e. underneath Hoggar) due to the absence of magmatic rocks preserved on the WAC. Continual dextral deformation is preserved throughout Hoggar until ca. 530 Ma, suggesting that there was still relative motion until the Cambrian (Liégeois et al., 2003; Paquette et al., 1998). The major regime of the Hoggar block between the Ediacaran and early Cambrian was transpressive, resulting in extensive faulting and upwelling of the asthenosphere; causing partial melting of lower Archaean crust in some areas (Hadj-Kaddour et al., 1998). We interpret the final amalgamation of Hoggar to occur at ca. 580 Ma, as this is the age of the syntectonic, deformed plutons found among the shear zones that bind the SM and the WAC. Here, a suite of ages include: Rb–Sr whole rock ages from dykes affected by the transpressive event yield an age of 592 ± 6 Ma (Hadj-Kaddour et al., 1998); a 583 ± 7 Ma U–Pb age on zircons extracted from the syn-to-late tectonic, elongated Imezzarene pluton (Lapique et al., 1986); a 594 ± 4 Ma and 593 ± 17 Ma U–Pb age of zircon extracted from the Ohergehem and Adaf plutons, respectively (Henry et al., 2009). Fezaa et al. (2010) identified younger (ca. 575–555 Ma) deformation in the Murzoq area of Hoggar, however, they suggested that it was unrelated to the main convergence between WAC and SM.

The Borborema block sits between Congo-SF and the Nigeria-Benin Shield in a reconstructed Gondwana (Fig. 18a). This small block consists of Archaean–Proterozoic basement that was strongly reworked and deformed during the Gondwana amalgamation events between Africa and Amazonia (dos Santos et al., 2010). Magmatism in the Transversal Domain of Central Borborema is thought to represent a local, early Tonian orogeny called the Cariri Velhos Orogeny (da Silva Filho et al., 2002; dos Santos et al., 2010). Late Stenian rift deposits are preserved in the Cariri Velhos belt, suggesting that the Pernambuco-Alagoas domain (PEAL) (the crystalline basement of Southern Borborema) originally rifted from this margin (Guimarães et al., 2012), before the ocean inverted and closed. Our model places the Northern and Transversal Domains of Borborema fixed to the Nigeria-Benin-SM blocks, while the PEAL closed the small Stenian-aged relict ocean basin as it collided with the northern and central Borborema provinces by ca. 920 Ma (Caxito et al., 2014a), forming the Cariri Velhos Orogen. An ocean basin remained on the southern margin of PEAL until the Ediacaran, as the final collision between Borborema and SF did not occur until this time forming the Sergipano belt, which preserves relict oceanic crust (e.g. Caxito et al., 2014b; Ganade de Araujo et al., 2014) (e.g. Fig. 9). To accommodate the Tonian closure, while maintaining an open ocean basin to the south of PEAL, we follow Caxito et al. (2014a, 2016) who suggested that the synchronous rifting and aulacogen formation preserved in SF (Pedrosa-Soares et al., 2001), which in our model is reconstructed to be adjacent to PEAL, are relicts of the divergent motion necessary to achieve this.

The Avalonian terranes, currently preserved in the east coast of modern day North America and western Europe, have a well-documented Neoproterozoic history (e.g. Murphy and Nance, 1989). The Avalonian terrane is interpreted to be underlain by ca. 1.0 Ga juvenile basement on the basis of 1.3–0.8 Ga Sm–Nd depleted mantle model ages in in younger Neoproterozoic rocks (Murphy et al., 2000; Thorogood, 1990). These younger rocks consist of magmatic gneiss and plutonic complexes, along with tuffs, pelitic schists and quartzites. U–Pb ages of the complexes and tuffs range from ca. 750–650 Ma (Bevier et al., 1993; Doig et al., 1993; Keppie and Dostal, 1998; Krogh et al., 1988; O'Brien et al., 2001) and detrital zircons from the (meta-)sedimentary rocks suggest they were sourced from a juvenile arc (metapelites, Murphy, 2002) and a cratonic source (quartzite), typically inferred to be Amazonia or the WAC (Nance et al., 2008). This magmatism is followed by amphibolite–granulite metamorphism from 660–630 Ma (Keppie et al., 1998; Strachan et al., 2007). Younger magmatism (ca. 640–550 Ma) is more voluminous and includes abundant arc derived volcanic, plutonic complexes and coeval volcanic-sedimentary successions (Bevier et al., 1993; Compston et al., 2002; Doig et al., 1993; Nance et al., 2008; O'Brien et al., 2001; White et al., 2020). Subduction does not continue into the Cambrian, instead a clastic platform and transition to rift environment begins to form, culminating in the opening of the Rheic Ocean (Domeier, 2016; Nance et al., 2008; Nance and Linnemann, 2008).

To a first order, Ganderia and Carolina, both preserved in North America, record a similar Neoproterozoic history to Avalonia, differing predominantly in that key metamorphic and magmatic events are ca. 30–40 Ma younger than in Avalonia (Hibbard et al., 2007; Nance et al., 2008; van Staal et al., 2012). Depleted mantle model ages from Sm–Nd isotopes also hint at the presence of ca. 1.2–0.8 Ga juvenile crust in Carolina (Hibbard et al., 2007). However, the principal period of magmatism in both Ganderia and Carolina is preserved from 650 to 580 Ma and is inferred to have occurred in an ocean-arc environment (Hibbard et al., 2007). Metamorphism, up to eclogite facies, occurs at the end of this period and continues into the earliest Cambrian (580–540 Ma) (Barker et al., 1998; Shervais et al., 2003). Younger magmatism (to ca. 520 Ma, White et al., 2002) linked to the rifting and opening of the Rheic Ocean, is only preserved in Ganderia (Hibbard et al., 2007). Finally, the Suwannee terrane of Florida is linked tectonically to both the West African Craton and Amazonia throughout the Neoproterozoic (Dallmeyer, 1989), lacking the Neoproterozoic arc development preserved in Avalonia, Ganderia and Carolina. Instead, 550 Ma calc-alkaline volcanic rocks are inferred to represent the remnants of a continental arc (Heatherington et al., 1996).

We follow the model of Nance et al. (2008) and Murphy et al. (2004) for the Neoproterozoic evolution of these terranes. An early Tonian (1–0.8 Ga) oceanic arc outboard of Baltica-Amazonia-WAC dipping under the Rodinian plate, formed the earliest portions of crust preserved in these terranes (Fig. 18c–e). The relative positioning of the terranes follows that of DOM16, with East Avalonia most easterly (Fig. 18b), then West Avalonia, and Ganderia and Carolina furthest west, with Ganderia sitting oceanward of Carolina. This arrangement follows the same logic outlined in Section 5.2.2, as by maintaining this relative positioning we avoid having to laterally re-organise the terranes during the Palaeozoic. This is slightly different from the positioning in Nance et al. (2008), who model West Avalonia more easterly (relative to a fixed WAC) than East Avalonia and invoke wrench-tectonics to laterally translate the terranes. Nonetheless, at ca. 750 Ma this subduction polarity reversed and the adjacent ocean basin between WAC-Baltica began to subduct underneath Avalonia. We model Ganderia and Carolina slightly further away from the active subduction front–behind Western Avalonia, to account for their lack of Cryogenian magmatism. This arc front collided with WAC at ca. 650 Ma when the subduction ceased and reset outboard of the now amalgamated Avalonian-WAC continent as a continental arc

(Fig. 18f, g). This subduction continued until the Cambrian when the area transitioned into a rift environment when the Rheic Ocean opened.

This last phase of our model is preliminary and needs further development, though we hope that it provides a framework that can assist with testing alternative scenarios. By fitting the latitude of the ca. 520–500 Ma poles of Baltica (Section 5.2.1), subduction must consume most of the relic ocean basin immediately north of the Avalonian margin of Gondwana between 550 and 520 Ma. The magmatism in Ganderia easily accounts for this, however Baltica needs to be further east at 520 Ma, otherwise it must undergo 4000 km of dextral motion (relative to Gondwana) to allow for the initial stages of the Rheic Ocean opening at ca 500 Ma (e.g. Domeier, 2016; von Raumer and Stampfli, 2008), which we suggest is not a reasonable scenario. As such, our model places a subduction zone slightly outboard of Avalonia, but acknowledge that this is a simplification that needs further refinement.

6. Plate model

Having discussed the motions of the evolution of continental configurations in previous sections, here we discuss the more speculative elements of the reconstruction—the oceanic plates and plate boundaries. For further in-depth discussion of the continental portions of the model, in particular the major Gondwana forming sutures and evolution of the post-Cambrian world, we point readers to the studies that produced the base models used here (MER17, DOM16/18, YOU19, DT14). We also provide in our supplementary material the associated plate model files (SM1), as well we a tectonic summary of seafloor production and consumption rates, mid-ocean ridge length and subduction zone length (SM2).

6.1. Synthetic ocean plates

The construction of synthetic ocean plates is required to maintain tectonic congruency (Section 2.7). But, with few exceptions (e.g. ophiolites), there is no direct evidence of the configuration or tectonic parameters (e.g. spreading rate, asymmetry) of oceanic crust for the pre-Mesozoic due to the constant subduction of oceanic lithosphere. However, we know that oceanic crust typical of present-day (i.e. MORB) did exist in the Palaeozoic and Neoproterozoic, as evidenced by ophiolitic remains preserved in orogens (Furnes et al., 2014). We therefore use one key assumption when constructing oceanic plates: we assume that the production (rate of motion, orthogonal spreading etc.) and subduction of oceanic crust in the Neoproterozoic was fundamentally similar to the Cenozoic. We note that this may not be a valid assumption for the early Neoproterozoic, since abundant ophiolite preservation only occurs after Rodinia breakup (Stern and Miller, 2018) and pre-1 Ga ophiolites suggest thicker oceanic crust (Moores, 2002), which, along with secular changes in Earth's heat loss (Brown et al., 2020b), could have an influence on spreading and subduction dynamics. Nonetheless, we maintain that if available palaeomagnetic and geological data can be reconciled within a uniformitarian framework of oceanic crust production and destruction, then our model becomes a useful reference model for future models that explore alternative hypotheses. Measurements of seafloor production, crustal consumption, ridge length and subduction zone length are provided in the supplementary material.

6.1.1. Early Tonian until Rodinia breakup (1000–750 Ma)

In our model, three prominent ocean basins existed in the early Tonian: the Mirovoi Ocean (McMenamin et al., 1990; Meert and Lieberman, 2008), the Mawson Sea (Meert, 2003; Meert and Lieberman, 2008) and the Mozambique Ocean (Fig. 8) (Collins et al., 2003; Collins and Pisarevsky, 2005). These ocean basins have been defined previously in the same context as they appear in our model, however, given differences between our model and the original publications, the geographical boundaries of each ocean are slightly different.

We define the Mirovoi Ocean as the large ocean bordering Rodinia in its west and India-South China and the Sahara Metacraton in the north east and south east respectively. The Mirovoi is the largest and most prominent ocean basin for the Neoproterozoic in our model, existing until ca. 520 Ma with the opening of the Proto-Tethyan Ocean and Ran Sea (Fig. 9, Hartz and Torsvik, 2002). It is (conceptually) equivalent to the external Panthalassic and Pacific oceans of the Phanerozoic, as it consists almost entirely of oceanic lithosphere and is ringed by subduction for the majority of its existence. At 1000 Ma, we model a triple junction spreading ridge located roughly in the centre of the ocean basin. The triple junction provides three directions of spreading to account for convergence in three areas: (i) the closure of the ocean basin separating India-South China from Tarim, Qaidam-Qilian, Lut, Afghanistan, Kunlun and Tarim (*this study*); (ii) the Taimyr subduction zone outboard of *northern* Siberia (Metelkin et al., 2012; Vernikovsky et al., 2004) and the Valhalla Orogen outboard of Greenland (Cawood et al., 2010), and; (iii) the Proto-Avalonian-Cadomian subduction zone outboard of Baltica and Amazonia (Murphy et al., 2000) that extends northwards to São Francisco and further north where it is preserved in the Iskel Island Arc of Hoggar (Liégeois et al., 2003).

The spreading arms of the triple junction span north, east-southeast and southwest. The northern arm separates Siberia and the India-China accretionary zone and extends partway into the Mawson Sea. The east-southeastern arm extends towards India, where we connect it via a transform fault to the mid-ocean ridge in the Mozambique Ocean. The southwestern arm intersects the Proto-Avalonian subduction zone. We model this configuration (triple junction) as being stable through the early Tonian until ca. 870–850 Ma, where a plate-reorganisation event occurs. We link this organisation to a change in kinematics of Rodinia, suggested through palaeomagnetic data. At this time, palaeomagnetic data from the Baltica (Walderhaug et al., 2007) suggest that Rodinia had drifted to southerly latitudes, before returning to equatorial latitudes by ca. 750 Ma (Eyster et al., 2019). MER17 modelled significant relative dextral motion between Congo-SF-Azania and Rodinia during this time (870–750 Ma) as well, as suggested by palaeomagnetic data (Evans et al., 2016). Geological data from Congo-Azania also supports the rotation, with onset of sedimentation interpreted to be a rift event in the Damara region (Armstrong et al., 2005; McGee et al., 2012) and the onset of a massive subduction system outboard of Azania (Archibald et al., 2017; Handke et al., 1999). During this transition (850–800 Ma), we model the Mirovoi Ocean as a single spreading ridge, orientated subparallel to the north-facing arm in the original triple junction, extending northwards toward Siberia and intersecting an oceanic arc outboard of Baltica.

For the Tonian, until 750 Ma, the South China-India continent moved to polar latitudes on the north-eastern side of the Mirovoi Ocean basin. Comparably, Siberia started dextral motion relative to Rodinia, from a position near Australia-North China to one near Greenland (Pisarevsky et al., 2013). To account for this motion, alongside ongoing subduction in the Taimyr region of Siberia, we have extended the spreading ridge from the Mozambique Ocean into the Mirovoi Ocean (running E–W) and have a northern arm accounting for divergence between Tarim and the Taimyr subduction zone. This interpretation necessitates the presence of a triple junction, with a third ridge arm intersecting the subduction zone outboard of Baltica, similar to the configuration at the start of the Tonian.

The Mawson Sea is defined as the ocean basin between Australia and India-South China that closed with the amalgamation of Gondwana (Meert, 2003). In the early Tonian, this basin is large in our model, necessitated by MER17s removal of India-South China from Rodinia. The large size is because relative longitude prevents India-South China (at this point in time travelling north from the equator) from being any closer to Australia, as Azania occupied the same latitude as India and lay between India and Australia. We model a single spreading ridge in the centre of the ocean basin, accounting for the subduction on the India-South China margin as suggested in the Eastern Ghats of India and accretion of the Ruker Terrane to Indo-Antarctica (e.g. Corvino et al.,

2008; Liu et al., 2017). In South China, this subduction is more sparse, but recent work has suggested that part of present-day Vietnam is associated with the southwestern Yangtze craton (Minh et al., 2020) and could record the late Tonian portion of a subduction system and be the focus of future work. At 930 Ma the spreading direction of the ridge changes, to compensate for the southerly drift of Rodinia. The change in spreading direction coincides with the docking of North China-Australia-Antarctica with Laurentia as the final amalgamation event of Rodinia (Mulder et al., 2018b). At this time we model subduction initiating outboard of Australia, against Lhasa, (e.g. Guynn et al., 2006) and into the ocean outboard of Antarctica further *south*. Preserved evidence of subduction here is sparse due to ice cover in Antarctica. However, this area of the ocean (just outboard of the western margin of the Mawson craton) is positioned at the centre of Antarctica in the nexus between the TOAST terrane and Mawson craton, so it could be possible some arcs are preserved in Antarctica. Further south, this subduction zone transitions into a transform boundary and separates relative motion between Azania-Congo and Rodinia between 930 Ma and 850 Ma. We model continual spreading in the Mawson Sea until 850 Ma, at which time the ocean basin begins to close and we do not model an active ridge. By 750 Ma the Mawson Sea is extremely narrow, with only 2500–3500 km of ocean basin separating Australia and India. A narrow ocean basin is supported geologically by the strong evidence suggesting that a large sinistral shear zone was present outboard of western Australia and Antarctica during the Cryogenian and Ediacaran, suggesting that there was close proximity without collision between Australia-Antarctica and another continent (Collins, 2003; Fitzsimons, 2003; Halpin et al., 2017; Merdith et al., 2017b; Powell and Pisarevsky, 2002).

The Mozambique Ocean is described as the ocean that closed with the collision of India and Congo along the East African Orogen reacted to Gondwana amalgamation during the Cryogenian and Ediacaran (e.g. Collins and Pisarevsky, 2005). For the sake of continuity, we refer to this ocean as the Mozambique in the Tonian as well. A small ocean (in our model, roughly equivalent in size to the Tasman Sea between Australia and New Zealand), termed 'Neomozambique Ocean' also closed with the formation of the East African Orogen, however this ocean was located between ANS-Azania-TOAST and Congo (Fig. 8).

Geographically, the location of the Mozambique ocean is difficult to determine in the early Tonian due to overlapping latitudes between Azania and India (they are separated longitudinally by ~120° in our model). In our model there is no spreading in this ocean basin at this time, because Congo-Azania was latitudinally stable while India-South China moves towards the North Pole on a different longitude, accounted for by spreading in the Mirovoi Ocean. The spreading ridge in the Mawson Sea at ca. 900 Ma extends sufficiently south so that the ocean lithosphere generated here is subducted during closure of the Mozambique Ocean. We model active spreading in a clearly defined Mozambique Ocean beginning at 850 Ma, by which time India-South China had a similar longitude to Azania-Congo, making it easier to delineate the geographical extent of the ocean distinct from the Mawson Sea. Between 820 and 750 Ma the ocean basin closes rapidly, in order to fit palaeomagnetic constraints at 750 Ma that show India at ~60°N (Gregory et al., 2009; Torsvik et al., 2001) and Congo at 15°S (Meert et al., 1995) (placing Azania at the equator).

At 800 Ma, we model the birth of the Pacific/Panthalassic Ocean, here defined as the ocean basin separating Laurentia from North China, Australia and Antarctica, which most likely opened as Rodinia broke-up (although terrane migration across this ocean basin cannot be ruled out, e.g. Mulder et al. (2020). We note here that the pre-Mesozoic Pacific Ocean is already universally referred to as the Panthalassic Ocean. Consequently, we refer to the ocean separating North China-Australia-Antarctica and Laurentia between Rodinia and Gondwana times (ca. 800–520 Ma) as the proto-Pacific Ocean, the ocean surrounding Gondwana as the Panthalassic Ocean ('Panthalassa', ca. 520–200 Ma) and the ocean that has existed from 200 Ma to present-day as the Pacific Ocean, noting that all three of these oceans essentially refer to the same ocean basin (in a geographical sense) that existed between North China-Australia-Antarctica and Laurentia. From 800 to 720 Ma we have a single ridge system separating Australia-Antarctica and Laurentia. This ridge produces a highly angular divergence, with spreading rates faster towards northern Australia and Canada than in Antarctica, resulting in a wider ocean basin in the north and narrower in the south. These variable spreading rates are required fit the ca. 750 Ma palaeomagnetic data, which require Australia to be 'upright' (same orientation as present-day) and perpendicular to Laurentia (Wingate and Giddings, 2000).

6.1.2. late Tonian–Cambrian (Rodinia breakup–Gondwana Assembly, 720–520 Ma)

By 720 Ma, continental motions around the Mirovoi Ocean are latitudinally stable with no polar excursions thus, the simplest way to account for the necessary subduction is with a stable triple junction. At this time, we show subduction along the western margin of the Mirovoi Ocean, outboard of Siberia in the Taimyr region, as well further south outboard of the WAC and Baltica where the Avalonian and Cadomian terranes were coalescing (Murphy et al., 1999; Murphy and Nance, 1989) and along the *northern* margin of the Sahara Metacraton in the east. This latter subduction zone is speculative since there are no known rocks of this age in the Sahara Metacraton (Blades et al., submitted). The Mirovoi ocean basin does not grow appreciably during the Ediacaran due to onset of subduction around its periphery, however, at 590 Ma Baltica begins moving north, resulting in the consumption of the Mirovoi Ocean basin and necessitating a change in mid-ocean ridge configuration. At this point we model a single ridge parallel to the Gondwanan margin, from Amazonia in the west towards India in the northeast. This ridge also accommodates the final motion of India as it collides with Congo. It is difficult to identify when the Mirovoi Ocean ceased to exist, but by ca. 490 Ma, expansion in the Proto-Tethyan ocean basin outboard of northwest Gondwana (e.g. Fig. 12), as well as the easterly drift of Siberia amalgamates the Siberian subduction zones outboard of North China and Chu-Yili-Tianshan, probably indicating that the majority of Mirovoi crust produced during the Cryogenian and Ediacaran has been consumed.

An obvious issue with this discussion on the size of the Mirovoi is the longitudinal uncertainty between the position of Congo and Laurentia during the Ediacaran. This uncertainty is because the distance between these two cratons dictates the size of the Adamastor Ocean (between Kalahari and Congo), which grew at expense of the Mirovoi Ocean. Earliest evidence of subduction in the Damara belt exists from 650 Ma, with final closure occurring at 550 Ma. A conservative convergence rate of 40–60 km/Ma (roughly equivalent to present-day Pacific convergence rates) would make the ocean basin at 4000–6000 km wide, roughly equivalent to the present-day Atlantic Ocean (this width is similar in our model to that of the Adamastor Ocean). However, faster divergence during Rodinia breakup would increase the size of this ocean basin, in turn reducing the size of the Mirovoi Ocean during the Ediacaran, similar to how the size of the modern Pacific Ocean would become smaller or larger depending on the changing size of the Atlantic Ocean.

The Mawson Sea remains very small in size during the Cryogenian due to the close proximity between India and Australia-Antarctica. There is no active ridge, instead a transform fault separates the two continents. There is little evidence of subduction-related magmatism on either cratonic Australia or India or this time (e.g. Halpin et al., 2017), suggesting the intervening lithosphere that eventually closed with Gondwana amalgamation could have also involved a more complex scenario of terrane accretion. The veracity of that statement is strongly dependent on the configuration and relative positioning of other terranes that are typically reconstructed to the north-western margin of Australia in the late Palaeozoic, such as Sibumasu and Indochina (Metcalfe, 2011) or other terranes preserved in Antarctica that are speculated to have rifted off the Indo-Antarctica and accreted to the western margin of the Mawson Craton (Daczko et al., 2018; Mulder et al., 2019). Neither set of terranes are yet considered explicitly in our

model. By 520 Ma Australia-Antarctica is sutured with India, closing any remnants of the Mawson Sea.

Both the Mozambique and NeoMozambique oceans close orthogonally from 720 to 550 Ma due to the continual southward motion of India towards Congo-SM. We do not model an active spreading ridge during this time, as subduction is only preserved on the African side of the collision (Collins and Pisarevsky, 2005). The presence of an earlier ridge does, however, suggest that at least two ridges (in our model they are extinct) were subducted during the East African Orogeny.

The Proto-Pacific Ocean grows predominantly longitudinally during the Cryogenian–Cambrian. In our model, we show separation between Australia-Antarctica-North China and Laurentia using a single ridge system that propagates southwards, around *southern* Laurentia to eventually separate the Kalahari Craton and DML at ca. 700 Ma. We maintain a single ridge system until the Ediacaran, although when Kalahari begins drifting from Laurentia, we follow Merdith et al. (2017b) in inferring a ridge jump to re-align spreading between Australia and Laurentia with the incipient ridge separating Kalahari and Laurentia. This ridge jump also assists with reconciling the necessary motion of Australia to Ediacaran palaeomagnetic data, which require a ~35–45° counter-clockwise rotation from its present-day orientation (Schmidt and Williams, 2010). At 580 Ma we model a triple junction in the Proto-Pacific Ocean that coincides with the equatorial excursion of Baltica and cessation of triple junction spreading in the Mirovoi Ocean. The arms of this triple junction intersect sub-perpendicular to subduction outboard of Laurentia, a transform fault outboard of North China and another transform boundary outboard of Baltica.

Between 500 and 410 Ma, we refer to the ocean as the Panthalassic Ocean and for this time interval we extended the triple junction of YOU19 backwards through DOM16 and DOM18. We found at 500 Ma when Cuyania rifts off the promontory of Laurentia (Domeier, 2016), that the position of the triple junction and orientation of the ridges extended backwards from YOU19 was parallel to the direction of spreading separating Cuyania from Laurentia. While coincidental, given the arbitrary nature of pre-Mesozoic ocean plates, we find it useful to use the configuration at this time as a transition from the Proto-Pacific Ocean to the Panthalassic Ocean.

7. Conclusions

We present here the first continuous full-plate model from 1 Ga to present-day. The model traces the kinematic evolution of all cratonic crust and links the Neoproterozoic to the Phanerozoic, encompassing an entire supercontinent cycle, and enabling quantitative analysis of tectonic features for deep time. We present the model in a palaeomagnetic reference frame, including a new APWP for Gondwana from 540 to 320 Ma and a GAPWaP from 320 to 0 Ma. For the Neoproterozoic, the model uses a hybrid hierarchy, where relative plate motions are tied to a key plate, forming distinct nodes. This cluster-approach allows for the model to be iterated, constructed and modified in the future more easily in light of sparse palaeomagnetic data, but abundant geological data. Our revised Neoproterozoic model incorporates a late amalgamation of Rodinia with a novel configuration, in particular through the removal of India, South China and Tarim from the supercontinent. We incorporate major plate re-organisation events at ca. 850 Ma and again at ca. 750–700 Ma, corresponding to the counter-clockwise rotation of Congo-São Francisco-Sahara Metacraton relative to Rodinia and the initial closing of the Mozambique Ocean and coeval opening of the Proto-Pacific Ocean, respectively. Our model also includes preliminary interpretations of the Neoproterozoic history of many regional areas, such as terrane amalgamation outboard of India-South China, Hoggar and Avalonia, that then link coherently with their more established Phanerozoic histories. We reiterate that this model is a non-unique solution of global palaeogeography and tectonics for the Neoproterozoic but we hope it can provide a framework on which future studies can build upon. To facilitate this, we include in our supplementary material (SM2) the tectonic parameters of seafloor production and consumption as extracted from the model.

Because our model has continuous plate boundaries, it enables a range of new scientific experiments such as those seeking to link plate boundary processes to other aspects of the Earth system. This includes experiments related to the biosphere, hydrosphere and atmosphere investigating events surrounding oxygenation of Earth's atmosphere, Snowball Earth and animal radiation (e.g. (Gernon et al., 2016; Goddéris et al., 2017; He et al., 2019; Hoffman et al., 1998; Hoffman and Schrag, 2002; Lenton et al., 2016; Mills et al., 2019) and those studying the deep Earth (e.g. Heron et al., 2020). There are a number of limitations of this study, in particular, we do not address TPW in this model. Most previous studies looked at TPW purely from a palaeomagnetic framework, however the incorporation of geological data in the form of plate boundaries in this model (and others like it) open up opportunities for to analyse whole-lithospheric motion from other directions (e.g. Tetley et al., 2019).

Declaration of Competing Interest

The authors declare that they have no known competing financial interests or personal relationships that could have appeared to influence the work reported in this paper.

Acknowledgements

The authors thank Sergei Pisarevsky for advice on palaeomagnetic data. ASM is currently supported by the Deep Energy Community of the Deep Carbon Observatory and the Richard Lounsbery Foundation. ASM, SEW, RDM and SZ were supported by Australian Research Council grant IH130200012. SEW is supported by NSFC Grant No. 41972237. ASC and MLB are supported by Australian Research Council grants FT120100340 and LP160101353. MGT was supported by European Research Council Grant Agreement 617588 and Agence Nationale de la Recherche project ANR-18-ERC1-0005. JAM is supported by ARC grant FL160100168. AY and SA are supported by an Australian Government Research Training Program Scholarship. SZ was supported by Australian Research Council grant IH130200012, a University of Sydney Robinson Fellowship. SZ and RDM were supported by Alfred P. Sloan grants G-2017-9997 and G-2018-11296 through the Deep Carbon Observatory. JC and RDM were also supported by the AuScope National Collaborative Research Infrastructure System (NCRIS) program. pyGPlates and GPlates development is funded by the AuScope National Collaborative Research Infrastructure System (NCRIS) program. The authors are grateful for thorough reviews by D. J. J. van Hinsbergen, C. Scotese and B. Murphy, all of which greatly improved the focus and clarity of the manuscript.

Appendix A. Supplementary data

Supplementary data to this article can be found online at https://doi.org/10.1016/j.earscirev.2020.103477.

References

Ahmad, M., Munson, T.J., 2013. Geology and mineral resources of the Northern Territory. Northern Territory Geological Survey Special Publication 5.

Alessio, B.L., Blades, M.L., Murray, G., Thorpe, B., Collins, A.S., Kelsey, D.E., Foden, J., Payne, J., Al-Khirbash, S., Jourdan, F., 2018. Origin and tectonic evolution of the NE basement of Oman: a window into the Neoproterozoic accretionary growth of India? Geol. Mag. 155 (5), 1150–1174. https://doi.org/10.1017/S0016756817000061.

Alexeiev, D.V., Ryazantsev, A.V., Kröner, A., Tretyakov, A.A., Xia, X., Liu, D.Y., 2011. Geochemical data and zircon ages for rocks in a high-pressure belt of Chu-Yili Mountains, southern Kazakhstan: Implications for the earliest stages of accretion in Kazakhstan and the Tianshan. J. Asian Earth Sci. 42 (5), 805–820. https://doi.org/10.1016/j.jseaes.2010.09.004.

Alexeiev, D.V., Kröner, A., Kovach, V.P., Tretyakov, A.A., Rojas-Agramonte, Y., Degtyarev, K.E., Mikolaichuk, A.V., Wong, J., Kiselev, V.V., 2019. Evolution of Cambrian and Early Ordovician arcs in the Kyrgyz North Tianshan: Insights from U-

Pb zircon ages and geochemical data. Gondwana Res. 66, 93–115. https://doi.org/10.1016/j.gr.2018.09.005.
Alexeiev, D.V., Biske, G.S., Kröner, A., Tretyakov, A.A., Kovach, V.P., Rojas-Agramonte, Y., 2020. Ediacaran, Early Ordovician and early Silurian arcs in the South Tianshan orogen of Kyrgyzstan. J. Asian Earth Sci. 190 (1), 104194 https://doi.org/10.1016/j.jseaes.2019.104194.
Archibald, D.B., Collins, A.S., Foden, J.D., Razakamanana, T., 2017. Tonian arc magmatism in central Madagascar: the petrogenesis of the Imorona-Itsindro Suite. J. Geol. 125 (3), 271–297. https://doi.org/10.1086/691185.
Archibald, D.B., Collins, A.S., Foden, J.D., Payne, J.L., Macey, P.H., Holden, P., Razakamanana, T., 2018. Stenian–Tonian arc magmatism in west–central Madagascar: the genesis of the Dabolava Suite. J. Geol. Soc. London 175 (1), 111–129. https://doi.org/10.1144/jgs2017-028.
Armistead, S.E., Collins, A.S., Merdith, A.S., Payne, J.L., Cox, G.M., Foden, J.D., Razakamanana, T., De Waele, B., 2019. Evolving marginal terranes during Neoproterozoic supercontinent reorganisation: constraints from the Bemarivo Domain in northern Madagascar. Tectonics 38 (6), 2019–2035. https://doi.org/10.1029/2018TC005384.
Armstrong, R.A., Master, S., Robb, L.J., 2005. Geochronology of the Nchanga Granite, and constraints on the maximum age of the Katanga Supergroup, Zambian Copperbelt. J. Afr. Earth. Sci. 42 (1–5), 32–40. https://doi.org/10.1016/j.jafrearsci.2005.08.012.
Arthaud, F., Matte, P., 1977. Late Paleozoic strike-slip faulting in southern Europe and northern Africa: Result of a right-lateral shear zone between the Appalachians and the Urals. GSA Bulletin 88 (9), 1305–1320. https://doi.org/10.1130/0016-7606(1977)88<1305:LPSFIS>2.0.CO;2.
Ashwal, L.D., Solanki, A.M., Pandit, M.K., Corfu, F., Hendriks, B.W.H., Burke, K., Torsvik, T.H., 2013. Geochronology and geochemistry of Neoproterozoic Mt. Abu granitoids, NW India: Regional correlation and implications for Rodinia paleogeography. Precambrian Res. 236, 265–281. https://doi.org/10.1016/j.precamres.2013.07.018.
Austermann, J., Ben-Avraham, Z., Bird, P., Heidbach, O., Schubert, G., Stock, J.M., 2011. Quantifying the forces needed for the rapid change of Pacific plate motion at 6Ma. Earth Planet. Sci. Lett. 307 (3–4), 289–297. https://doi.org/10.1016/j.epsl.2011.04.043.
Austermann, J., Kaye, B.T., Mitrovica, J.X., Huybers, P., 2014. A statistical analysis of the correlation between large igneous provinces and lower mantle seismic structure. Geophys. J. Int. 197 (1), 1–9. https://doi.org/10.1093/gji/ggt500.
Barker, C.A., Secor, T.D., Pray, J.R., Wright, J.E., 1998. Age and Deformation of the Longtown Metagranite, South Carolina Piedmont: A Possible Constraint on the Origin of the Carolina Terrane. J. Geol. 106 (6), 713–726. https://doi.org/10.1086/516055.
Bebout, G.E., 1995. The impact of subduction-zone metamorphism on mantle-ocean chemical cycling. Chemical Geology 126 (2), 191–218. https://doi.org/10.1016/0009-2541(95)00118-5.
Berry, R.F., Steele, D.A., Meffre, S., 2008. Proterozoic metamorphism in Tasmania: Implications for tectonic reconstructions. Precambrian Res. 166 (1–4), 387–396. https://doi.org/10.1016/j.precamres.2007.05.004.
Bevier, M.L., Barr, S.M., White, C.E., Macdonald, A.S., 1993. U–Pb geochronologic constraints on the volcanic evolution of the Mira (Avalon) terrane, southeastern Cape Breton Island, Nova Scotia. Can. J. Earth Sci. 30 (1), 1–10. https://doi.org/10.1139/e93-001.
Black, R., Latouche, L., Liegeois, J.P., Caby, R., Bertrand, J.M., 1994. Pan-African displaced terranes in the Tuareg shield (central Sahara). Geology 22 (7), 641–644. https://doi.org/10.1130/0091-7613(1994)022<0641:PADTIT>2.3.CO;2.
Blades, M.L., Collins, A.S., Foden, J., Payne, J.L., Xu, X., Alemu, T., Woldetinsae, G., Clark, C., Taylor, R.J.M., 2015. Age and hafnium isotopic evolution of the Didesa and Kemashi Domains, western Ethiopia. Precambrian Res. 270, 267–284. https://doi.org/10.1016/j.precamres.2015.09.018.
Black, L.P., Seymour, D.B., Corbett, K.D., Cox, S.E., Streit, J.E., Bottrill, R.S., Calver, C.R., Everard, J.L., Green, G.R., McClenaghan, M.P., Pemberton, J., Taheri, J., Turner, N.J., 1997. Dating Tasmania's oldest geological events. In: Canberra, ACT: AustralianGeological Survey Organisation Record 1997/15 (57pp).
Blades, M.L., Alessio, B.L., Collins, A.S., Foden, J., Payne, J.L., Glorie, S., Holden, P., Thorpe, B., Al-Khirbash, S., 2020. Unravelling the Neoproterozoic accretionary history of Oman, using an array of isotopic systems in zircon. J. Geol. Soc. 177 (2), 357–378. https://doi.org/10.1144/jgs2018-125.
Blades, M.L., Foden, J., Collins, A.S., Alemu, T., Woldetinsae, G., 2019. The origin of the ultramafic rocks of the Tulu Dimtu Belt, western Ethiopia–do they represent remnants of the Mozambique Ocean? Geol. Mag. 156 (1), 62–82. https://doi.org/10.1017/S0016756817000802.
Blades, M.L., Collins, A.S., Foden, J., Payne, J.L., Stüwe, K., Hassan, M., Abu-Alam, T., submitted. Age and Hafnium Isotope Evolution of Sudanese Butana and Chad Illuminates the Stenian to Ediacaran Evolution of the Southeast Sahara Metacraton. Precambrian Res.
Bleeker, W., 2003. The late Archean record: a puzzle in ca. 35 pieces. Lithos 71 (2–4), 99–134. https://doi.org/10.1016/j.lithos.2003.07.003.
Bodorkos, S., Crowley, J.L., Claoué-Long, J.C., Anderson, J.R., Magee, C.W., 2020. Precise U–Pb baddeleyite dating of the Derim Derim Dolerite, McArthur Basin, Northern Territory: old and new SHRIMP and ID-TIMS constraints. Aust. J. Earth Sci. 1–15. https://doi.org/10.1080/08120099.2020.1749929.
Bower, D.J., Gurnis, M., Seton, M., 2013. Lower mantle structure from paleogeographically constrained dynamic Earth models. Geochem. Geophys. Geosyst. 14 (1), 44–63. https://doi.org/10.1029/2012GC004267.
Boyden, J.A., Müller, R.D., Gurnis, M., Torsvik, T.H., Clark, J.A., Turner, M., Ivey-Law, H., Watson, R.J., Cannon, J.S., 2011. Next-generation plate tectonic reconstructions. In: Keller, G.R., Baru, C. (Eds.), Geoinformatics: Cyberinfrastructure for the Solid Earth Sciences. Cambridge University Press, Cambridge, pp. 95–113.
Brenner, A.R., Fu, R.R., Evans, D.A.D., Smirnov, A.V., Trubko, R., Rose, I.R., 2020. Paleomagnetic evidence for modern-like plate motion velocities at 3.2 Ga. Science Advances 6 (17), eaaz8670. https://doi.org/10.1126/sciadv.aaz8670.
Brown, M., Johnson, T.E., Gardiner, N.J., 2020a. Plate Tectonics and the Archean Earth. Annu. Rev. Earth Planet. Sci. 48 (1), 291–320. https://doi.org/10.1146/annurev-earth-081619-052705.
Brown, M., Kirkland, C.L., Johnson, T.E., 2020b. Evolution of geodynamics since the Archean: Significant change at the dawn of the Phanerozoic. Geology 48 (5), 488–492. https://doi.org/10.1130/G47417.1.
Brune, S., Williams, S.E., Müller, R.D., 2017. Potential links between continental rifting, CO2 degassing and climate change through time. Nat. Geosci. 10, 941–946. https://doi.org/10.1038/s41561-017-0003-6.
Burke, K., Torsvik, T.H., 2004. Derivation of Large Igneous Provinces of the past 200 million years from long-term heterogeneities in the deep mantle. Earth Planet. Sci. Lett. 227 (3–4), 531–538. https://doi.org/10.1016/j.epsl.2004.09.015.
Burrett, C., Long, J., Stait, B., 1990. Early-Middle Palaeozoic biogeography of Asian terranes derived from Gondwana. Geological Society, London, Memoirs 12, 163–174. https://doi.org/10.1144/GSL.MEM.1990.012.01.14.
Burrett, C., Zaw, Khin, Meffre, S., Lai, C.K., Khositanont, S., Chaodumrong, P., Udchachon, M., Ekins, S., Halpin, J., 2014. The configuration of Greater Gondwana—Evidence from LA ICPMS, U–Pb geochronology of detrital zircons from the Palaeozoic and Mesozoic of Southeast Asia and China. Gondwana Res. 26 (1), 31–51. https://doi.org/10.1016/j.gr.2013.05.020.
Caby, R., 2003. Terrane assembly and geodynamic evolution of central–western Hoggar: a synthesis. J. Afr. Earth. Sci. 37 (3–4), 133–159. https://doi.org/10.1016/j.jafrearsci.2003.05.003.
Caby, R., Andreopoulos-Renaud, U., Gravelle, M., 1982. Cadre geologique et geochronologique U/Pb sur zircon des batholites precoces dans le segment pan-africain du Hoggar central (Algerie). Bulletin de la Société Géologique de France S7-XXIV, 677–684. https://doi.org/10.2113/gssgfbull.S7-XXIV.4.677.
Caby, R., Andreopoulos-Renaud, U., Pin, C., 1989. Late Proterozoic arc–continent and continent–continent collision in the pan-African trans-Saharan belt of Mali. Can. J. Earth Sci. 26 (6), 1136–1146. https://doi.org/10.1139/e89-097.
Calver, C.R., 2011. Neoproterozoic glacial deposits of Tasmania. In: Arnaud, E., Halverson, G.P., Shields-Zhou, G. (Eds.), The Geological Record of Neoproterozoic Glaciations, 36. Geological Society of London, Memoirs, pp. 649–658.
Calver, C.R., Meffre, S., Everard, J.L., 2013. Felsic Porphyry Sills in Surprise Bay Formation Near Currie, King Island, Dated at 775 Ma (LA-ICPMS, U-Pb on Zircon), 04. Tasmanian Geological Survey Record, pp. 1–10.
Calver, C.R., Everard, J.L., Berry, R.F., Bottrill, R.S., Seymour, D.B., 2014. Proterozoic Tasmania. In: Corbett, K.D., Quilty, P.G., Calver, C.R. (Eds.), Geological Evolution of Tasmania. Geological Society of Australia (Tasmania Division), Hobart, TAS, pp. 33–94 (Special Publication 24).
Cao, W., Williams, S., Flament, N., Zahirovic, S., Scotese, C., Dietmar Müller, R., 2019. Palaeolatitudinal distribution of lithologic indicators of climate in a palaeogeographic framework. Geol. Mag. 156 (2), 331–354. https://doi.org/10.1017/S0016756818000110.
Cawood, P.A., Buchan, C., 2007. Linking accretionary orogenesis with supercontinent assembly. Earth-Sci. Rev. 82 (3–4), 217–256. https://doi.org/10.1016/j.earscirev.2007.03.003.
Cawood, P.A., Pisarevsky, S.A., 2006. Was Baltica right-way-up or upside-down in the Neoproterozoic? J. Geol. Soc. London 163 (5), 753–759. https://doi.org/10.1144/0016-76492005-126.
Cawood, P.A., Nemchin, A.A., Leverenz, A., Saeed, A., Balance, P.F., 1999. U/Pb dating of detrital zircons: Implications for the provenance record of Gondwana margin terranes. GSA Bulletin 111 (8), 1107–1119. https://doi.org/10.1130/0016-7606(1999)111<1107:UPDODZ>2.3.CO;2.
Cawood, P.A., Nemchin, A.A., Smith, M., Loewy, S., 2003. Source of the Dalradian Supergroup constrained by U–Pb dating of detrital zircon and implications for the East Laurentian margin. J. Geol. Soc. London 160, 231–246. https://doi.org/10.1144/0016-764902-039.
Cawood, P.A., Strachan, R., Cutts, K., Kinny, P.D., Hand, M., Pisarevsky, S., 2010. Neoproterozoic orogeny along the margin of Rodinia: Valhalla orogen, North Atlantic. Geology 38 (2), 99–102. https://doi.org/10.1130/G30450.1.
Cawood, P.A., Hawkesworth, C.J., Dhuime, B., 2013a. The continental record and the generation of continental crust. GSA Bulletin 125 (1-2), 14–32. https://doi.org/10.1130/B30722.1.
Cawood, P.A., Wang, Y., Xu, Y., Zhao, G., 2013b. Locating South China in Rodinia and Gondwana: A fragment of greater India lithosphere? Geology 41 (8), 903–906. https://doi.org/10.1130/G34395.1.
Cawood, P.A., Strachan, R.A., Pisarevsky, S.A., Gladkochub, D.P., Murphy, J.B., 2016. Linking collisional and accretionary orogens during Rodinia assembly and breakup: Implications for models of supercontinent cycles. Earth Planet. Sci. Lett. 449, 118–126. https://doi.org/10.1016/j.epsl.2016.05.049.
Cawood, P.A., Hawkesworth, C.J., Pisarevsky, S.A., Dhuime, B., Capitanio, F.A., Nebel, O., 2018a. Geological archive of the onset of plate tectonics. Philos. Trans. A Math. Phys. Eng. Sci. 376 (2132) https://doi.org/10.1098/rsta.2017.0405.
Cawood, P.A., Zhao, G., Yao, J., Wang, W., Xu, Y., Wang, Y., 2018b. Reconstructing South China in Phanerozoic and Precambrian supercontinents. Earth-Sci. Rev. 186, 173–194. https://doi.org/10.1016/j.earscirev.2017.06.001.
Cawood, P.A., Wang, W., Zhao, T., Xu, Y., Mulder, J.A., Pisarevsky, S.A., Zhang, L., Gan, C., He, H., Liu, H., Qi, L., Wang, Y., Yao, J., Zhao, G., Zhou, M.-F., Zi, J.-W., 2020. Deconstructing South China and consequences for reconstructing Nuna and

Rodinia. Earth-Sci. Rev. 204, 103169 https://doi.org/10.1016/j.earscirev.2020.103169.
Caxito, F.A., Uhlein, A., Dantas, E.L., 2014a. The Afeição augen-gneiss Suite and the record of the Cariris Velhos Orogeny (1000–960 Ma) within the Riacho do Pontal fold belt, NE Brazil. J. South Amer. Earth Sci. 51, 12–27. https://doi.org/10.1016/j.jsames.2013.12.012.
Caxito, F.A., Uhlein, A., Stevenson, R., Uhlein, G.J., 2014b. Neoproterozoic oceanic crust remnants in northeast Brazil. Geology 42, 387–390. https://doi.org/10.1130/G35479.1.
Caxito, F.A., Uhlein, A., Dantas, E.L., Stevenson, R., Salgado, S.S., Dussin, I.A., Sial, A. da N., 2016. A complete Wilson Cycle recorded within the Riacho do Pontal Orogen, NE Brazil: Implications for the Neoproterozoic evolution of the Borborema Province at the heart of West Gondwana. Precambrian Res. 282, 97–120. https://doi.org/10.1016/j.precamres.2016.07.001.
Cayley, R.A., 2011. Exotic crustal block accretion to the eastern Gondwanaland margin in the Late Cambrian–Tasmania, the Selwyn Block, and implications for the Cambrian–Silurian evolution of the Ross, Delamerian, and Lachlan orogens. Gondwana Res. 19 (3), 628–649. https://doi.org/10.1016/j.gr.2010.11.013.
Channell, J.E.T., McCabe, C., 1992. Palaeomagnetic data from the Borrowdale Volcanic Group: volcano-tectonics and Late Ordovician palaeolatitudes. J. Geol. Soc. London 149, 881–888. https://doi.org/10.1144/gsjgs.149.6.0881.
Channell, J.E.T., McCabe, C., Woodcock, N.H., 1993. Palaeomagnetic study of Llandovery (Lower Silurian) red beds in north-west England. Geophys. J. Int. 115 (3), 1085–1094. https://doi.org/10.1111/j.1365-246X.1993.tb01511.x.
Charvet, J., Shu, L., Laurent-Charvet, S., Wang, B., Faure, M., Cluzel, D., Chen, Y., De Jong, K., 2011. Palaeozoic tectonic evolution of the Tianshan belt, NW China. Sci. China Earth Sci. 54, 166–184. https://doi.org/10.1007/s11430-010-4138-1.
Chen, N.S., Li, X.Y., Zhang, K.X., Wang, G.C., Zhu, Y.H., Hou, G.J., Bai, Y.S., 2006a. Lithological characteristics of the baishahe formation to the south of Xiangride town, eastern kunlun mountains and its age constrained from zircon Pb-Pb dating. Geological Science and Technology Information 25 (6), 1–7.
Chen, N.S., Li, X.Y., Wang, X.Y., Chen, Q., Wang, Q.Y., Wan, Y.S., 2006b. Zircon SHRIMP U-Pb age of neoproterozoic metagranite in the north kunlun Unit on the southern margin of the qaidam block in China. Geol. Bull. China 25 (11), 1311–1314.
Chen, Nengsong, Sun, Min, Wang, Qinyan, Zhang, Kexin, Wan, Yusheng, Chen, Haihong, 2008. U-Pb dating of zircon from the central zone of the east kunlun orogen and its implications for tectonic evolution. Science in China. Series D, Earth Sciences / Chinese Academy of Sciences 51 (7), 929–938.
Chen, Y., Xu, B., Zhan, S., Li, Y., 2004. First mid-Neoproterozoic paleomagnetic results from the Tarim Basin (NW China) and their geodynamic implications. Precambrian Res. 133 (3–4), 271–281. https://doi.org/10.1016/j.precamres.2004.05.002.
Claesson, C., 1979. Early Palaeozoic geomagnetism of Gotland. Geologiska Föreningen i Stockholm Förhandlingar 101 (2), 149–155. https://doi.org/10.1080/11035897909452573.
Clennett, E.J., Sigloch, K., Mihalynuk, M.G., Seton, M., Henderson, M.A., Hosseini, K., Mohammadzaheri, A., Johnston, S.T., Müller, R.D., 2020. A Quantitative Tomotectonic Plate Reconstruction of Western North America and the Eastern Pacific Basin. Geochemistry, Geophysics, Geosystems 21 (8), 1–25. https://doi.org/10.1029/2020GC009117.
Cocks, L.R.M., Fortey, R.A., 1997. A new Hirnantia faunafrom Thailand and the biogeography of the latest Ordovician of south-east Asia. Geobios 30 (1), 117–126. https://doi.org/10.1016/S0016-6995(97)80017-4.
Cocks, L.R.M., Torsvik, T.H., 2007. Siberia, the wandering northern terrane, and its changing geography through the Palaeozoic. Earth-Sci. Rev. 82, 29–74. https://doi.org/10.1016/j.earscirev.2007.02.001.
Collins, A.S., 2003. Structure and age of the northern Leeuwin Complex, Western Australia: Constraints from field mapping and U–Pb isotopic analysis. Aust. J. Earth Sci. 50, 585–599. https://doi.org/10.1046/j.1440-0952.2003.01014.x.
Collins, A.S., 2006. Madagascar and the amalgamation of Central Gondwana. Gondwana Res. 9 (1–2), 3–16. https://doi.org/10.1016/j.gr.2005.10.001.
Collins, A.S., Pisarevsky, S.A., 2005. Amalgamating eastern Gondwana: The evolution of the Circum-Indian Orogens. Earth-Sci. Rev. 71, 229–270. https://doi.org/10.1016/j.earscirev.2005.02.004.
Collins, A.S., Kröner, A., Fitzsimons, I.C.W., Razakamanana, T., 2003. Detrital footprint of the Mozambique ocean: U–Pb SHRIMP and Pb evaporation zircon geochronology of metasedimentary gneisses in eastern Madagascar. Tectonophysics 375 (1–4), 77–99. https://doi.org/10.1016/S0040-1951(03)00334-2.
Collins, W.J., Belousova, E.A., Kemp, A.I.S., Murphy, J.B., 2011. Two contrasting Phanerozoic orogenic systems revealed by hafnium isotope data. Nat. Geosci. 4, 333–337. https://doi.org/10.1038/ngeo1127.
Collins, A.S., Blades, M.L., Merdith, A.S., Foden, J.D., in revision. A late Tonian plate reorganization event revealed by a full-plate Proterozoic reconstruction. Communications Earth Environment.
Colpron, M., Logan, J.M., Mortensen, J.K., 2002. U-Pb zircon age constraint for late Neoproterozoic rifting and initiation of the lower Paleozoic passive margin of western Laurentia. Can. J. Earth Sci. 39 (2), 133–143. https://doi.org/10.1139/e01-069.
Compston, W., Wright, A.E., Toghill, P., 2002. Dating the Late Precambrian volcanicity of England and Wales. J. Geol. Soc. London 159, 323–339. https://doi.org/10.1144/0016-764901-010.
Corvino, A.F., Boger, S.D., Henjes-Kunst, F., Wilson, C.J.L., Fitzsimons, I.C.W., 2008. Superimposed tectonic events at 2450 Ma, 2100 Ma, 900 Ma and 500 Ma in the North Mawson Escarpment, Antarctic Prince Charles Mountains. Precambrian Res. 167 (3–4), 281–302. https://doi.org/10.1016/j.precamres.2008.09.001.
Cox, G.M., Halverson, G.P., Denyszyn, S., Foden, J., Macdonald, F.A., 2018. Cryogenian magmatism along the north-western margin of Laurentia: Plume or rift? Precambrian Res. 319, 144–157. https://doi.org/10.1016/j.precamres.2017.09.025.
da Silva Filho, A.F., Guimarães, I.P., Van Schmus, W.R., 2002. Crustal Evolution of the Pernambuco-Alagoas Complex, Borborema Province, NE Brazil: Nd Isotopic Data from Neoproterozoic Granitoids. Gondwana Res. 5 (2), 409–422. https://doi.org/10.1016/S1342-937X(05)70732-2.
Daczko, N.R., Halpin, J.A., Fitzsimons, I.C.W., Whittaker, J.M., 2018. A cryptic Gondwana-forming orogen located in Antarctica. Sci. Rep. 8, 8371. https://doi.org/10.1038/s41598-018-26530-1.
Dallmeyer, R.D., 1989. Contrasting accreted terranes in the southern Appalachian Orogen, basement beneath the Atlantic and Gulf Coastal Plains, and West African orogens. Precambrian Res. 42 (3–4), 387–409. https://doi.org/10.1016/0301-9268(89)90021-1.
Dalziel, I.W.D., 1991. Pacific margins of Laurentia and East Antarctica-Australia as a conjugate rift pair: Evidence and implications for an Eocambrian supercontinent. Geology 19 (6), 598–601. https://doi.org/10.1130/0091-7613(1991)019<0598:PMOLAE>2.3.CO;2.
Dalziel, I.W., 1992. On the organization of American plates in the Neoproterozoic and the breakout of Laurentia. GSA Today 2 (11), 239–241.
Dalziel, I.W.D., 1997. Neoproterozoic-Paleozoic geography and tectonics: Review, hypothesis, environmental speculation. GSA Bull. 109 (1), 16–42. https://doi.org/10.1130/0016-7606(1997)109<0016:ONPGAT>2.3.CO;2.
Dalziel, I.W.D., Dewey, J.F., 2019. The classic Wilson cycle revisited. Geological Society, London, Special Publications 470, 19–38. https://doi.org/10.1144/SP470.1.
Danukalov, N.F., Kondruchina, L.S., Chernikov, A.P., 1983. Paleozoic paleomagnetism of the South and Central Urals. BF AN SSSR, Ufa.
Davies, R.G., Crawford, A.R., 1971. Petrography and age of the rocks of Bulland Hill, Kirana Hills, Sarghoda District, West Pakistan. Geol. Mag. 108 (3), 235–246. https://doi.org/10.1017/S001675680005158X.
Davies, D.R., Goes, S., Sambridge, M., 2015. On the relationship between volcanic hotspot locations, the reconstructed eruption sites of large igneous provinces and deep mantle seismic structure. Earth Planet. Sci. Lett. 411, 121–130. https://doi.org/10.1016/j.epsl.2014.11.052.
Davis, J.K., Meert, J.G., Pandit, M.K., 2014. Paleomagnetic analysis of the Marwar Supergroup, Rajasthan, India and proposed interbasinal correlations. J. Asian Earth Sci. 91, 339–351. https://doi.org/10.1016/j.jseaes.2013.09.027.
Deb, M., Thorpe, R.I., Krstic, D., Corfu, F., Davis, D.W., 2001. Zircon U–Pb and galena Pb isotope evidence for an approximate 1.0 Ga terrane constituting the western margin of the Aravalli–Delhi orogenic belt, northwestern India. Precambrian Res. 108 (3–4), 195–213. https://doi.org/10.1016/S0301-9268(01)00134-6.
Degtyarev, K.E., 2011. Tectonic evolution of Early Paleozoic island-arc systems and continental crust formation in the Caledonides of Kazakhstan and the North Tien Shan. Geotectonics/Geotektonika 45, 23–50. https://doi.org/10.1134/S0016852111010031.
Degtyarev, K.E., Shatagin, K.N., Kotov, A.B., Sal'Nikova, E.B., Luchitskaya, M.V., Tret'yakov, A.A., Yakovleva, S.Z., 2008. Late Precambrian volcanoplutonic association of the Aktau-Dzhungar massif, Central Kazakhstan: Structural position and age, in: Doklady Earth Sciences, , 2nd421. Springer Nature BV, pp. 879–883.
Degtyarev, K.E., Tret'yakov, A.A., Ryazantsev, A.V., Kotov, A.B., Sal'nikova, E.B., Aleksandrov, P.A., Anisimova, I.V., 2011. Stenian granitoids of the west Kyrgyz Ridge (North Tien Shan): Position, structure, and age determination. Dokl. Earth Sci. 441, 1484–1488. https://doi.org/10.1134/S1028334X11110134.
Degtyarev, K., Yakubchuk, A., Tretyakov, A., Kotov, A., Kovach, V., 2017. Precambrian geology of the Kazakh Uplands and Tien Shan: An overview. Gondwana Res. 47, 44–75. https://doi.org/10.1016/j.gr.2016.12.014.
Denyszyn, S.W., Halls, H.C., Davis, D.W., Evans, D.A.D., 2009. Paleomagnetism and U–Pb geochronology of Franklin dykes in High Arctic Canada and Greenland: a revised age and paleomagnetic pole constraining block rotations in the Nares Strait region. Can. J. Earth Sci. 46 (9), 689–705. https://doi.org/10.1139/E09-042.
Deutsch, E.R., 1980. Magnetism of the Mid-Ordovician Tramore Volcanics, SE Ireland, and the Question of a Wide Proto-Atlantic Ocean. J. Geomagn. Geoelectr. 32, SIII77–SIII98. https://doi.org/10.5636/jgg.32.Supplement3_SIII77.
Deutsch, E.R., Prasad, J.N., 1987. Ordovician paleomagnetic results from the St. George and Table Head carbonates of western Newfoundland. Can. J. Earth Sci. 24, 1785–1796. https://doi.org/10.1139/e87-170.
Direen, N.G., Crawford, A.J., 2003. Fossil seaward-dipping reflector sequences preserved in southeastern Australia: a 600 Ma volcanic passive margin in eastern Gondwanaland. J. Geol. Soc. London 160, 985–990. https://doi.org/10.1144/0016-764903-010.
Doig, R., Murphy, J.B., Nance, R.D., 1993. Tectonic significance of the Late Proterozoic Economy River gneiss, Cobequid Highlands, Avalon Composite Terrane, Nova Scotia. Can. J. Earth Sci. 30, 474–479. https://doi.org/10.1139/e93-035.
Domeier, M., 2016. A plate tectonic scenario for the Iapetus and Rheic oceans. Gondwana Res. 36, 275–295. https://doi.org/10.1016/j.gr.2015.08.003.
Domeier, M., 2018. Early Paleozoic tectonics of Asia: Towards a full-plate model. Geoscience Frontiers 9, 789–862. https://doi.org/10.1016/j.gsf.2017.11.012.
Domeier, M., Torsvik, T.H., 2014. Plate tectonics in the late Paleozoic. Geoscience Frontiers 5, 303–350. https://doi.org/10.1016/j.gsf.2014.01.002.
Domeier, M., Torsvik, T.H., 2017. Full-plate modelling in pre-Jurassic time. Geol. Mag. 1–20. https://doi.org/10.1017/S0016756817001005.
Domeier, M., Van der Voo, R., Torsvik, T.H., 2012. Paleomagnetism and Pangea: The road to reconciliation. Tectonophysics 514–517, 14–43. https://doi.org/10.1016/j.tecto.2011.10.021.

Domeier, M., Shephard, G.E., Jakob, J., Gaina, C., Doubrovine, P.V., Torsvik, T.H., 2017. Intraoceanic subduction spanned the Pacific in the Late Cretaceous-Paleocene. Sci Adv 3. https://doi.org/10.1126/sciadv.aao2303.

Domeier, M., Font, E., Youbi, N., Davies, J., Nemkin, S., Van der Voo, R., Perrot, M., Benabbou, M., Boumehdi, M.A., Torsvik, T.H., 2020. On the Early Permian shape of Pangea from paleomagnetism at its core. Gondwana Res. doi:https://doi.org/10.1016/j.gr.2020.11.005.

Dong, Y., Santosh, M., 2016. Tectonic architecture and multiple orogeny of the Qinling Orogenic Belt, Central China. Gondwana Res. 29, 1–40. https://doi.org/10.1016/j.gr.2015.06.009.

Dong, Y., Yang, Z., Liu, X., Zhang, X., He, D., Li, W., Zhang, F., Sun, S., Zhang, H., Zhang, G., 2014. Neoproterozoic amalgamation of the Northern Qinling terrain to the North China Craton: Constraints from geochronology and geochemistry of the Kuanping ophiolite. Precambrian Res. 255, 77–95. https://doi.org/10.1016/j.precamres.2014.09.008.

dos Santos, E.J., Van Schmus, W.R., Kozuch, M., Neves, B.B. de B., 2010. The Cariris Velhos tectonic event in Northeast Brazil. J. South Amer. Earth Sci. 29, 61–76. https://doi.org/10.1016/j.jsames.2009.07.003.

Doubrovine, P.V., Steinberger, B., Torsvik, T.H., 2016. A failure to reject: Testing the correlation between large igneous provinces and deep mantle structures with EDF statistics. Geochem. Geophys. Geosyst. 17 (3), 1130–1163. https://doi.org/10.1002/2015GC006044.

Doucet, L.S., Li, Z.-X., Gamal El Dien, H., Pourteau, A., Murphy, J.B., Collins, W.J., Mattielli, N., Olierook, H.K.H., Spencer, C.J., Mitchell, R.N., 2020. Distinct formation history for deep-mantle domains reflected in geochemical differences. Nat. Geosci. 13, 511–515. https://doi.org/10.1038/s41561-020-0599-9.

Douglass, D.N., 1988. Paleomagnetics of Ringerike Old Red Sandstone and related rocks, southern Norway: implications for pre-Carboniferous separation of Baltica and British terranes. Tectonophysics 148, 11–27. https://doi.org/10.1016/0040-1951(88)90157-6.

Dunn, W.J., Elmore, R.D., 1985. Paleomagnetic and petrographic investigation of the Taum Sauk Limestone, southeast Missouri. Journal of Geophysical Research [Solid Earth] 90 (B13), 11469. https://doi.org/10.1029/JB090iB13p11469.

Dutkiewicz, A., Dietmar Müller, R., Cannon, J., Vaughan, S., Zahirovic, S., 2019. Sequestration and subduction of deep-sea carbonate in the global ocean since the Early Cretaceous. Geology 47, 91–94. https://doi.org/10.1130/G45424.1.

Elburg, M.A., Andersen, T., Jacobs, J., Läufer, A., Ruppel, A., Krohne, N., Damaske, D., 2015. One hundred fifty million years of intrusive activity in the Sør Rondane Mountains (East Antarctica): Implications for Gondwana assembly. J. Geol. 124 (1), 1–26. https://doi.org/10.1086/684052.

Elming, S.-Å., Pisarevsky, S.A., Layer, P., Bylund, G., 2014. A palaeomagnetic and 40Ar/39Ar study of mafic dykes in southern Sweden: A new Early Neoproterozoic key-pole for the Baltic Shield and implications for Sveconorwegian and Grenville loops. Precambrian Res. 244, 192–206. https://doi.org/10.1016/j.precamres.2013.12.007.

Elston, D.P., Bressler, S.L., 1977. Paleomagnetic poles and polarity zonation from Cambrian and Devonian strata of Arizona. Earth Planet. Sci. Lett. 36, 423–433. https://doi.org/10.1016/0012-821X(77)90067-X.

Embleton, B.J.J., Williams, G.E., 1986. Low palaeolatitude of deposition for late Precambrian periglacial varvites in South Australia: implications for palaeoclimatology. Earth Planet. Sci. Lett. 79, 419–430. https://doi.org/10.1016/0012-821X(86)90197-4.

England, P., Molnar, P., 1990. Surface uplift, uplift of rocks, and exhumation of rocks. Geology 18 (12), 1173–1177. https://doi.org/10.1130/0091-7613(1990)018<1173:SUUORA>2.3.CO;2.

Evans, D.A.D., 2003. True polar wander and supercontinents. Tectonophysics. 362 (1–4), 303–320. https://doi.org/10.1016/S0040-1951(02)00642-X.

Evans, D.A.D., 2009. The palaeomagnetically viable, long-lived and all-inclusive Rodinia supercontinent reconstruction, 327. Geological Society, London, pp. 371–404. https://doi.org/10.1144/SP327.16.

Evans, D.A.D., 2013. Reconstructing pre-Pangean supercontinents. GSA Bulletin 125 (11–12), 1735–1751. https://doi.org/10.1130/B30950.1.

Evans, D.A.D., Li, Z.X., Kirschvink, J.L., Wingate, M.T.D., 2000. A high-quality mid-Neoproterozoic paleomagnetic pole from South China, with implications for ice ages and the breakup configuration of Rodinia. Precambrian Res. 100, 313–334. https://doi.org/10.1016/S0301-9268(99)00079-0.

Evans, D.A.D., Trindade, R.I.F., Catelani, E.L., D'Agrella-Filho, M.S., Heaman, L.M., Oliveira, E.P., Söderlund, U., Ernst, R.E., Smirnov, A.V., Salminen, J.M., 2016. Return to Rodinia? Moderate to high palaeolatitude of the São Francisco/Congo craton at 920 Ma. Geological Society, London, Special Publications 424, 167–190. https://doi.org/10.1144/SP424.1.

Eyster, A., Weiss, B.P., Karlstrom, K., Macdonald, F.A., 2019. Paleomagnetism of the Chuar Group and evaluation of the late Tonian Laurentian apparent polar wander path with implications for the makeup and breakup of Rodinia. GSA Bulletin. 132 (3–4), 710–738. https://doi.org/10.1130/B32012.1.

Fang, D.-J., Jin, G.-H., Jiang, L.-P., Wang, P.-Y., Wang, Z.-L., 1996. Paleozoic paleomagnetic results and the tectonic significance of Tarim Plate. Acta Geophysica Sinica 39, 532–542.

Fang, D., Wang, P., Shen, Z., Tan, X., 1998. Cenozoic paleomagnetic results and phanerozoic apparent polar wandering path of Tarim Block. Sci. China Ser. D Earth Sci. 41, 105–112. https://doi.org/10.1007/BF02984518.

Farr, M.R., Gose, W.A., 1991. Paleomagnetism of the Cambrian Moore Hollow Group, Texas: Evidence for a primary magnetization carried by detrital magnetite. J. Geophys. Res. 96, 9895. https://doi.org/10.1029/91JB00337.

Fezaa, N., Liégeois, J.-P., Abdallah, N., Cherfouh, E.H., De Waele, B., Bruguier, O., Ouabadi, A., 2010. Late Ediacaran geological evolution (575–555 Ma) of the Djanet Terrane, Eastern Hoggar, Algeria, evidence for a Murzukian intracontinental episode. Precambrian Res. 180 (3–4), 299–327. https://doi.org/10.1016/j.precamres.2010.05.011.

Fioretti, A.M., Black, L.P., Foden, J., Visonà, D., 2005. Grenville-age magmatism at the South Tasman Rise (Australia): A new piercing point for the reconstruction of Rodinia. Geology 33 (10), 769–772. https://doi.org/10.1130/G21671.1.

Fitzsimons, I.C.W., 2003. Proterozoic basement provinces of southern and southwestern Australia, and their correlation with Antarctica. Geological Society, London, Special Publications 206, 93–130. https://doi.org/10.1144/GSL.SP.2003.206.01.07.

Flament, N., Williams, S., Müller, R.D., Gurnis, M., Bower, D.J., 2017. Origin and evolution of the deep thermochemical structure beneath Eurasia. Nat. Commun. 8, 14164 https://doi.org/10.1038/ncomms14164.

French, A.N., Van der Voo, R., 1979. The magnetization of the Rose Hill Formation at the classical site of Graham's Fold Test. J. Geophys. Res. 84, 7688–7696. https://doi.org/10.1029/JB084iB13p07688.

Fu, X., Zhang, S., Li, Haiyan, Ding, J., Li, Huaikun, Yang, T., Wu, H., Yuan, H., Lv, J., 2015. New paleomagnetic results from the Huaibei Group and Neoproterozoic mafic sills in the North China Craton and their paleogeographic implications. Precambrian Res. 269, 90–106. https://doi.org/10.1016/j.precamres.2015.08.013.

Furnes, H., de Wit, M., Dilek, Y., 2014. Four billion years of ophiolites reveal secular trends in oceanic crust formation. Geoscience Frontiers 5, 571–603. https://doi.org/10.1016/j.gsf.2014.02.002.

Gallet, Y., Pavlov, V., 1996. Magnetostratigraphy of the Moyero River Section (North-Western Siberia): Constraints On Geomagnetic Reversal Frequency During the Early Palaeozoic. Geophys. J. Int. 125, 95–105. https://doi.org/10.1111/j.1365-246X.1996.tb06536.x.

Gallet, Y., Pavlov, V., Courtillot, V., 2003. Magnetic reversal frequency and apparent polar wander of the Siberian platform in the earliest Palaeozoic, inferred from the Khorbusuonka river section (northeastern Siberia). Geophys. J. Int. 154 (3), 829–840. https://doi.org/10.1046/j.1365-246X.2003.01996.x.

Ganade de Araujo, C.E., Cordani, U.G., Weinberg, R.F., Basei, M.A.S., Armstrong, R., Sato, K., 2014. Tracing Neoproterozoic subduction in the Borborema Province (NE-Brazil): Clues from U-Pb geochronology and Sr-Nd-Hf-O isotopes on granitoids and migmatites. Lithos 202–203, 167–189. https://doi.org/10.1016/j.lithos.2014.05.015.

Gao, R.F., Huang, H.L., Zhu, Z.W., Liu, H.S., Fan, Y.Q., Qing, X.J., 1983. The study of paleomagnetism in northeastern Sino-Korean massif during Pre-late Paleozoic. Contr. Project of Plate Tectonics in North China 1, 265–274.

Gao, J., Wang, X.-S., Klemd, R., Jiang, T., Qian, Q., Mu, L.-X., Ma, Y.-Z., 2015. Record of assembly and breakup of Rodinia in the Southwestern Altaids: Evidence from Neoproterozoic magmatism in the Chinese Western Tianshan Orogen. J. Asian Earth Sci. 113, 173–193. https://doi.org/10.1016/j.jseaes.2015.02.002.

Garnero, E.J., Lay, T., McNamara, A., 2007. Implications of lower-mantle structural heterogeneity for the existence and nature of whole-mantle plumes. In: Foulgerand, G.R., Jurdy, D.M. (Eds.), The Origin of Melting Anomalies: Plates, Plumes and Planetary Processes, pp. 79–101. https://doi.org/10.1130/2007.2430(05) (Spec. Pap. Geol. Soc. Am., 430).

Ge, R., Zhu, W., Wilde, S.A., He, J., Cui, X., Wang, X., Bihai, Z., 2014. Neoproterozoic to Paleozoic long-lived accretionary orogeny in the northern Tarim Craton: accretionary orogeny in northern Tarim. Tectonics 33, 302–329. https://doi.org/10.1002/2013TC003501.

Geissman, J.W., Jackson, M., Harlan, S.S., Van Der Voo, R., 1991. Paleomagnetism of Latest Cambrian-Early Ordovician and Latest Cretaceous-Early Tertiary rocks of the Florida Mountains, southwest New Mexico. J. Geophys. Res. [Solid Earth] 96 (B4), 6053–6071. https://doi.org/10.1029/90JB02701.

Gernon, T.M., Hincks, T.K., Tyrrell, T., Rohling, E.J., Palmer, M.R., 2016. Snowball Earth ocean chemistry driven by extensive ridge volcanism during Rodinia breakup. Nat. Geosci. 9, 242. https://doi.org/10.1038/ngeo2632.

Gerya, T., 2014. Precambrian geodynamics: Concepts and models. Gondwana Res. 25, 442–463. https://doi.org/10.1016/j.gr.2012.11.008.

Goddéris, Y., Le Hir, G., Macouin, M., Donnadieu, Y., Hubert-Théou, L., Dera, G., Aretz, M., Fluteau, F., Li, Z.X., Halverson, G.P., 2017. Paleogeographic forcing of the strontium isotopic cycle in the Neoproterozoic. Gondwana Res. 42, 151–162. https://doi.org/10.1016/j.gr.2016.09.013.

Goodge, J.W., Fanning, C.M., Fisher, C.M., Vervoort, J.D., 2017. Proterozoic crustal evolution of central East Antarctica: Age and isotopic evidence from glacial igneous clasts, and links with Australia and Laurentia. Precambrian Res. 299, 151–176. https://doi.org/10.1016/j.precamres.2017.07.026.

Gordon, R.G., Cox, A., O'Hare, S., 1984. Paleomagnetic Euler poles and the apparent polar wander and absolute motion of North America since the Carboniferous. Tectonics 3, 499–537. https://doi.org/10.1029/TC003i005p00499.

Granot, R., 2016. Palaeozoic oceanic crust preserved beneath the eastern Mediterranean. Nat. Geosci. 9, 701–705. https://doi.org/10.1038/ngeo2784.

Gregory, L.C., Meert, J.G., Bingen, B., Pandit, M.K., Torsvik, T.H., 2009. Paleomagnetism and geochronology of the Malani Igneous Suite, Northwest India: Implications for the configuration of Rodinia and the assembly of Gondwana. Precambrian Res. 170, 13–26. https://doi.org/10.1016/j.precamres.2008.11.004.

Guimarães, I.P., Van Schmus, W.R., de Brito Neves, B.B., Bretas Bittar, S.M., Silva Filho, A.F., Armstrong, R., 2012. U–Pb zircon ages of orthogneisses and supracrustal rocks of the Cariris Velhos belt: Onset of Neoproterozoic rifting in the Borborema Province, NE Brazil. Precambrian Res. 192–195, 52–77. https://doi.org/10.1016/j.precamres.2011.10.008.

Gurnis, M., Turner, M., Zahirovic, S., DiCaprio, L., Spasojevic, S., Müller, R.D., Boyden, J., Seton, M., Manea, V.C., Bower, D.J., 2012. Plate tectonic reconstructions with continuously closing plates. Comput. Geosci. 38, 35–42. https://doi.org/10.1016/j.cageo.2011.04.014.

Gurnis, M., Yang, T., Cannon, J., Turner, M., Williams, S., Flament, N., Müller, R.D., 2018. Global tectonic reconstructions with continuously deforming and evolving rigid plates. Comput. Geosci. 116, 32–41. https://doi.org/10.1016/j.cageo.2018.04.007.

Guynn, J.H., Kapp, P., Pullen, A., Heizler, M., Gehrels, G., Ding, L., 2006. Tibetan basement rocks near Amdo reveal "missing" Mesozoic tectonism along the Bangong suture, central Tibet. Geology 34, 505–508. https://doi.org/10.1130/G22453.1.

Guynn, J., Kapp, P., Gehrels, G.E., Ding, L., 2012. U–Pb geochronology of basement rocks in central Tibet and paleogeographic implications. J. Asian Earth Sci. 43, 23–50. https://doi.org/10.1016/j.jseaes.2011.09.003.

Hadj-Kaddour, Z., Liégeois, J.-P., Demaiffe, D., Caby, R., 1998. The alkaline–peralkaline granitic post-collisional Tin Zebane dyke swarm (Pan-African Tuareg shield, Algeria): prevalent mantle signature and late agpaitic differentiation. Lithos 45, 223–243. https://doi.org/10.1016/S0024-4937(98)00033-4.

Haldar, S.K., Deb, M., 2001. Geology and mineralization of Rajpura-Dariba lead-zinc belt, Rajasthan. In: Deb, M., Goodfellow, W.D. (Eds.), Sediment-Hosted Lead-Zink Deposit Modeling Program. Delhi-Udaipur, Elsevier, New Dehli, pp. 177–187.

Hall, S.A., Evans, I., 1988. Paleomagnetic study of the Ordovician Table Head Group, Port au Port Peninsula, Newfoundland. Can. J. Earth Sci. 25, 1407–1419. https://doi.org/10.1139/e88-135.

Halpin, J.A., Jensen, T., McGoldrick, P., Meffre, S., Berry, R.F., Everard, J.L., Calver, C. R., Thompson, J., Goemann, K., Whittaker, J.M., 2014. Authigenic monazite and detrital zircon dating from the Proterozoic Rocky Cape Group, Tasmania: Links to the Belt-Purcell Supergroup, North America. Precambrian Res. 250, 50–67. https://doi.org/10.1016/j.precamres.2014.05.025.

Halpin, J.A., Daczko, N.R., Kobler, M.E., Whittaker, J.M., 2017. Strike-slip tectonics during the Neoproterozoic–Cambrian assembly of East Gondwana: Evidence from a newly discovered microcontinent in the Indian Ocean (Batavia Knoll). Gondwana Res. 51, 137–148. https://doi.org/10.1016/j.gr.2017.08.002.

Hamilton, M.A., Murphy, J.B., 2004. Tectonic significance of a Llanvirn age for the Dunn Point volcanic rocks, Avalon terrane, Nova Scotia, Canada: implications for the evolution of the Iapetus and Rheic Oceans. Tectonophysics 379, 199–209. https://doi.org/10.1016/j.tecto.2003.11.006.

Han, Z., Yang, Z., Tong, Y., Jing, X., 2015. New paleomagnetic results from Late Ordovician rocks of the Yangtze Block, South China, and their paleogeographic implications. J. Geophys. Res. [Solid Earth] 120 (7), 4759–4772. https://doi.org/10.1002/2015JB012005.

Handke, M.J., Tucker, R.D., Ashwal, L.D., 1999. Neoproterozoic continental arc magmatism in west-central Madagascar. Geology 27 (4), 351–354. https://doi.org/10.1130/0091-7613(1999)027<0351:NCAMIW>2.3.CO;2.

Hargraves, R.B., Dawson, E.M., Houten, F.B., 1987. Palaeomagnetism and age of mid-Palaeozoic ring complexes in Niger, West Africa, and tectonic implications. Geophys. J. Int. 90, 705–729. https://doi.org/10.1111/j.1365-246X.1987.tb00750.x.

Harlan, S.S., Geissman, J.W., Snee, L.W., 2008. Paleomagnetism of Proterozoic mafic dikes from the Tobacco Root Mountains, southwest Montana. Precambrian Res. 163, 239–264. https://doi.org/10.1016/j.precamres.2007.12.002.

Hartz, E.H., Torsvik, T.H., 2002. Baltica upside down: A new plate tectonic model for Rodinia and the Iapetus Ocean. Geology 30 (3), 255–258. https://doi.org/10.1130/0091-7613(2002)030<0255:BUDANP>2.0.CO;2.

He, T., Zhu, M., Mills, B.J.W., Wynn, P.M., Zhuravlev, A.Y., Tostevin, R., Pogge von Strandmann, P.A.E., Yang, A., Poulton, S.W., Shields, G.A., 2019. Possible links between extreme oxygen perturbations and the Cambrian radiation of animals. Nat. Geosci. 12, 468–474. https://doi.org/10.1038/s41561-019-0357-z.

Heatherington, A.L., Mueller, P.A., Nutman, A.P., 1996. Neoproterozoic magmatism in the Suwan-nee terrane: Implications for terrane correlation. In: Nance, R.D., Thompson, M.D. (Eds.), Avalonian and Related Peri-Gondwanan Terranes of the Circum-North Atlantic. Geological Society of America, pp. 257–268. https://doi.org/10.1130/SPE304 (Special Papers, 304).

Henry, B., Liégeois, J.P., Nouar, O., Derder, M.E.M., Bayou, B., Bruguier, O., Ouabadi, A., Belhai, D., Amenna, M., Hemmi, A., Ayache, M., 2009. Repeated granitoid intrusions during the Neoproterozoic along the western boundary of the Saharan metacraton, Eastern Hoggar, Tuareg shield, Algeria: An AMS and U–Pb zircon age study. Tectonophysics 474, 417–434. https://doi.org/10.1016/j.tecto.2009.04.022.

Heron, P.J., Murphy, J.B., Nance, D.R., Pysklywec, R.N., 2020. Pannotia's mantle signature: the quest for supercontinent identification. Geological Society, London, Special Publications 503. https://doi.org/10.1144/SP503-2020-7.

Hibbard, J.P., van Staal, C.R., Miller, C.A., 2007. Links among Carolinia, Avalonia, and Ganderia in the Appalachian peri-Gondwanan realm. In: Sears, J.W., Harms, T.A., Evenchick, T.A. (Eds.), Whence the Mountains? Inquiries into the Evolution of Orogenic Systems: A Volume in Honor of Raymond A. Price. Geological Society of America, pp. 291–311. https://doi.org/10.1130/2007.2433(14) (Special Papers, 433).

Hochmuth, K., Gohl, K., Uenzelmann-Neben, G., 2015. Playing jigsaw with large igneous provinces—A plate tectonic reconstruction of Ontong Java Nui, West Pacific. Geochem. Geophys. Geosyst. 16 (11), 3789–3807. https://doi.org/10.1002/2015GC006036.

Hodych, J.P., 1989. Limestones of western Newfoundland that magnetized before Devonian folding but after Middle Ordovician lithification. Geophys. Res. Lett. 16, 93–96. https://doi.org/10.1029/GL016i001p00093.

Hodych, J.P., Buchan, K.L., 1998. Palaeomagnetism of the ca. 440 Ma Cape St Mary's sills of the Avalon Peninsula of Newfoundland: implications for Iapetus Ocean closure. Geophys. J. Int. 135, 155–164. https://doi.org/10.1046/j.1365-246X.1998.00263.x.

Hodych, J.P., Cox, R.A., Košler, J., 2004. An equatorial Laurentia at 550 Ma confirmed by Grenvillian inherited zircons dated by LAM ICP-MS in the Skinner Cove volcanics of western Newfoundland: implications for inertial interchange true polar wander. Precambrian Res. 129, 93–113. https://doi.org/10.1016/j.precamres.2003.10.012.

Hoffman, P.F., 1991. Did the breakout of Laurentia turn Gondwanaland inside-out? Science 252, 1409–1412. https://doi.org/10.1126/science.252.5011.1409.

Hoffman, P.F., Schrag, D.P., 2002. The snowball Earth hypothesis: testing the limits of global change. Terra Nova 14, 129–155. https://doi.org/10.1046/j.1365-3121.2002.00408.x.

Hoffman, P.F., Kaufman, A.J., Halverson, G.P., Schrag, D.P., 1998. A Neoproterozoic snowball earth. Science 281, 1342–1346. https://doi.org/10.1126/science.281.5381.1342.

Hofmann, M., Linnemann, U., Rai, V., Becker, S., Gärtner, A., Sagawe, A., 2011. The India and South China cratons at the margin of Rodinia—Synchronous Neoproterozoic magmatism revealed by LA-ICP-MS zircon analyses. Lithos 123 (1–4), 176–187. https://doi.org/10.1016/j.lithos.2011.01.012.

Hopper, E., Fischer, K.M., Wagner, L.S., Hawman, R.B., 2017. Reconstructing the end of the Appalachian orogeny. Geology 45, 15–18. https://doi.org/10.1130/G38453.1.

Hounslow, M.W., Domeier, M., Biggin, A.J., 2018. Subduction flux modulates the geomagnetic polarity reversal rate. Tectonophysics 742–743, 34–49. https://doi.org/10.1016/j.tecto.2018.05.018.

Hu, X., Garzanti, E., Wang, J., Huang, W., An, W., Webb, A., 2016. The timing of India-Asia collision onset–Facts, theories, controversies. Earth-Sci. Rev. 160, 264–299. https://doi.org/10.1016/j.earscirev.2016.07.014.

Hu, P.-Y., Zhai, Q.-G., Wang, J., Tang, Y., Wang, H.-T., Hou, K.-J., 2018. Precambrian origin of the North Lhasa terrane, Tibetan Plateau: Constraint from early Cryogenian back-arc magmatism. Precambrian Res. 313, 51–67. https://doi.org/10.1016/j.precamres.2018.05.014.

Huang, B., Yang, Z., Otofuji, Y.-I., Zhu, R., 1999a. Early Paleozoic paleomagnetic poles from the western part of the North China Block and their implications. Tectonophysics 308, 377–402. https://doi.org/10.1016/S0040-1951(99)00098-0.

Huang, B.C., Otofuji, Y., Yang, Z.Y., 1999b. Paleomagnetic constraints on the tectonic relationship between the Alashan/Hexi Corridor Terrane and the North China Block. Geophys. Res. Lett. 26, 787–790. https://doi.org/10.1029/1999GL900097.

Huang, K., Opdyke, N.D., Zhu, R., 2000. Further paleomagnetic results from the Silurian of the Yangtze Block and their implications. Earth Planet. Sci. Lett. 175, 191–202. https://doi.org/10.1016/S0012-821X(99)00302-7.

Huang, B., Xu, B., Zhang, C., Li, Y., Zhu, R., 2005. Paleomagnetism of the Baiyisi volcanic rocks (ca. 740Ma) of Tarim, Northwest China: A continental fragment of Neoproterozoic Western Australia? Precambrian Res. 142, 83–92. https://doi.org/10.1016/j.precamres.2005.09.006.

Huang, B., He, Z., Zong, K., Zhang, Z., 2014. Zircon U–Pb and Hf isotopic study of Neoproterozoic granitic gneisses from the Alatage area, Xinjiang: constraints on the Precambrian crustal evolution in the Central Tianshan Block. Chin. Sci. Bull. 59, 100–112. https://doi.org/10.1007/s11434-013-0010-y.

Huang, Z., Long, X., Kröner, A., Yuan, C., Wang, Y., Chen, B., Zhang, Y., 2015. Neoproterozoic granitic gneisses in the Chinese Central Tianshan Block: Implications for tectonic affinity and Precambrian crustal evolution. Precambrian Res. 269, 73–89. https://doi.org/10.1016/j.precamres.2015.08.005.

Huang, H., Cawood, P.A., Hou, M., Xiong, F., Ni, S., 2019. Provenance of latest Mesoproterozoic to early Neoproterozoic (meta)-sedimentary rocks and implications for paleographic reconstruction of the Yili Block. Gondwana Res. 72, 120–138. https://doi.org/10.1016/j.gr.2019.03.010.

Iosifidi, A.G., Khramov, A.N., Rodionov, V.P., Pisarevskii, S.A., Popov, V.V., 1999. Geomagnetic reversals in the Early Paleozoic: 2. A nonsynchronous record of Middle Ordovician reversals in the Berezovskaya section, southern Siberian Platform. Izv. Phys. Solid Earth 35, 24–32.

Jackson, M., Van der Voo, R., 1985. A Lower Ordovician paleomagnetic pole from the Oneota dolomite, Upper Mississippi River Valley. J. Geophys. Res., Geol. Soc. Am. 90, 10449. https://doi.org/10.1029/JB090iB12p10449.

Jacobs, J., Elburg, M., Läufer, A., Kleinhanns, I.C., Henjes-Kunst, F., Estrada, S., Ruppel, A.S., Damaske, D., Montero, P., Bea, F., 2015. Two distinct Late Mesoproterozoic/Early Neoproterozoic basement provinces in central/eastern Dronning Maud Land, East Antarctica: The missing link, 15–21°E. Precambrian Res. 265, 249–272. https://doi.org/10.1016/j.precamres.2015.05.003.

Jacobs, J., Opås, B., Elburg, M.A., Läufer, A., Estrada, S., Ksienzyk, A.K., Damaske, D., Hofmann, M., 2017. Cryptic sub-ice geology revealed by a U-Pb zircon study of glacial till in Dronning Maud Land, East Antarctica. Precambrian Res. 294, 1–14. https://doi.org/10.1016/j.precamres.2017.03.012.

Jarrard, R.D., 2003. Subduction fluxes of water, carbon dioxide, chlorine, and potassium. Geochem. Geophys. Geosyst., Geophys. Monogr. Ser. 4 (5), 1–50. https://doi.org/10.1029/2002GC000392.

Jeleńska, M., Bakhmutov, V., Konstantinienko, L., 2005. Paleomagnetic and rock magnetic data from the Silurian succession of the Dniester basin, Ukraine. Phys. Earth Planet. Inter. 149, 307–320. https://doi.org/10.1016/j.pepi.2004.10.005.

Jeleńska, M., Kądziałko-Hofmokl, M., Bakhmutov, V., Poliachenko, I., Ziółkowski, P., 2015. Palaeomagnetic and rock magnetic study of Lower Devonian sediments from Podolia, SW Ukraine: remagnetization problems. Geophys. J. Int. 200, 557–573. https://doi.org/10.1093/gji/ggu411.

Jian, P., Kröner, A., Jahn, B.-M., Windley, B.F., Shi, Y., Zhang, W., Zhang, F., Miao, L., Tomurhuu, D., Liu, D., 2014. Zircon dating of Neoproterozoic and Cambrian ophiolites in West Mongolia and implications for the timing of orogenic processes in the central part of the Central Asian Orogenic Belt. Earth-Sci. Rev. 133, 62–93. https://doi.org/10.1016/j.earscirev.2014.02.006.

Jiang, G., Sohl, L.E., Christie-Blick, N., 2003. Neoproterozoic stratigraphic comparison of the Lesser Himalaya (India) and Yangtze block (south China): Paleogeographic implications. Geology 31, 917–920. https://doi.org/10.1130/G19790.1.

Jing, X.-Q., Yang, Z., Tong, Y., Han, Z., 2015. A revised paleomagnetic pole from the mid-Neoproterozoic Liantuo Formation in the Yangtze block and its paleogeographic implications. Precambrian Res. 268, 194–211. https://doi.org/10.1016/j.precamres.2015.07.007.

Johnson, R.J.E., Van der Voo, R., 1985. Middle Cambrian paleomagnetism of the Avalon Terrane in Cape Breton Island, Nova Scotia. Tectonics 4, 629–651. https://doi.org/10.1029/TC004i007p00629.

Johnson, R.J.E., Van Der Voo, R., 1990. Pre-folding magnetization reconfirmed for the Late Ordovician-Early Silurian Dunn Point volcanics, Nova Scotia. Tectonophysics 178, 193–205. https://doi.org/10.1016/0040-1951(90)90146-Y.

Johnson, P.R., Andresen, A., Collins, A.S., Fowler, A.R., Fritz, H., Ghebreab, W., Kusky, T., Stern, R.J., 2011. Late Cryogenian–Ediacaran history of the Arabian–Nubian Shield: a review of depositional, plutonic, structural, and tectonic events in the closing stages of the northern East African Orogen. J. Afr. Earth. Sci. 61 (3), 167–232. https://doi.org/10.1016/j.jafrearsci.2011.07.003.

Just, J., Schulz, B., de Wall, H., Jourdan, F., Pandit, M.K., 2011. Monazite CHIME/EPMA dating of Erinpura granitoid deformation: Implications for Neoproterozoic tectono-thermal evolution of NW India. Gondwana Res. 19, 402–412. https://doi.org/10.1016/j.gr.2010.08.002.

Kamo, S.L., Gower, C.F., 1994. Note: U-Pb baddeleyite dating clarifies age of characteristic paleomagnetic remanence of Long Range dykes, southeastern Labrador. Atlantic Geol. 259–262. https://doi.org/10.4138/2133.

Karlsen, K.S., Conrad, C.P., Magni, V., 2019. Deep Water Cycling and Sea Level Change Since the Breakup of Pangea. Geochem. Geophys. Geosyst. 20, 2919–2935. https://doi.org/10.1029/2019GC008232.

Keppie, J.D., Dostal, J., 1998. Birth of the Avalon arc in Nova Scotia, Canada: geochemical evidence for 700–630 Ma back-arc rift volcanism off Gondwana. Geol. Mag. 135 (2), 171–181. https://doi.org/10.1017/S0016756898008322.

Keppie, J.D., Davis, D.W., Krogh, T.E., 1998. U-Pb geochronological constraints on Precambrian stratified units in the Avalon Composite Terrane of Nova Scotia, Canada: tectonic implications. Can. J. Earth Sci. 35, 222–236. https://doi.org/10.1139/e97-109.

Khramov, A.N., Iosifidi, A.G., 2009. Paleomagnetism of the Lower Ordovician and Cambrian sedimentary rocks in the section of the Narva river right bank: For the construction of the Baltic kinematic model in the Early Paleozoic. Izv. Phys. Solid Earth 45, 465–481.

Kirschvink, J.L., Ripperdan, R.L., Evans, D.A., 1997. Evidence for a Large-Scale Reorganization of Early Cambrian Continental Masses by Inertial Interchange True Polar Wander. Science 277, 541–545. https://doi.org/10.1126/science.277.5325.541.

Knesel, K.M., Cohen, B.E., Vasconcelos, P.M., Thiede, D.S., 2008. Rapid change in drift of the Australian plate records collision with Ontong Java plateau. Nature 454, 754–757. https://doi.org/10.1038/nature07138.

Konstantinovskaya, E.A., 2002. The mechanism of continental crust accretion: an example of Western Kamchatka. Geotectonics/Geotektonika 36 (5), 393–411.

Krogh, T.E., Strong, D.F., O'Brien, S.J., Papezik, V.S., 1988. Precise U–Pb zircon dates from the Avalon Terrane in Newfoundland. Can. J. Earth Sci. 25, 442–453. https://doi.org/10.1139/e88-045.

Kröner, A., Alexeiev, D.V., Hegner, E., Rojas-Agramonte, Y., Corsini, M., Chao, Y., Wong, J., Windley, B.F., Liu, D., Tretyakov, A.A., 2012. Zircon and muscovite ages, geochemistry, and Nd–Hf isotopes for the Aktyuz metamorphic terrane: Evidence for an Early Ordovician collisional belt in the northern Tianshan of Kyrgyzstan. Gondwana Res. 21, 901–927. https://doi.org/10.1016/j.gr.2011.05.010.

Kröner, A., Windley, B.F., Badarch, G., Tomurtogoo, O., Hegner, E., Jahn, B.M., Gruschka, S., Khain, E.V., Demoux, A., Wingate, M.T.D., 2007. Accretionary growth and crust formation in the Central Asian Orogenic Belt and comparison with the Arabian-Nubian shield. Memoirs-Geological Society of America 200, 181.

Lapique, F., Bertrand, J.M., Meriem, D., 1986. A major Pan-African crustal decoupling zone in the Timgaouine area (Western Hoggar, Algeria). J. Afr. Earth Sci. (1983). https://doi.org/10.1016/0899-5362(86)90028-x.

Lenton, T.M., Dahl, T.W., Daines, S.J., Mills, B.J.W., Ozaki, K., Saltzman, M.R., Porada, P., 2016. Earliest land plants created modern levels of atmospheric oxygen. Proc. Natl. Acad. Sci. U. S. A. 113, 9704–9709. https://doi.org/10.1073/pnas.1604787113.

Levashova, N.M., Bazhenov, M.L., Meert, J.G., Kuznetsov, N.B., Golovanova, I.V., Danukalov, K.N., Fedorova, N.M., 2013. Paleogeography of Baltica in the Ediacaran: Paleomagnetic and geochronological data from the clastic Zigan Formation, South Urals. Precambrian Res. 236, 16–30. https://doi.org/10.1016/j.precamres.2013.06.006.

Li, M., McNamara, A.K., 2013. The difficulty for subducted oceanic crust to accumulate at the Earth's core-mantle boundary. J. Geophys. Res. [Solid Earth] 118, 1807–1816.

Li, Z.-X., Zhong, S., 2009. Supercontinent–superplume coupling, true polar wander and plume mobility: Plate dominance in whole-mantle tectonics. Phys. Earth Planet. Inter. 176, 143–156. https://doi.org/10.1016/j.pepi.2009.05.004.

Li, Z.-X., Zhang, L., Powell, C.M., 1995. South China in Rodinia: Part of the missing link between Australia–East Antarctica and Laurentia? Geology 23 (5), 407–410. https://doi.org/10.1130/0091-7613(1995)023<0407:SCIRPO>2.3.CO;2.

Li, Z.X., Evans, D.A.D., Zhang, S., 2004. A 90° spin on Rodinia: possible causal links between the Neoproterozoic supercontinent, superplume, true polar wander and low-latitude glaciation. Earth Planet. Sci. Lett. 220, 409–421. https://doi.org/10.1016/S0012-821X(04)00064-0.

Li, Z.X., Bogdanova, S.V., Collins, A.S., Davidson, A., De Waele, B., Ernst, R.E., Fitzsimons, I.C.W., Fuck, R.A., Gladkochub, D.P., Jacobs, J., Karlstrom, K.E., Lu, S., Natapov, L.M., Pease, V., Pisarevsky, S.A., Thrane, K., Vernikovsky, V., 2008. Assembly, configuration, and break-up history of Rodinia: A synthesis. Precambrian Res. 160, 179–210. https://doi.org/10.1016/j.precamres.2007.04.021.

Li, Z.-X., Evans, D.A.D., Halverson, G.P., 2013. Neoproterozoic glaciations in a revised global palaeogeography from the breakup of Rodinia to the assembly of Gondwanaland. Sediment. Geol. 294, 219–232. https://doi.org/10.1016/j.sedgeo.2013.05.016.

Li, Z., Ding, L., Lippert, P.C., Song, P., Yue, Y., van Hinsbergen, D.J.J., 2016. Paleomagnetic constraints on the Mesozoic drift of the Lhasa terrane (Tibet) from Gondwana to Eurasia. Geology 44, 727–730. https://doi.org/10.1130/G38030.1.

Li, Z., Ding, L., Song, P., Fu, J., Yue, Y., 2017. Paleomagnetic constraints on the paleolatitude of the Lhasa block during the Early Cretaceous: implications for the onset of India–Asia collision and latitudinal shortening estimates across Tibet and stable Asia. Gondwana Res. 41, 352–372. https://doi.org/10.1016/j.gr.2015.05.013.

Li, Yianping, McWillams, M., Sharps, R., Cox, A., Li, Yongan, Li, Q., Gao, Z., Zhang, Z., Zhai, Y., 1990. A Devonian paleomagnetic pole from red beds of the Tarim Block, China. J. Geophys. Res., Geodyn. Ser. 95, 19185. https://doi.org/10.1029/JB095iB12p19185.

Li, Z.X., Mitchell, R.N., Spencer, C.J., Ernst, R., Pisarevsky, S., Kirscher, U., Murphy, J.B., 2019. Decoding Earth's rhythms: modulation of supercontinent cycles by longer superocean episodes. Precambrian Res. 323, 1–5. https://doi.org/10.1016/j.precamres.2019.01.009.

Liégeois, J.P., Black, R., Navez, J., Latouche, L., 1994. Early and late Pan-African orogenies in the Aïr assembly of terranes (Tuareg shield, Niger). Precambrian Res. 67, 59–88. https://doi.org/10.1016/0301-9268(94)90005-1.

Liégeois, J.P., Latouche, L., Boughrara, M., Navez, J., Guiraud, M., 2003. The LATEA metacraton (Central Hoggar, Tuareg shield, Algeria): behaviour of an old passive margin during the Pan-African orogeny. J. Afr. Earth. Sci. 37, 161–190. https://doi.org/10.1016/j.jafrearsci.2003.05.004.

Liu, L., Spasojevic, S., Gurnis, M., 2008. Reconstructing Farallon plate subduction beneath North America back to the Late Cretaceous. Science 322, 934–938. https://doi.org/10.1126/science.1162921.

Liu, L., Gurnis, M., Seton, M., Saleeby, J., Müller, R.D., Jackson, J.M., 2010. The role of oceanic plateau subduction in the Laramide orogeny. Nat. Geosci. 3, 353–357. https://doi.org/10.1038/ngeo829.

Liu, X., Zhao, Y., Chen, H., Song, B., 2017. New zircon U–Pb and Hf–Nd isotopic constraints on the timing of magmatism, sedimentation and metamorphism in the northern Prince Charles Mountains, East Antarctica. Precambrian Res. 299, 15–33. https://doi.org/10.1016/j.precamres.2017.07.012.

Lixin, B., Rixiang, Z., Harming, W., Bin, G., Jianjun, L., 1998. New Cambrian paleomagnetic pole for Yangtze Block. Sci. China Ser. D Earth Sci. 41, 66–71. https://doi.org/10.1007/BF02984514.

Llanos, M.P.I., Tait, J.A., Popov, V., Abalmassova, A., 2005. Palaeomagnetic data from Ediacaran (Vendian) sediments of the Arkhangelsk region, NW Russia: An alternative apparent polar wander path of Baltica for the Late Proterozoic–Early Palaeozoic. Earth Planet. Sci. Lett. 240, 732–747. https://doi.org/10.1016/j.epsl.2005.09.063.

Loucks, V., Elmore, D.R., 1986. Absolute dating of dedolomitization and the origin of magnetization in the Cambrian Morgan Creek Limestone, central Texas. GSA Bulletin 97 (4), 486–496. https://doi.org/10.1130/0016-7606(1986)97<486:ADODAT>2.0.CO;2.

Lubnina, N.V., Iosifidi, A.G., Khramov, A.N., Popov, V.V., Lewandowski, M., 2007. Paleomagnetism of the Silurian and Devoni-an sedimentary formations of Podolia, Ukraine. In: Khramov, A.N. (Ed.), Paleomagnetism of the Northern Eurasia Sedimentary Basins (IN RUSSIAN), pp. 105–125.

Lubnina, N.V., Pisarevsky, S.A., Puchkov, V.N., Kozlov, V.I., Sergeeva, N.D., 2014. New paleomagnetic data from Late Neoproterozoic sedimentary successions in Southern Urals, Russia: implications for the Late Neoproterozoic paleogeography of the Iapetan realm. Int. J. Earth Sci. 103, 1317–1334. https://doi.org/10.1007/s00531-014-1013-x.

Macdonald, F.A., Prave, A.R., Petterson, R., Smith, E.F., Pruss, S.B., Oates, K., Waechter, F., Trotzuk, D., Fallick, A.E., 2013. The Laurentian record of Neoproterozoic glaciation, tectonism, and eukaryotic evolution in Death Valley, California. GSA Bulletin 125, 1203–1223. https://doi.org/10.1130/B30789.1.

Martin, M.W., Grazhdankin, D.V., Bowring, S.A., Evans, D.A., Fedonkin, M.A., Kirschvink, J.L., 2000. Age of Neoproterozoic bilatarian body and trace fossils, White Sea, Russia: implications for metazoan evolution. Science 288, 841–845. https://doi.org/10.1126/science.288.5467.841.

Matthews, K.J., Williams, S.E., Whittaker, J.M., Müller, R.D., Seton, M., Clarke, G.L., 2015. Geologic and kinematic constraints on Late Cretaceous to mid Eocene plate boundaries in the southwest Pacific. Earth-Sci. Rev. 140, 72–107. https://doi.org/10.1016/j.earscirev.2014.10.008.

Matthews, K.J., Maloney, K.T., Zahirovic, S., Williams, S.E., Seton, M., Müller, R.D., 2016. Global plate boundary evolution and kinematics since the late Paleozoic. Glob. Planet. Change 146, 226–250. https://doi.org/10.1016/j.gloplacha.2016.10.002.

McCabe, C., Channell, J.E.T., 1990. Paleomagnetic results from volcanic rocks of the Shelve Inlier, Wales: evidence for a wide Late Ordovician Iapetus Ocean in Britain. Earth Planet. Sci. Lett. 96, 458–468. https://doi.org/10.1016/0012-821X(90)90020-X.

McCabe, C., Van der Voo, R., Wilkinson, B.H., Devaney, K., 1985. A Middle/Late Silurian paleomagnetic pole from limestone reefs of the Wabash Formation, Indiana, USA. Journal of Geophysical Research [Solid Earth] 90 (B4), 2959–2965. https://doi.org/10.1029/JB090iB04p02959.

McCabe, C., Channell, J.E.T., Woodcock, N.H., 1992. Further paleomagnetic results from the Builth Wells Ordovician inlier, Wales. Journal of Geophysical Research [Solid Earth] 97 (B6), 9357–9370. https://doi.org/10.1029/92JB00638.

McCausland, P.J.A., Hodych, J.P., 1998. Paleomagnetism of the 550 Ma Skinner Cove volcanics of western Newfoundland and the opening of the Iapetus Ocean. Earth Planet. Sci. Lett. 163, 15–29. https://doi.org/10.1016/S0012-821X(98)00171-X.

McCausland, P.J.A., Van der Voo, R., Hall, C.M., 2007. Circum-Iapetus paleogeography of the Precambrian–Cambrian transition with a new paleomagnetic constraint from Laurentia. Precambrian Res. 156, 125–152. https://doi.org/10.1016/j.precamres.2007.03.004.

McElhinny, M.W., Cowley, J.A., Edwards, D.J., 1978. Palaeomagnetism of some rocks from Peninsular India and Kashmir. Tectonophysics 50, 41–54. https://doi.org/10.1016/0040-1951(78)90198-1.

McGee, B., Halverson, G.P., Collins, A.S., 2012. Cryogenian rift-related magmatism and sedimentation: South-western Congo Craton, Namibia. J. Afr. Earth. Sci. 76, 34–49. https://doi.org/10.1016/j.jafrearsci.2012.09.003.

McKenzie, D.P., Parker, R.L., 1967. The North Pacific: an Example of Tectonics on a Sphere. Nature 216, 1276–1280. https://doi.org/10.1038/2161276a0.

McKenzie, R.N., Hughes, N.C., Gill, B.C., Myrow, P.M., 2014. Plate tectonic influences on Neoproterozoic–early Paleozoic climate and animal evolution. Geology 42, 127–130. https://doi.org/10.1130/G34962.1.

McKerrow, W.S., Mac Niocaill, C., Ahlberg, P.E., Clayton, G., Cleal, C.J., Eagar, R.M.C., 2000. The Late Palaeozoic relations between Gondwana and Laurussia. Geological Society, London, Special Publications 179, 9–20. https://doi.org/10.1144/GSL.SP.2000.179.01.03.

McMenamin, M.A., McMenamin, M.A., McMenamin, D.L.S., 1990. The emergence of animals: the Cambrian breakthrough. Columbia University Press.

Meert, J.G., 2002. Paleomagnetic Evidence for a Paleo-Mesoproterozoic Supercontinent Columbia. Gondwana Res. 5, 207–215. https://doi.org/10.1016/S1342-937X(05)70904-7.

Meert, J.G., 2003. A synopsis of events related to the assembly of eastern Gondwana. Tectonophysics 362, 1–40. https://doi.org/10.1016/S0040-1951(02)00629-7.

Meert, J.G., 2014. Ediacaran–Early Ordovician paleomagnetism of Baltica: A review. Gondwana Res. 25, 159–169. https://doi.org/10.1016/j.gr.2013.02.003.

Meert, J.G., Lieberman, B.S., 2008. The Neoproterozoic assembly of Gondwana and its relationship to the Ediacaran–Cambrian radiation. Gondwana Res. 14, 5–21. https://doi.org/10.1016/j.gr.2007.06.007.

Meert, J.G., van der Voo, R., Ayub, S., 1995. Paleomagnetic investigation of the Neoproterozoic Gagwe lavas and Mbozi complex, Tanzania and the assembly of Gondwana. Precambrian Res. 74, 225–244. https://doi.org/10.1016/0301-9268(95)00012-T.

Meert, J.G., Pandit, M.K., Pradhan, V.R., Banks, J., Sirianni, R., Stroud, M., Newstead, B., Gifford, J., 2010. Precambrian crustal evolution of Peninsular India: A 3.0 billion year odyssey. J. Asian Earth Sci. 39, 483–515. https://doi.org/10.1016/j.jseaes.2010.04.026.

Meert, J.G., Pandit, M.K., Kamenov, G.D., 2013. Further geochronological and paleomagnetic constraints on Malani (and pre-Malani) magmatism in NW India. Tectonophysics 608, 1254–1267. https://doi.org/10.1016/j.tecto.2013.06.019.

Meffre, S., Direen, N.G., Crawford, A.J., Kamenetsky, V., 2004. Mafic volcanic rocks on King Island, Tasmania: evidence for 579 Ma break-up in east Gondwana. Precambrian Res. 135 (3), 177–191. https://doi.org/10.1016/j.precamres.2004.08.004.

Merdith, A.S., Collins, A.S., Williams, S.E., Pisarevsky, S., Foden, J.D., Archibald, D.B., Blades, M.L., Alessio, B.L., Armistead, S., Plavsa, D., Clark, C., Müller, R.D., 2017a. A full-plate global reconstruction of the Neoproterozoic. Gondwana Res. 50, 84–134. https://doi.org/10.1016/j.gr.2017.04.001.

Merdith, A.S., Williams, S.E., Müller, R.D., Collins, A.S., 2017b. Kinematic constraints on the Rodinia to Gondwana transition. Precambrian Res. 299, 132–150. https://doi.org/10.1016/j.precamres.2017.07.013.

Merdith, A.S., Atkins, S.E., Tetley, M.G., 2019a. Tectonic Controls on Carbon and Serpentinite Storage in Subducted Upper Oceanic Lithosphere for the Past 320 Ma. Front Earth Sci. Chin. 7, 332. https://doi.org/10.3389/feart.2019.00332.

Merdith, A.S., Williams, S.E., Brune, S., Collins, A.S., Müller, R.D., 2019b. Rift and plate boundary evolution across two supercontinent cycles. Glob. Planet. Change 173, 1–14. https://doi.org/10.1016/j.gloplacha.2018.11.006.

Metcalfe, I., 2011. Palaeozoic–Mesozoic history of SE Asia. Geological Society, London, Special Publications 355, 7–35. https://doi.org/10.1144/SP355.2.

Metcalfe, I., 2013. Gondwana dispersion and Asian accretion: Tectonic and palaeogeographic evolution of eastern Tethys. J. Asian Earth Sci. 66, 1–33. https://doi.org/10.1016/j.jseaes.2012.12.020.

Metelkin, D.V., Vernikovsky, V.A., Kazansky, A.Y., 2012. Tectonic evolution of the Siberian paleocontinent from the Neoproterozoic to the Late Mesozoic: paleomagnetic record and reconstructions. Russ. Geol. Geophys. 53, 675–688. https://doi.org/10.1016/j.rgg.2012.05.006.

Miller, J.D., Kent, D.V., 1988. Paleomagnetism of the Silurian-Devonian Andreas redbeds: Evidence for an Early Devonian supercontinent? Geology 16 (3), 195–198. https://doi.org/10.1130/0091-7613(1988)016<0195:POTSDA>2.3.CO;2.

Mills, B., Watson, A.J., Goldblatt, C., Boyle, R., Lenton, T.M., 2011. Timing of Neoproterozoic glaciations linked to transport-limited global weathering. Nat. Geosci. 4, 861–864. https://doi.org/10.1038/ngeo1305.

Mills, B.J.W., Krause, A.J., Scotese, C.R., Hill, D.J., Shields, G.A., Lenton, T.M., 2019. Modelling the long-term carbon cycle, atmospheric CO2, and Earth surface temperature from late Neoproterozoic to present day. Gondwana Res. 67, 172–186. https://doi.org/10.1016/j.gr.2018.12.001.

Millward, D., Evans, J.A., 2003. U–Pb chronology and duration of late Ordovician magmatism in the English Lake District. J. Geol. Soc. London 160, 773–781. https://doi.org/10.1144/0016-764902-160.

Minh, P., Hieu, P.T., Thuy, N.T.B., Dung, L.T., Kawaguchi, K., Dung, P.T., 2020. Neoproterozoic granitoids from the Phan Si Pan Zone, NW Vietnam: geochemistry and geochronology constraints on reconstructing South China–India Palaeogeography. Int. Geol. Rev. 1–16. https://doi.org/10.1080/00206814.2020.1728584.

Minibaev, R.A., Sulutdinov, R.M., 1991. Paleomagnitniye kharakteristiki siluriyskikh obrazovanii sakmarskoy zoni Yuzhnogo Urala. Bashkirian Natl.Cttee.Ural.Branch Acad.Sci.USSR (Ufa) 3, 30.

Mitchell, R.N., Kilian, T.M., Evans, D.A.D., 2012. Supercontinent cycles and the calculation of absolute palaeolongitude in deep time. Nature 482, 208–211. https://doi.org/10.1038/nature10800.

Moores, E.M., 1991. Southwest U.S.-East Antarctic (SWEAT) connection: A hypothesis. Geology 19 (5), 425–428. https://doi.org/10.1130/0091-7613(1991)019<0425:SUSEAS>2.3.CO;2.

Moores, E.M., 2002. Pre–1 Ga (pre-Rodinian) ophiolites: Their tectonic and environmental implications. GSA Bulletin 114 (1), 80–95. https://doi.org/10.1130/0016-7606(2002)114<0080:PGPROT>2.0.CO;2.

Morgan, W.J., 1968. Rises, trenches, great faults, and crustal blocks. J. Geophys. Res. 73, 1959–1982. https://doi.org/10.1029/JB073i006p01959.

Morrison, J., Ellwood, B.B., 1986. Paleomagnetism of Silurian-Ordovician sediments from the Valley and Ridge province, northwest Georgia. Geophys. Res. Lett. 13 (3), 189–192. https://doi.org/10.1029/GL013i003p00189.

Mulder, J.A., Halpin, J.A., Daczko, N.R., 2015. Mesoproterozoic Tasmania: Witness to the East Antarctica–Laurentia connection within Nuna. Geology 43, 759–762. https://doi.org/10.1130/G36850.1.

Mulder, J.A., Berry, R.F., Halpin, J.A., Meffre, S., Everard, J.L., 2018a. Depositional age and correlation of the Oonah Formation: refining the timing of Neoproterozoic basin formation in Tasmania. Aust. J. Earth Sci. 65, 391–407. https://doi.org/10.1080/08120099.2018.1426629.

Mulder, J.A., Karlstrom, K.E., Halpin, J.A., Merdith, A.S., Spencer, C.J., Berry, R.F., McDonald, B., 2018b. Rodinian devil in disguise: Correlation of 1.25–1.10 Ga strata between Tasmania and Grand Canyon. Geology 46, 991–994. https://doi.org/10.1130/G45225.1.

Mulder, J.A., Halpin, J.A., Daczko, N.R., Orth, K., Meffre, S., Thompson, J.M., Morrissey, L.J., 2019. A Multiproxy provenance approach to uncovering the assembly of East Gondwana in Antarctica. Geology 47, 645–649. https://doi.org/10.1130/G45952.1.

Mulder, J.A., Everard, J.L., Cumming, G., Meffre, S., Bottrill, R.S., Merdith, A.S., Halpin, J.A., McNeill, A.W., Cawood, P.A., 2020. Neoproterozoic opening of the Pacific Ocean recorded by multi-stage rifting in Tasmania, Australia. Earth-Sci. Rev. 201, 103041 https://doi.org/10.1016/j.earscirev.2019.103041.

Müller, R.D., Royer, J.-Y., Lawver, L.A., 1993. Revised plate motions relative to the hotspots from combined Atlantic and Indian Ocean hotspot tracks. Geology 21 (3), 275–278. https://doi.org/10.1130/0091-7613(1993)021<0275:RPMRTT>2.3.CO;2.

Müller, R.D., Sdrolias, M., Gaina, C., Steinberger, B., Heine, C., 2008. Long-term sea-level fluctuations driven by ocean basin dynamics. Science 319, 1357–1362. https://doi.org/10.1126/science.1151540.

Müller, R.D., Seton, M., Zahirovic, S., Williams, S.E., Matthews, K.J., Wright, N.M., Shephard, G.E., Maloney, K.T., Barnett-Moore, N., Hosseinpour, M., Bower, D.J., Cannon, J., 2016. Ocean Basin Evolution and Global-Scale Plate Reorganization Events Since Pangea Breakup. Annu. Rev. Earth Planet. Sci. 44, 107–138. https://doi.org/10.1146/annurev-earth-060115-012211.

Müller, R.D., Cannon, J., Qin, X., Watson, R.J., Gurnis, M., Williams, S., Pfaffelmoser, T., Seton, M., Russell, S.H.J., Zahirovic, S., 2018. GPlates: Building a Virtual Earth Through Deep Time. Geochem. Geophys. Geosyst. 19, 2243–2261. https://doi.org/10.1029/2018GC007584.

Müller, R.D., Zahirovic, S., Williams, S.E., Cannon, J., Seton, M., Bower, D.J., Tetley, M., Heine, C., Le Breton, E., Liu, S., Russell, S.H.J., Yang, T., Leonard, J., Gurnis, M., 2019. A global plate model including lithospheric deformation along major rifts and orogens since the Triassic. Tectonics. https://doi.org/10.1029/2018TC005462.

Murphy, J.B., 2002. Geochemistry of the Neoproterozoic metasedimentary Gamble Brook Formation, Avalon terrane, Nova Scotia: evidence for a rifted-arc environment along the west Gondwanan margin of Rodinia. J. Geol. 110 (4), 407–419. https://doi.org/10.1086/340630.

Murphy, J.B., Nance, R.D., 1989. Model for the evolution of the Avalonian-Cadomian belt. Geology 17 (8), 735–738. https://doi.org/10.1130/0091-7613(1989)017<0735:MFTEOT>2.3.CO;2.

Murphy, J.B., Keppie, J.D., Dostal, J., Nance, R.D., 1999. Neoproterozoic-early Paleozoic evolution ofAvalonia. Laurentia-Gondwana Connections Before Pangea 336, 253–266. https://doi.org/10.1130/0-8137-2336-1.253.

Murphy, J.B., Strachan, R.A., Nance, R.D., Parker, K.D., Fowler, M.B., 2000. Proto-Avalonia: A 1.2–1.0 Ga tectonothermal event and constraints for the evolution of Rodinia. Geology 28 (12), 1071–1074. https://doi.org/10.1130/0091-7613(2000)28<1071:PAGTEA>2.0.CO;2.

Murphy, J.B., Pisarevsky, S.A., Nance, R.D., Keppie, J.D., 2004. Neoproterozoic—Early Paleozoic evolution of peri-Gondwanan terranes: implications for Laurentia-Gondwana connections. Int. J. Earth Sci. 93, 659–682. https://doi.org/10.1007/s00531-004-0412-9.

Murphy, J.B., Waldron, J.W.F., Kontak, D.J., Pe-Piper, G., Piper, D.J.W., 2011. Minas Fault Zone: Late Paleozoic history of an intra-continental orogenic transform fault in the Canadian Appalachians. J. Struct. Geol. 33, 312–328. https://doi.org/10.1016/j.jsg.2010.11.012.

Murthy, G., Gower, C., Tubrett, M., Pätzold, R., 1992. Paleomagnetism of Eocambrian Long Range dykes and Double Mer Formation from Labrador, Canada. Can. J. Earth Sci. 29, 1224–1234. https://doi.org/10.1139/e92-098.

Nance, R.D., Linnemann, U., 2008. The Rheic Ocean: origin, evolution, and significance. GSA Today 18 (12), 4–12. https://doi.org/10.1130/GSATG24A.1.

Nance, R.D., Murphy, J.B., Strachan, R.A., Keppie, J.D., Gutiérrez-Alonso, G., Fernández-Suárez, J., Quesada, C., Linnemann, U., D'lemos, R., Pisarevsky, S.A., 2008. Neoproterozoic-early Palaeozoic tectonostratigraphy and palaeogeography of the

peri-Gondwanan terranes: Amazonian v. West African connections. Geological Society, London, Special Publications 297, 345–383. https://doi.org/10.1144/SP297.17.
Nick, K.E., Elmore, R.D., 1990. Paleomagnetism of the Cambrian Royer Dolomite and Pennsylvanian Collings Ranch Conglomerate, southern Oklahoma: An early Paleozoic magnetization and nonpervasive remagnetization by weathering. Geol. Soc. Am. Bull. 102 (11), 1517–1525. https://doi.org/10.1130/0016-7606(1990)102<1517:POTCRD>2.3.CO;2.
Niu, J., Li, Z.-X., Zhu, W., 2016. Palaeomagnetism and geochronology of mid-Neoproterozoic Yanbian dykes, South China: implications for a c. 820–800 Ma true polar wander event and the reconstruction of Rodinia. Geological Society, London, Special Publications 424, 191–199. https://doi.org/10.1144/SP424.11.
Noel, J.R., Spariosu, D.J., Dallmeyer, R.D., 1988. Paleomagnetism and 40Ar/39Ar ages from the Carolina slate belt, Albemarle, North Carolina: Implications for terrane amalgamation with North America. Geology 16 (1), 64–68. https://doi.org/10.1130/0091-7613(1988)016<0064:PAAAAF>2.3.CO;2.
O'Brien, S.J., Dunning, G.R., Dube, B., O'Driscoll, C.F., Sparkes, B., Israel, S., Ketchum, J., 2001. New insights into the Neoproterozoic geology of the central Avalon Peninsula (parts of NTS map areas 1N/6, 1N/7 and 1N/3), eastern Newfoundland. In: Current Research. Newfoundland Department of Mines and Energy, pp. 169–189 (Geological Survey Report, 2001-1).
O'Neill, C., Müller, D., Steinberger, B., 2005. On the uncertainties in hot spot reconstructions and the significance of moving hot spot reference frames. Geochem. Geophys. Geosyst., Spec. Pap. Geol. Soc. Am 6. https://doi.org/10.1029/2004GC000784.
Opdyke, N.D., Huang, K., Xu, G., Zhang, W.Y., Kent, D.V., 1987. Paleomagnetic results from the Silurian of the Yangtze paraplatform. Tectonophysics 139, 123–132. https://doi.org/10.1016/0040-1951(87)90201-0.
Palin, R.M., Santosh, M., Cao, W., Li, S.S., Hernández-Uribe, D., Parsons, A., 2020. Secular change and the onset of plate tectonics on Earth. Earth-Sci. Rev. 207, 103172. https://doi.org/10.1016/j.earscirev.2020.103172.
Pan, B., Brock, G.A., Skovsted, C.B., Betts, M.J., Topper, T.P., Li, G., 2018. Paterimitra pyramidalis Laurie, 1986, the first tommotiid discovered from the early Cambrian of North China. Gondwana Res. 63, 179–185. https://doi.org/10.1016/j.gr.2018.05.014.
Pandit, M.K., Carter, L.M., Ashwal, L.D., Tucker, R.D., Torsvik, T.H., Jamtveit, B., Bhushan, S.K., 2003. Age, petrogenesis and significance of 1 Ga granitoids and related rocks from the Sendra area, Aravalli Craton, NW India. J. Asian Earth Sci. 22 (4), 363–381. https://doi.org/10.1016/S1367-9120(03)00070-1.
Paquette, J.L., Caby, R., Djouadi, M.T., Bouchez, J.L., 1998. U–Pb dating of the end of the Pan-African orogeny in the Tuareg shield: the post-collisional syn-shear Tioueine pluton (Western Hoggar, Algeria). Lithos 45, 245–253. https://doi.org/10.1016/S0024-4937(98)00034-6.
Parsons, A.J., Hosseini, K., Palin, R.M., Sigloch, K., 2020. Geological, geophysical and plate kinematic constraints for models of the India-Asia collision and the post-Triassic central Tethys oceans. Earth-Sci. Rev. 208, 103084 https://doi.org/10.1016/j.earscirev.2020.103084.
Pavlov, V., Gallet, Y., 1998. Upper Cambrian to Middle Ordovician magnetostratigraphy from the Kulumbe river section (northwestern Siberia). Phys. Earth Planet. Inter. 108, 49–59. https://doi.org/10.1016/S0031-9201(98)00087-9.
Pavlov, V., Bachtadse, V., Mikhailov, V., 2008. New Middle Cambrian and Middle Ordovician palaeomagnetic data from Siberia: Llandelian magnetostratigraphy and relative rotation between the Aldan and Anabar–Angara blocks. Earth Planet. Sci. Lett. 276 (3–4), 229–242. https://doi.org/10.1016/j.epsl.2008.06.021.
Pavlov, V.E., Veselovskiy, R.V., Shatsillo, A.V., Gallet, Y., 2012. Magnetostratigraphy of the Ordovician Angara/Rozhkova River section: Further evidence for the Moyero reversed superchron. Izv. Phys. Solid Earth 48, 297–305. https://doi.org/10.1134/S1069351312040052.
Pavlov, V.E., Shatsillo, A.V., Petrov, P.Y., 2015. Paleomagnetism of the upper Riphean deposits in the Turukhansk and Olenek uplifts and Uda Pre-Sayan region and the neoproterozoic drift of the Siberian Platform. Izv. Phys. Solid Earth 51, 716–747. https://doi.org/10.1134/S1069351315050092.
Pedrosa-Soares, A.C., Noce, C.M., Wiedemann, C.M., Pinto, C.P., 2001. The Araçuaí-West-Congo Orogen in Brazil: an overview of a confined orogen formed during Gondwanaland assembly. Precambrian Res. 110 (1–4), 307–323. https://doi.org/10.1016/S0301-9268(01)00174-7.
Pehrsson, S.J., Berman, R.G., Eglington, B., Rainbird, R., 2013. Two Neoarchean supercontinents revisited: The case for a Rae family of cratons. Precambrian Res. 232, 27–43. https://doi.org/10.1016/j.precamres.2013.02.005.
Peng, Y., Yu, S., Li, S., Zhang, J., Liu, Y., Li, Y., Santosh, M., 2019. Early Neoproterozoic magmatic imprints in the Altun-Qilian-Kunlun region of the Qinghai-Tibet Plateau: Response to the assembly and breakup of Rodinia supercontinent. Earth-Sci. Rev. 199, 102954 https://doi.org/10.1016/j.earscirev.2019.102954.
Pisarevsky, S., Bylund, G., 1998. Neoproterozoic palaeomagnetic directions in rocks from a key section of the Protogine Zone, southern Sweden. Geophys. J. Int. 133, 185–200. https://doi.org/10.1046/j.1365-246X.1998.1331497.x.
Pisarevsky, S.A., Natapov, L.M., 2003. Siberia and Rodinia. Tectonophysics 375, 221–245. https://doi.org/10.1016/j.tecto.2003.06.001.
Pisarevsky, S.A., Gurevich, E.L., Khramov, A.N., 1997. Palaeomagnetism of Lower Cambrian sediments from the Olenek River section (northern Siberia): palaeopoles and the problem of magnetic polarity in the Early Cambrian. Geophys. J. Int. 130, 746–756. https://doi.org/10.1111/j.1365-246X.1997.tb01869.x.
Pisarevsky, S.A., Wingate, M.T.D., Stevens, M.K., Haines, P.W., 2007. Palaeomagnetic results from the Lancer 1 stratigraphic drillhole, Officer Basin, Western Australia, and implications for Rodinia reconstructions. Aust. J. Earth Sci. 54, 561–572. https://doi.org/10.1080/08120090701188962.
Pisarevsky, S.A., Murphy, J.B., Cawood, P.A., Collins, A.S., 2008. Late Neoproterozoic and Early Cambrian palaeogeography: models and problems. Geological Society, London, Special Publications 294, 9–31. https://doi.org/10.1144/SP294.2.
Pisarevsky, S.A., Gladkochub, D.P., Konstantinov, K.M., Mazukabzov, A.M., Stanevich, A.M., Murphy, J.B., Tait, J.A., Donskaya, T.V., Konstantinov, I.K., 2013. Paleomagnetism of Cryogenian Kitoi mafic dykes in South Siberia: Implications for Neoproterozoic paleogeography. Precambrian Res. 231, 372–382. https://doi.org/10.1016/j.precamres.2013.04.007.
Pisarevsky, S.A., Elming, S.-Å., Pesonen, L.J., Li, Z.-X., 2014. Mesoproterozoic paleogeography: Supercontinent and beyond. Precambrian Res. 244, 207–225. https://doi.org/10.1016/j.precamres.2013.05.014.
Plavsa, D., Collins, A.S., Foden, J.D., Clark, C., 2015. The evolution of a Gondwanan collisional orogen: A structural and geochronological appraisal from the Southern Granulite Terrane, South India. Tectonics 34 (5), 820–857. https://doi.org/10.1002/2014TC003706.
Popov, V., Iosifidi, A., Khramov, A., Tait, J., Bachtadse, V., 2002. Paleomagnetism of Upper Vendian sediments from the Winter Coast, White Sea region, Russia: implications for the paleogeography of Baltica during Neoproterozoic times. J. Geophys. Res. [Solid Earth] 107 (B11), 1–8. https://doi.org/10.1029/2001JB001607.
Popov, V.V., Khramov, A.N., Bachtadse, V., 2005. Palaeomagnetism, magnetic stratigraphy, and petromagnetism of the Upper Vendian sedimentary rocks in the sections of the Zolotitsa River and in the Verkhotina Hole, Winter Coast of the White Sea, Russia. Russian Journal of Earth Sciences 7.
Powell, C.M., Pisarevsky, S.A., 2002. Late Neoproterozoic assembly of East Gondwana. Geology 30 (1), 3–6. https://doi.org/10.1130/0091-7613(2002)030<0003:LNAOEG>2.0.CO;2.
Powerman, V., Shatsillo, A., Coe, R., Zhao, X., Gladkochub, D., Buchwaldt, R., Pavlov, V., 2013. Palaeogeography of the Siberian platform during middle Palaeozoic Times (450–400 Ma): new palaeomagnetic evidence from the Lena and Nyuya rivers. Geophys. J. Int. 194 (3), 1412–1440. https://doi.org/10.1093/gji/ggt197.
Qiantao, B., Shanlin, G., Dihui, L., Zhengren, Y., Chengfa, C., Xiaoquan, L., 2001. A study of the Kunlun-Qilian-Qinling suture system. Acta Geologica Sinica-English Edition 75, 364–374.
Rapalini, A.E., 2006. New late Proterozoic paleomagnetic pole for the Rio de la Plata craton: Implications for Gondwana. Precambrian Res. 147, 223–233. https://doi.org/10.1016/j.precamres.2006.01.016.
Rapalini, A.E., Cingolani, C.A., 2004. First Late Ordovician Paleomagnetic Pole for the Cuyania (Precordillera) Terrane of Western Argentina: a Microcontinent or a Laurentian Plateau. Gondwana Res. 7, 1089–1104. https://doi.org/10.1016/S1342-937X(05)71086-8.
Rapalini, A.E., Tohver, E., Bettucci, L.S., Lossada, A.C., Barcelona, H., Pérez, C., 2015. The late Neoproterozoic Sierra de las Ánimas Magmatic Complex and Playa Hermosa Formation, southern Uruguay, revisited: Paleogeographic implications of new paleomagnetic and precise geochronologic data. Precambrian Res. 259, 143–155. https://doi.org/10.1016/j.precamres.2014.11.021.
Raub, T.D., Kirschvink, J.L., Evans, D.A.D., 2007. True polar wander: Linking deep and shallow geodynamics to hydro-and biospheric hypotheses. In: Treatise on geophysics, 5, pp. 565–589.
Raza, M., Khan, A., Bhardwaj, V.R., Rais, S., 2012. Geochemistry of Mesoproterozoic sedimentary rocks of upper Vindhyan Group, southeastern Rajasthan and implications for weathering history, composition and tectonic setting of continental crust in the northern part of Indian shield. J. Asian Earth Sci. 48, 160–172. https://doi.org/10.1016/j.jseaes.2011.11.012.
Robert, B., Besse, J., Blein, O., Greff-Lefftz, M., Baudin, T., Lopes, F., Meslouh, S., Belbadaoui, M., 2017. Constraints on the Ediacaran inertial interchange true polar wander hypothesis: A new paleomagnetic study in Morocco (West African Craton). Precambrian Res. 295, 90–116. https://doi.org/10.1016/j.precamres.2017.04.010.
Robert, B., Domeier, M., Jakob, J., 2020. Iapetan Oceans: An analog of Tethys? Geology 48 (9), 929–933. https://doi.org/10.1130/G47513.1.
Rodionov, V.P., 1966. Dipole character of the Geomagnetic field in the Late Cambrian and the Ordovician in the south of the Siberian Platform. Geol. Geofiz. 1, 94–101.
Rodionov, V.P., Khramov, A.N., Pisarevskii, S.A., Popov, V.V., Iosifidi, A.G., 1998. Geomagnetic Reversals in the Early Paleozoic. 1. A Late Cambrian Reversal Recorded in the Ichera Section, Southern Siberian Platform. Izv. Phys. Solid Earth 34, 1009–1017.
Rodionov, V.P., Dekkers, M.J., Khramov, A.N., Gurevich, E.L., Krijgsman, W., Duermeijer, C.E., Heslop, D., 2003. Paleomagnetism and cyclostratigraphy of the Middle Ordovician Krivolutsky suite, Krivaya Luka section, southern Siberian platform: record of non-synchronous NRM-components or a non-axial geomagnetic field? Studia Geophys. Geodaetica 47, 255–274.
Rogers, J.J.W., Santosh, M., 2002. Configuration of Columbia, a Mesoproterozoic Supercontinent. Gondwana Res. 5, 5–22. https://doi.org/10.1016/S1342-937X(05)70883-2.
Ross, M.I., Scotese, C.R., 1988. A hierarchical tectonic model of the Gulf of Mexico and Caribbean region. Tectonophysics 155 (1–4), 139–168. https://doi.org/10.1016/0040-1951(88)90263-6.
Ruppel, A., Jacobs, J., Eagles, G., Läufer, A., Jokat, W., 2018. New geophysical data from a key region in East Antarctica: Estimates for the spatial extent of the Tonian Oceanic Arc Super Terrane (TOAST). Gondwana Res. 59, 97–107. https://doi.org/10.1016/j.gr.2018.02.019.
Safonova, I., Biske, G., Romer, R.L., Seltmann, R., Simonov, V., Maruyama, S., 2016. Middle Paleozoic mafic magmatism and ocean plate stratigraphy of the South Tianshan, Kyrgyzstan. Gondwana Res. 30, 236–256. https://doi.org/10.1016/j.gr.2015.03.006.

Schellart, W.P., Lister, G.S., Toy, V.G., 2006. A Late Cretaceous and Cenozoic reconstruction of the Southwest Pacific region: Tectonics controlled by subduction and slab rollback processes. Earth-Sci. Rev. 76, 191–233. https://doi.org/10.1016/j.earscirev.2006.01.002.

Scherstén, A., Årebäck, H., Cornell, D., Hoskin, P., Åberg, A., Armstrong, R., 2000. Dating mafic–ultramafic intrusions by ion-microprobing contact-melt zircon: examples from SW Sweden. Contrib. Mineral. Petrol. 139, 115–125. https://doi.org/10.1007/s004100050577.

Schmidt, P.W., Williams, G.E., 1995. The Neoproterozoic climatic paradox: Equatorial palaeolatitude for Marinoan glaciation near sea level in South Australia. Earth Planet. Sci. Lett. 134, 107–124. https://doi.org/10.1016/0012-821X(95)00106-M.

Schmidt, P.W., Williams, G.E., 1996. Palaeomagnetism of the ejecta-bearing Bunyeroo Formation, late Neoproterozoic, Adelaide fold belt, and the age of the Acraman impact. Earth Planet. Sci. Lett. 144, 347–357. https://doi.org/10.1016/S0012-821X(96)00169-0.

Schmidt, P.W., Williams, G.E., 2010. Ediacaran palaeomagnetism and apparent polar wander path for Australia: no large true polar wander. Geophys. J. Int. 182, 711–726. https://doi.org/10.1111/j.1365-246X.2010.04652.x.

Schmidt, P.W., Williams, G.E., Embleton, B.J.J., 1991. Low palaeolatitude of Late Proterozoic glaciation: early timing of remanence in haematite of the Elatina Formation, South Australia. Earth Planet. Sci. Lett. 105, 355–367. https://doi.org/10.1016/0012-821X(91)90177-J.

Schmidt, P.W., Williams, G.E., McWilliams, M.O., 2009. Palaeomagnetism and magnetic anisotropy of late Neoproterozoic strata, South Australia: Implications for the palaeolatitude of late Cryogenian glaciation, cap carbonate and the Ediacaran System. Precambrian Res. 174, 35–52. https://doi.org/10.1016/j.precamres.2009.06.002.

Scotese, C.R., 2004. A Continental Drift Flipbook. J. Geol. 112, 729–741. https://doi.org/10.1086/424867.

Scotese, C.R., 2016. PALEOMAP PaleoAtlas for GPlates and the PaleoData Plotter Program. PALEOMAP Project. See http://www. earthbyte. org/paleomap-paleoatlas-for-gplates.

Seton, M., Müller, R.D., Zahirovic, S., Gaina, C., Torsvik, T., Shephard, G., Talsma, A., Gurnis, M., Turner, M., Maus, S., Chandler, M., 2012. Global continental and ocean basin reconstructions since 200 Ma. Earth-Sci. Rev. 113, 212–270. https://doi.org/10.1016/j.earscirev.2012.03.002.

Shapiro, M.N., Solov'ev, A.V., 2009. Formation of the Olyutorsky–Kamchatka foldbelt: a kinematic model. Russ. Geol. Geophys. 50, 668–681. https://doi.org/10.1016/j.rgg.2008.10.006.

Shatsillo, A.V., Paverman, V.I., Pavlov, V.E., 2007. Middle paleozoic segment of the apparent polar wander path from the Siberian platform: New paleomagnetic evidence for the Silurian of the Nyuya-Berezovskii facial province. Izv. Phys. Solid Earth 43, 880–889. https://doi.org/10.1134/S1069351307100102.

Shephard, G.E., Müller, R.D., Seton, M., 2013. The tectonic evolution of the Arctic since Pangea breakup: Integrating constraints from surface geology and geophysics with mantle structure. Earth-Sci. Rev. 124, 148–183. https://doi.org/10.1016/j.earscirev.2013.05.012.

Shervais, J.W., Dennis, A.J., McGee, J.J., Secor, D., 2003. Deep in the heart of Dixie: Pre-Alleghanian eclogite and HP granulite metamorphism in the Carolina Terrane, South Carolina, USA. J. Metamorph. Geol. 21, 65–80.

Shi, R., Yang, J., Wu, C., Wooden, J., 2004. First SHRIMP dating for the formation of the late Sinian Yushigou Ophiolite, North Qilian Mountains. ACTA GEOLOGICA SINICA-CHINESE EDITION 78, 649–657.

Shi, Y., Zhang, W., Kröner, A., Li, L., Jian, P., 2018. Cambrian ophiolite complexes in the Beishan area, China, southern margin of the Central Asian Orogenic Belt. J. Asian Earth Sci. 153, 193–205. https://doi.org/10.1016/j.jseaes.2017.05.021.

Sigloch, K., Mihalynuk, M.G., 2013. Intra-oceanic subduction shaped the assembly of Cordilleran North America. Nature 496, 50–56. https://doi.org/10.1038/nature12019.

Slagstad, T., Kulakov, E., Kirkland, C.L., Roberts, N.M.W., Ganerød, M., 2019. Breaking the Grenville–Sveconorwegian link in Rodinia reconstructions. Terra Nova 31, 430–437. https://doi.org/10.1111/ter.12406.

Smethurst, M.A., Khramov, A.N., 1992. A new Devonian palaeomagnetic pole for the Russian platform and Baltica, and related apparent polar wander. Geophys. J. Int. 108, 179–192. https://doi.org/10.1111/j.1365-246X.1992.tb00848.x.

Smethurst, M.A., Khramov, A.N., Pisarevsky, S., 1998. Palaeomagnetism of the Lower Ordovician Orthoceras Limestone, St. Petersburg, and a revised drift history for Baltica in the early Palaeozoic. Geophys. J. Int. 133, 44–56. https://doi.org/10.1046/j.1365-246X.1998.1331463.x.

Smirnov, A.V., Evans, D.A.D., Ernst, R.E., Söderlund, U., Li, Z.-X., 2013. Trading partners: Tectonic ancestry of southern Africa and western Australia, in Archean supercratons Vaalbara and Zimgarn. Precambrian Res. 224, 11–22. https://doi.org/10.1016/j.precamres.2012.09.020.

Sohl, L.E., Christie-Blick, N., Kent, D.V., 1999. Paleomagnetic polarity reversals in Marinoan (ca. 600 Ma) glacial deposits of Australia: Implications for the duration of low-latitude glaciation in Neoproterozoic time. GSA Bulletin 111 (8), 1120–1139. https://doi.org/10.1130/0016-7606(1999)111<1120:PPRIMC>2.3.CO;2.

Soldati, G., Boschi, L., Piersanti, A., Spada, G., 2001. The effect of global seismicity on the polar motion of a viscoelastic Earth. J. Geophys. Res. 106, 6761–6767. https://doi.org/10.1029/2000JB900354.

Song, S., Li, X.-H., 2019. A positive test for the Greater Tarim Block at the heart of Rodinia: Mega-dextral suturing of supercontinent assembly: COMMENT. Geology 47 (1), e453. https://doi.org/10.1130/G45470C.1.

Song, S., Niu, Y., Zhang, L., Wei, C., Liou, J.G., Su, L., 2009. Tectonic evolution of early Paleozoic HP metamorphic rocks in the North Qilian Mountains, NW China: New perspectives. J. Asian Earth Sci. 35, 334–353. https://doi.org/10.1016/j.jseaes.2008.11.005.

Song, S., Su, L., Li, X.-H., Niu, Y., Zhang, L., 2012. Grenville-age orogenesis in the Qaidam-Qilian block: The link between South China and Tarim. Precambrian Res. 220–221, 9–22. https://doi.org/10.1016/j.precamres.2012.07.007.

Song, S., Niu, Y., Su, L., Xia, X., 2013. Tectonics of the North Qilian orogen, NW China. Gondwana Res. 23, 1378–1401. https://doi.org/10.1016/j.gr.2012.02.004.

Stampfli, G.M., Borel, G.D., 2002. A plate tectonic model for the Paleozoic and Mesozoic constrained by dynamic plate boundaries and restored synthetic oceanic isochrons. Earth Planet. Sci. Lett. 196, 17–33. https://doi.org/10.1016/S0012-821X(01)00588-X.

Stearn, J.E.F., Piper, J.D.A., 1984. Palaeomagnetism of the Sveconorwegian mobile belt of the Fennoscandian Shield. Precambrian Res. 23 (3–4), 201–246. https://doi.org/10.1016/0301-9268(84)90045-7.

Steinberger, B., Torsvik, T.H., 2008. Absolute plate motions and true polar wander in the absence of hotspot tracks. Nature 452, 620–623. https://doi.org/10.1038/nature06824.

Stern, R.J., 1994. Arc Assembly and Continental Collision in the Neoproterozoic East African Orogen: Implications for the Consolidation of Gondwanaland. Annu. Rev. Earth Planet. Sci. 22, 319–351. https://doi.org/10.1146/annurev.ea.22.050194.001535.

Stern, R.J., Miller, N.R., 2018. Did the transition to plate tectonics cause Neoproterozoic Snowball Earth? Terra Nova 30, 87–94. https://doi.org/10.1111/ter.12321.

Strachan, R.A., Collins, A.S., Buchan, C., Nance, R.D., Murphy, J.B., D'Lemos, R.S., 2007. Terrane analysis along a Neoproterozoic active margin of Gondwana: insights from U–Pb zircon geochronology. J. Geol. Soc. London 164, 57–60. https://doi.org/10.1144/0016-76492006-014.

Sun, L.-S., Huang, B.-C., 2009. New paleomagnetic result for Ordovician rocks from the Tarim Block. Chin. J. Geophy. 52 (7), 1836–1848 (in Chinese with English abstract).

Surkis, Y.F., Rodionov, V.P., Khramov, A.N., Gurevich, E.L., Westfahl, M., 1999. Geomagnetic reversals in the early Paleozoic: 3. Reversals recorded in redbeds of the lower Ordovician Mandra section, Siberia. Izv. Phys. Solid Earth 35, 347–357.

Sutherland, R., Dickens, G.R., Blum, P., Agnini, C., Alegret, L., Asatryan, G., Bhattacharya, J., Bordenave, A., Chang, L., Collot, J., Cramwinckel, M.J., Dallanave, E., Drake, M.K., Etienne, S.J.G., Giorgioni, M., Gurnis, M., Harper, D.T., Huang, H.-H.M., Keller, A.L., Lam, A.R., Li, H., Matsui, H., Morgans, H.E.G., Newsam, C., Park, Y.-H., Pascher, K.M., Pekar, S.F., Penman, D.E., Saito, S., Stratford, W.R., Westerhold, T., Zhou, X., 2020. Continental-scale geographic change across Zealandia during Paleogene subduction initiation. Geology 48 (5), 419–424. https://doi.org/10.1130/G47008.1.

Swanson-Hysell, N.L., Maloof, A.C., Kirschvink, J.L., Evans, D.A.D., Halverson, G.P., Hurtgen, M.T., 2012. Constraints on Neoproterozoic paleogeography and Paleozoic orogenesis from paleomagnetic records of the Bitter Springs Formation, Amadeus Basin, central Australia. Am. J. Sci. 312, 817–884. https://doi.org/10.2475/08.2012.01.

Tetley, M.G., 2018. Constraining Earth's plate tectonic evolution through data mining and knowledge discovery (PhD). The University of Sydney.

Tetley, M.G., Williams, S.E., Gurnis, M., Flament, N., Müller, R.D., 2019. Constraining absolute plate motions since the Triassic. J. Geophys. Res. [Solid Earth]. https://doi.org/10.1029/2019JB017442.

Thomas, R.J., De Waele, B., Schofield, D.I., Goodenough, K.M., Horstwood, M., Tucker, R., Bauer, W., Annells, R., Howard, K., Walsh, G., Rabarimanana, M., Rafahatelo, J.M., Ralison, A.V., Randriamananjara, T., 2009. Geological evolution of the Neoproterozoic Bemarivo Belt, northern Madagascar. Precambrian Res. 172, 279–300. https://doi.org/10.1016/j.precamres.2009.04.008.

Thompson, M.D., Grunow, A.M., Ramezani, J., 2010. Cambro-Ordovician paleogeography of the Southeastern New England Avalon Zone: Implications for Gondwana breakup. GSA Bulletin 122, 76–88. https://doi.org/10.1130/B26581.1.

Thorogood, E.J., 1990. Provenance of the pre-Devonian sediments of England and Wales: Sm-Nd isotopic evidence. J. Geol. Soc. London 147, 591–594. https://doi.org/10.1144/gsjgs.147.4.0591.

Torsvik, T.H., Cocks, L.R.M., 2009. The Lower Palaeozoic palaeogeographical evolution of the northeastern and eastern peri-Gondwanan margin from Turkey to New Zealand. Geological Society, London, Special Publications 325, 3–21. https://doi.org/10.1144/SP325.2.

Torsvik, T.H., Cocks, L.R.M., 2016. Earth History and Palaeogeography. Cambridge University Press, United Kingdom.

Torsvik, T.H., Cocks, L.R.M., 2017. The integration of palaeomagnetism, the geological record and mantle tomography in the location of ancient continents. Geol. Mag. 1–19. https://doi.org/10.1017/S001675681700098X.

Torsvik, T.H., Domeier, M., 2017. Correspondence: Numerical modelling of the PERM anomaly and the Emeishan large igneous province. Nat. Commun. 8, 821. https://doi.org/10.1038/s41467-017-00125-2.

Torsvik, T.H., Rehnström, E.F., 2001. Cambrian palaeomagnetic data from Baltica: implications for true polar wander and Cambrian palaeogeography. J. Geol. Soc. London 158, 321–329. https://doi.org/10.1144/jgs.158.2.321.

Torsvik, T.H., Smethurst, M.A., 1989. GMAP32—Geographic Mapping and Reconstruction System. Geol. Surv of Norway, Oslo, p. 1997.

Torsvik, T.H., Trench, A., 1991. The Lower—Middle Ordovician palaeofield of Scandinavia: southern Sweden revisited. Phys. Earth Planet. Inter. 65, 283–291. https://doi.org/10.1016/0031-9201(91)90135-5.

Torsvik, T.H., Van der Voo, R., 2002. Refining Gondwana and Pangea palaeogeography: estimates of Phanerozoic non-dipole (octupole) fields. Geophys. J. Int. 151, 771–794. https://doi.org/10.1046/j.1365-246X.2002.01799.x.

Torsvik, T.H., Trench, A., Svensson, I., Walderhaug, H.J., 1993. Palaeogeographic significance of mid-Silurian palaeomagnetic results from southern Britain—major

revision of the apparent polar wander path for eastern Avalonia. Geophys. J. Int. 113 (3), 651–668. https://doi.org/10.1111/j.1365-246X.1993.tb04658.x.
Torsvik, T.H., Trench, A., McKerrow, W.S., 1994. Implications of palaeomagnetic data from the Tortworth Silurian inlier (southern Britain) to palaeogeography and Variscan tectonism. Geophys. J. Int. 119 (1), 91–100. https://doi.org/10.1111/j.1365-246X.1994.tb00915.x.
Torsvik, T.H., Tait, J., Moralev, V.M., McKerrow, W.S., Sturt, B.A., Roberts, D., 1995. Ordovician palaeogeography of Siberia and adjacent continents. J. Geol. Soc. London 152, 279–287. https://doi.org/10.1144/gsjgs.152.2.0279.
Torsvik, T.H., Smethurst, M.A., Meert, J.G., Van der Voo, R., McKerrow, W.S., Brasier, Sturt, Walderhaug, H.J., 1996. Continental break-up and collision in the Neoproterozoic and Palaeozoic — A tale of Baltica and Laurentia. Earth-Sci. Rev. 40, 229–258. https://doi.org/10.1016/0012-8252(96)00008-6.
Torsvik, T.H., Ashwal, L.D., Tucker, R.D., Eide, E.A., 2001. Neoproterozoic geochronology and palaeogeography of the Seychelles microcontinent: the India link. Precambrian Res. 110, 47–59. https://doi.org/10.1016/S0301-9268(01)00180-2.
Torsvik, T.H., Dietmar Muller, R., Van der Voo, R., Steinberger, B., Gaina, C., 2008. Global Plate Motion Frames: Toward a Unified Model. Reviews of Geophysics 46. https://doi.org/10.1029/2007RG000227.
Torsvik, T.H., Burke, K., Steinberger, B., Webb, S.J., Ashwal, L.D., 2010a. Diamonds sampled by plumes from the core-mantle boundary. Nature 466, 352–355. https://doi.org/10.1038/nature09216.
Torsvik, T.H., Steinberger, B., Gurnis, M., Gaina, C., 2010b. Plate tectonics and net lithosphere rotation over the past 150My. Earth Planet. Sci. Lett. 291, 106–112. https://doi.org/10.1016/j.epsl.2009.12.055.
Torsvik, T.H., Van der Voo, R., Preeden, U., Mac Niocaill, C., Steinberger, B., Doubrovine, P.V., van Hinsbergen, D.J.J., Domeier, M., Gaina, C., Tohver, E., Meert, J.G., McCausland, P.J.A., Cocks, L.R.M., 2012. Phanerozoic polar wander, palaeogeography and dynamics. Earth-Sci. Rev. 114, 325–368. https://doi.org/10.1016/j.earscirev.2012.06.007.
Torsvik, T.H., van der Voo, R., Doubrovine, P.V., Burke, K., Steinberger, B., Ashwal, L.D., Trønnes, R.G., Webb, S.J., Bull, A.L., 2014. Deep mantle structure as a reference frame for movements in and on the Earth. Proc. Natl. Acad. Sci. U. S. A. 111, 8735–8740. https://doi.org/10.1073/pnas.1318135111.
Trench, A., Torsvik, T.H., 1991. A revised Palaeozoic apparent polar wander path for Southern Britain (Eastern Avalonia). Geophys. J. Int. 104, 227–233. https://doi.org/10.1111/j.1365-246X.1991.tb02506.x.
Trench, A., Torsvik, T.H., Dentith, M.C., Walderhaug, H., Traynor, J.-J., 1992. A high southerly palaeolatitude for Southern Britain in Early Ordovician times: palaeomagnetic data from the Treffgarne Volcanic Formation SW Wales. Geophys. J. Int. 108 (1), 89–100. https://doi.org/10.1111/j.1365-246X.1992.tb00840.x.
Tretyakov, A.A., Degtyarev, K.E., Kovach, V.P., Kotov, A.B., Salnikova, E.B., Pilitsyna, A. V., Yakovleva, S.Z., 2016. The migmatite–gneiss complex of the Chuya–Kendyktas sialic massif (Southern Kazakhstan): Structure and age. Dokl. Earth Sci. 467, 236–240. https://doi.org/10.1134/S1028334X16030156.
Tucker, R.D., Ashwal, L.D., Torsvik, T.H., 2001. U–Pb geochronology of Seychelles granitoids: a Neoproterozoic continental arc fragment. Earth Planet. Sci. Lett. 187, 27–38. https://doi.org/10.1016/S0012-821X(01)00282-5.
Tucker, R.D., Roig, J.Y., Macey, P.H., Delor, C., Amelin, Y., Armstrong, R.A., Rabarimanana, M.H., Ralison, A.V., 2011. A new geological framework for south-central Madagascar, and its relevance to the "out-of-Africa" hypothesis. Precambrian Res. 185, 109–130. https://doi.org/10.1016/j.precamres.2010.12.008.
Tung, K., Yang, H.-J., Yang, H.-Y., Liu, D., Zhang, J., Wan, Y., Tseng, C.-Y., 2007. SHRIMP U-Pb geochronology of the zircons from the Precambrian basement of the Qilian Block and its geological significances. Chin. Sci. Bull. 52, 2687–2701. https://doi.org/10.1007/s11434-007-0356-0.
Vaes, B., Van Hinsbergen, D.J.J., Boschman, L.M., 2019. Reconstruction of subduction and back-arc spreading in the NW Pacific and Aleutian Basin: Clues to causes of Cretaceous and Eocene plate reorganizations. Tectonics 38 (4), 1367–1413. https://doi.org/10.1029/2018TC005164.
van der Meer, D.G., Spakman, W., van Hinsbergen, D.J.J., Amaru, M.L., Torsvik, T.H., 2010. Towards absolute plate motions constrained by lower-mantle slab remnants. Nat. Geosci. 3, 36–40. https://doi.org/10.1038/ngeo708.
Van der Voo, R., 1990. The reliability of paleomagnetic data. Tectonophysics 184, 1–9. https://doi.org/10.1016/0040-1951(90)90116-P.
Van der Voo, R., French, R.B., Williams, D.W., 1976. Paleomagnetism of the Wilberns Formation (Texas) and the late Cambrian palaeomagnetic field for North America. J. Geophys. Res. 81 (32), 5633–5638. https://doi.org/10.1029/JB081i032p05633.
van Hinsbergen, D.J.J., Lippert, P.C., Dupont-Nivet, G., McQuarrie, N., Doubrovine, P.V., Spakman, W., Torsvik, T.H., 2012. Greater India Basin hypothesis and a two-stage Cenozoic collision between India and Asia. Proc. Natl. Acad. Sci. U. S. A. 109, 7659–7664. https://doi.org/10.1073/pnas.1117262109.
van Hinsbergen, D.J.J., Torsvik, T.H., Schmid, S.M., Maţenco, L.C., Maffione, M., Vissers, R.L.M., Gürer, D., Spakman, W., 2020. Orogenic architecture of the Mediterranean region and kinematic reconstruction of its tectonic evolution since the Triassic. Gondwana Res. 81, 79–229. https://doi.org/10.1016/j.gr.2019.07.009.
Van Lente, B., Ashwal, L.D., Pandit, M.K., Bowring, S.A., Torsvik, T.H., 2009. Neoproterozoic hydrothermally altered basaltic rocks from Rajasthan, northwest India: Implications for late Precambrian tectonic evolution of the Aravalli Craton. Precambrian Res. 170, 202–222. https://doi.org/10.1016/j.precamres.2009.01.007.
van Staal, C.R., Barr, S.M., Brendan Murphy, J., 2012. Provenance and tectonic evolution of Ganderia: Constraints on the evolution of the Iapetus and Rheic oceans. Geology 40, 987–990. https://doi.org/10.1130/G33302.1.
Vernikovsky, V.A., Vernikovskaya, A.E., 2001. Central Taimyr accretionary belt (Arctic Asia): Meso–Neoproterozoic tectonic evolution and Rodinia breakup. Precambrian Res. 110, 127–141. https://doi.org/10.1016/S0301-9268(01)00184-X.
Vernikovsky, V.A., Vernikovskaya, A.E., Kotov, A.B., Sal'nikova, E.B., Kovach, V.P., 2003. Neoproterozoic accretionary and collisional events on the western margin of the Siberian craton: new geological and geochronological evidence from the Yenisey Ridge. Tectonophysics 375, 147–168. https://doi.org/10.1016/S0040-1951(03)00337-8.
Vernikovsky, V.A., Vernikovskaya, A.E., Pease, V.L., Gee, D.G., 2004. Neoproterozoic Orogeny along the margins of Siberia. Geological Society, London, Memoirs 30, 233–248. https://doi.org/10.1144/GSL.MEM.2004.030.01.18.
Veselovskiy, R.V., Arzamastsev, A.A., 2011. Evidence for the Mesozoic endogenous activity in the northeastern part of the Fennoscandian Shield. Dokl. Earth Sci. 438, 754–758. https://doi.org/10.1134/S1028334X11060377.
Vick, H.K., Channell, J.E.T., Opdyke, N.D., 1987. Ordovician docking of the Carolina Slate Belt: Paleomagnetic data. Tectonics 6, 573–583. https://doi.org/10.1029/TC006i005p00573.
Vizan, H., Carney, J.N., Turner, P., Ixer, R.A., Tomasso, M., Mullen, R.P., Clarke, P., 2003. Late Neoproterozoic to Early Palaeozoic palaeogeography of Avalonia: some palaeomagnetic constraints from Nuneaton, central England. Geol. Mag. 140, 685–705. https://doi.org/10.1017/S001675680300832X.
von Raumer, J.F., Stampfli, G.M., 2008. The birth of the Rheic Ocean—Early Palaeozoic subsidence patterns and subsequent tectonic plate scenarios. Tectonophysics 461 (1–4), 9–20. https://doi.org/10.1016/j.tecto.2008.04.012.
Walderhaug, H.J., Torsvik, T.H., Eide, E.A., Sundvoll, B., Bingen, B., 1999. Geochronology and palaeomagnetism of the Hunnedalen dykes, SW Norway: implications for the Sveconorwegian apparent polar wander loop. Earth Planet. Sci. Lett. 169, 71–83. https://doi.org/10.1016/S0012-821X(99)00066-7.
Walderhaug, H.J., Torsvik, T.H., Halvorsen, E., 2007. The Egersund dykes (SW Norway): a robust Early Ediacaran (Vendian) palaeomagnetic pole from Baltica. Geophys. J. Int. 168, 935–948. https://doi.org/10.1111/j.1365-246X.2006.03265.x.
Wang, C., Liu, L., Wang, Y.-H., He, S.-P., Li, R.-S., Li, M., Yang, W.-Q., Cao, Y.-T., Collins, A.S., Shi, C., Wu, Z.-N., 2015. Recognition and tectonic implications of an extensive Neoproterozoic volcano-sedimentary rift basin along the southwestern margin of the Tarim Craton, northwestern China. Precambrian Res. 257, 65–82. https://doi.org/10.1016/j.precamres.2014.11.022.
Wang, C.-C., Jacobs, J., Elburg, M.A., Läufer, A., Thomas, R.J., Elvevold, S., 2020. Grenville-age continental arc magmatism and crustal evolution in central Dronning Maud Land. Zircon geochronological and HfO isotopic evidence. Gondwana Res, East Antarctica). https://doi.org/10.1016/j.gr.2019.12.004.
Weil, A.B., Van der Voo, R., Mac Niocaill, C., Meert, J.G., 1998. The Proterozoic supercontinent Rodinia: paleomagnetically derived reconstructions for 1100 to 800 Ma. Earth Planet. Sci. Lett. 154, 13–24. https://doi.org/10.1016/S0012-821X(97)00127-1.
Weil, A.B., Geissman, J.W., Van der Voo, R., 2004. Paleomagnetism of the Neoproterozoic Chuar Group, Grand Canyon Supergroup, Arizona: implications for Laurentia's Neoproterozoic APWP and Rodinia break-up. Precambrian Res. 129, 71–92.
Weil, A.B., Geissman, J.W., Ashby, J.M., 2006. A new paleomagnetic pole for the Neoproterozoic Uinta Mountain supergroup, Central Rocky Mountain States, USA. Precambrian Res. 147, 234–259. https://doi.org/10.1016/j.precamres.2006.01.017.
Wen, B., Li, Y.-X., Zhu, W., 2013. Paleomagnetism of the Neoproterozoic diamictites of the Qiaoenbrak formation in the Aksu area, NW China: Constraints on the paleogeographic position of the Tarim Block. Precambrian Res. 226, 75–90. https://doi.org/10.1016/j.precamres.2012.10.018.
Wen, B., Evans, D.A.D., Li, Y.-X., 2017. Neoproterozoic paleogeography of the Tarim Block: An extended or alternative "missing-link" model for Rodinia? Earth Planet. Sci. Lett. 458, 92–106. https://doi.org/10.1016/j.epsl.2016.10.030.
Wen, B., Evans, D.A.D., Wang, C., Li, Y.-X., Jing, X., 2018. A positive test for the Greater Tarim Block at the heart of Rodinia: Mega-dextral suturing of supercontinent assembly. Geology 46, 687–690. https://doi.org/10.1130/G40254.1.
Wen, B., Evans, D.A.D., Wang, C., Li, Y.-X., Jing, X., 2019. A positive test for the Greater Tarim Block at the heart of Rodinia: Mega-dextral suturing of supercontinent assembly: REPLY. Geology 47 (1), e454. https://doi.org/10.1130/G45711Y.1.
White, C.E., Barr, S.M., Miller, B.V., Hamilton, M.A., 2002. Granitoid plutons of the Brookville terrane, southern New Brunswick: petrology, age, and tectonic setting. Atlantic Geol. 38 (1) https://doi.org/10.4138/1255.
White, C.E., Barr, S.M., Hamilton, M.A., Murphy, J.B., 2020. Age and tectonic setting of Neoproterozoic granitoid rocks, Antigonish Highlands, Nova Scotia, Canada: Implications for Avalonia in the northern Appalachian orogen. Can. J. Earth Sci. https://doi.org/10.1139/cjes-2020-0110.
Wilhem, C., Windley, B.F., Stampfli, G.M., 2012. The Altaids of Central Asia: A tectonic and evolutionary innovative review. Earth-Sci. Rev. 113, 303–341. https://doi.org/10.1016/j.earscirev.2012.04.001.
Williams, G.E., Schmidt, P.W., 2015. Low paleolatitude for the late Cryogenian interglacial succession, South Australia: paleomagnetism of the Angepena Formation, Adelaide Geosyncline. Aust. J. Earth Sci. 62, 243–253. https://doi.org/10.1080/08120099.2015.1003967.
Williams, S., Flament, N., Dietmar Müller, R., Butterworth, N., 2015. Absolute plate motions since 130 Ma constrained by subduction zone kinematics. Earth Planet. Sci. Lett. 418, 66–77. https://doi.org/10.1016/j.epsl.2015.02.026.
Windley, B.F., Alexeiev, D., Xiao, W., Kröner, A., Badarch, G., 2007. Tectonic models for accretion of the Central Asian Orogenic Belt. J. Geol. Soc. London 164, 31–47. https://doi.org/10.1144/0016-76492006-022.
Wingate, M.T.D., Giddings, J.W., 2000. Age and palaeomagnetism of the Mundine Well dyke swarm, Western Australia: implications for an Australia–Laurentia connection

at 755 Ma. Precambrian Res. 100, 335–357. https://doi.org/10.1016/S0301-9268(99)00080-7.
Wingate, M.T.D., Pisarevsky, S.A., De Waele, B., 2010. Paleomagnetism of the 765 Ma Luakela volcanics in Northwest Zambia and implications for Neoproterozoic positions of the Congo Craton. Am. J. Sci. 310, 1333–1344. https://doi.org/10.2475/10.2010.05.
Wu, J., Suppe, J., Lu, R., Kanda, R., 2016. Philippine Sea and East Asian plate tectonics since 52 Ma constrained by new subducted slab reconstruction methods. J. Geophys. Res. [Solid Earth] 121 (6), 4670–4741. https://doi.org/10.1002/2016JB012923.
Wu, C., Zuza, A.V., Yin, A., Liu, C., Reith, R.C., Zhang, J., Liu, W., Zhou, Z., 2017. Geochronology and geochemistry of Neoproterozoic granitoids in the central Qilian Shan of northern Tibet: Reconstructing the amalgamation processes and tectonic history of Asia. Lithosphere 9, 609–636. https://doi.org/10.1130/L640.1.
Wu, L., Murphy, J.B., Quesada, C., Li, Z.-X., Waldron, J.W.F., Williams, S., Pisarevsky, S., Collins, W.J., 2020. The amalgamation of Pangea: Paleomagnetic and geological observations revisited. GSA Bulletin. https://doi.org/10.1130/B35633.1.
Xia, B., Zhang, L., Du, Z., Xu, B., 2017. Petrology and age of Precambrian Aksu blueschist. NW China. Precambrian Res. https://doi.org/10.1016/j.precamres.2017.12.041.
Xiao, W., Windley, B.F., Yong, Y., Yan, Z., Yuan, C., Liu, C., Li, J., 2009. Early Paleozoic to Devonian multiple-accretionary model for the Qilian Shan, NW China. J. Asian Earth Sci. 35, 323–333. https://doi.org/10.1016/j.jseaes.2008.10.001.
Xiao, W.J., Mao, Q.G., Windley, B.F., Han, C.M., Qu, J.F., Zhang, J.E., Ao, S.J., Guo, Q.Q., Cleven, N.R., Lin, S.F., Shan, Y.H., Li, J.L., 2010. Paleozoic multiple accretionary and collisional processes of the Beishan orogenic collage. Am. J. Sci. 310, 1553–1594. https://doi.org/10.2475/10.2010.12.
Xiao, W., Windley, B.F., Allen, M.B., Han, C., 2013. Paleozoic multiple accretionary and collisional tectonics of the Chinese Tianshan orogenic collage. Gondwana Res. 23, 1316–1341. https://doi.org/10.1016/j.gr.2012.01.012.
Xu, D.-R., Xia, B., Li, P.-C., Chen, G.-H., Ma, C., Zhang, Y.-Q., 2007. Protolith natures and U-Pb sensitive high mass-resolution ion microprobe (SHRIMP) zircon ages of the metabasites in Hainan Island, South China: Implications for geodynamic evolution since the late Precambrian. Island Arc 16 (4), 575–597. https://doi.org/10.1111/j.1440-1738.2007.00584.x.
Xu, D., Xia, B., Bakun-Czubarow, N., Bachlinski, R., Li, P., Chen, G., Chen, T., 2008. Geochemistry and Sr-Nd isotope systematics of metabasites in the Tunchang area, Hainan Island, South China: implications for petrogenesis and tectonic setting. Mineral. Petrol. 92, 361–391. https://doi.org/10.1007/s00710-007-0198-0.
Xu, Y., Cawood, P.A., Du, Y., Zhong, Z., Hughes, N.C., 2014. Terminal suturing of Gondwana along the southern margin of South China Craton: Evidence from detrital zircon U-Pb ages and Hf isotopes in Cambrian and Ordovician strata, Hainan Island. Tectonics 33 (12), 2490–2504. https://doi.org/10.1002/2014TC003748.
Xu, X., Song, S., Su, L., Li, Z., Niu, Y., Allen, M.B., 2015. The 600–580Ma continental rift basalts in North Qilian Shan, northwest China: Links between the Qilian-Qaidam block and SE Australia, and the reconstruction of East Gondwana. Precambrian Res. 257, 47–64. https://doi.org/10.1016/j.precamres.2014.11.017.
Yakubchuk, A., 2017. Evolution of the Central Asian Orogenic Supercollage since Late Neoproterozoic revised again. Gondwana Res. 47, 372–398. https://doi.org/10.1016/j.gr.2016.12.010.
Yang, Z.-Y., Sun, Z.M., Ma, X.H., Huang, B.C., Dong, J.M., Zhou, Y.X., Zhu, H., 1996. Preliminary paleomagnetic results from the Lower Paleozoic of North China (Henan Province) and its implications. Chinese Science Bulletin (in Chinese) 42, 401.
Yang, Z., Otofuji, Y.-I., Sun, Z., Huang, B., 2002. Magnetostratigraphic constraints on the Gondwanan origin of North China: Cambrian/Ordovician boundary results. Geophys. J. Int. 151, 1–10. https://doi.org/10.1046/j.1365-246X.2002.01656.x.
Yang, Z., Sun, Z., Yang, T., Pei, J., 2004. A long connection (750–380 Ma) between South China and Australia: paleomagnetic constraints. Earth Planet. Sci. Lett. 220, 423–434. https://doi.org/10.1016/S0012-821X(04)00053-6.
Yang, J.S., Wu, C.L., Chen, S.Y., Shi, R.D., Zhang, J.X., Meng, F.C., Zuo, G.C., Wu, H.Q., Constantinovskaya, E., 2006. Neoproterozoic eclogitic metamorphic age of the Beishan eclogite of Gansu, China: evidence from SHRIMP U–Pb isotope dating. Geology in China 33, 317–325.
Yang, B., Collins, A.S., Blades, M.L., 2019. Middle–late Mesoproterozoic tectonic geography of the North Australia Craton: U–Pb and Hf isotopes of detrital zircon grains in the Beetaloo Sub-basin. Journal of the Geological Society 176, 771–784. https://doi.org/10.1144/jgs2018-159.
Yang, B., Collins, A.S., Cox, G.M., Jarrett, A.J.M., Denyszyn, S., Blades, M.L., Farkaš, J., Glorie, S., 2020. Using Mesoproterozoic sedimentary geochemistry to reconstruct basin tectonic geography and link organic carbon productivity to nutrient flux from a Northern Australian large igneous Province. Basin Res. 60, 175. https://doi.org/10.1111/bre.12450.
Yin, A., Harrison, T.M., 2000. Geologic Evolution of the Himalayan-Tibetan Orogen. Annu. Rev. Earth Planet. Sci. 28, 211–280. https://doi.org/10.1146/annurev.earth.28.1.211.
Young, A., Flament, N., Maloney, K., Williams, S., Matthews, K., Zahirovic, S., Müller, R. D., 2019. Global kinematics of tectonic plates and subduction zones since the late Paleozoic Era. Geoscience Frontiers 10, 989–1013. https://doi.org/10.1016/j.gsf.2018.05.011.
Yuan, C., Sun, M., Yang, J., Zhou, H., Zhou, M.-F., 2004. Nb-depleted, continental rift-related Akaz metavolcanic rocks (West Kunlun): implication for the rifting of the Tarim Craton from Gondwana. Geological Society, London, Special Publications 226, 131–143. https://doi.org/10.1144/GSL.SP.2004.226.01.07.
Zeng, Y.-C., Chen, Q., Xu, J.-F., Chen, J.-L., Huang, F., Yu, H.-X., Zhao, P.-P., 2018. Petrogenesis and geodynamic significance of Neoproterozoic (~925 Ma) high-Fe–Ti gabbros of the RenTso ophiolite, Lhasa Terrane, central Tibet. Precambrian Res. 314, 160–169. https://doi.org/10.1016/j.precamres.2018.06.005.
Zhan, S., Chen, Y., Xu, B., Wang, B., Faure, M., 2007. Late Neoproterozoic paleomagnetic results from the Sugetbrak Formation of the Aksu area, Tarim basin (NW China) and their implications to paleogeographic reconstructions and the snowball Earth hypothesis. Precambrian Res. 154, 143–158. https://doi.org/10.1016/j.precamres.2007.01.001.
Zhang, Q.R., Piper, J.D.A., 1997. Palaeomagnetic study of Neoproterozoic glacial rocks of the Yangzi Block: palaeolatitude and configuration of South China in the late Proterozoic Supercontinent. Precambrian Res. 85, 173–199. https://doi.org/10.1016/S0301-9268(97)00031-4.
Zhang, J., Mattinson, C.G., Meng, F., Wan, Y., Tung, K., 2008. Polyphase tectonothermal history recorded in granulitized gneisses from the north Qaidam HP/UHP metamorphic terrane, western China: Evidence from zircon U-Pb geochronology. Geol. Soc. Am. Bull. 120, 732–749.
Zhang, C.-L., Li, Z.-X., Li, X.-H., Ye, H.-M., 2009. Neoproterozoic mafic dyke swarms at the northern margin of the Tarim Block, NW China: Age, geochemistry, petrogenesis and tectonic implications. J. Asian Earth Sci. 35, 167–179. https://doi.org/10.1016/j.jseaes.2009.02.003.
Zhang, N., Zhong, S., Leng, W., Li, Z.X., 2010. A model for the evolution of the Earth's mantle structure since the Early Paleozoic. J. Geophy. Res. Solid Earth 115 (B6), 1–22. https://doi.org/10.1029/2009JB006896.
Zhang, C.-L., Li, H.-K., Santosh, M., Li, Z.-X., Zou, H.-B., Wang, H., Ye, H., 2012. Precambrian evolution and cratonization of the Tarim Block, NW China: Petrology, geochemistry, Nd-isotopes and U–Pb zircon geochronology from Archaean gabbro-TTG–potassic granite suite and Paleoproterozoic metamorphic belt. J. Asian Earth Sci. 47, 5–20. https://doi.org/10.1016/j.jseaes.2011.05.018.
Zhang, C.-L., Zou, H.-B., Li, H.-K., Wang, H.-Y., 2013a. Tectonic framework and evolution of the Tarim Block in NW China. Gondwana Res. 23, 1306–1315. https://doi.org/10.1016/j.gr.2012.05.009.
Zhang, S., Evans, D.A.D., Li, H., Wu, H., Jiang, G., Dong, J., Zhao, Q., Raub, T.D., Yang, T., 2013b. Paleomagnetism of the late Cryogenian Nantuo Formation and paleogeographic implications for the South China Block. J. Asian Earth Sci. 72, 164–177. https://doi.org/10.1016/j.jseaes.2012.11.022.
Zhang, S., Li, H., Jiang, G., Evans, D.A.D., Dong, J., Wu, H., Yang, T., Liu, P., Xiao, Q., 2015. New paleomagnetic results from the Ediacaran Doushantuo Formation in South China and their paleogeographic implications. Precambrian Res. 259, 130–142. https://doi.org/10.1016/j.precamres.2014.09.018.
Zhang, S.-H., Zhao, Y., Li, X.-H., Ernst, R.E., Yang, Z.-Y., 2017. The 1.33–1.30 Ga Yanliao large igneous province in the North China Craton: Implications for reconstruction of the Nuna (Columbia) supercontinent, and specifically with the North Australian Craton. Earth Planet. Sci. Lett. 465, 112–125. https://doi.org/10.1016/j.epsl.2017.02.034.
Zhao, X., Coe, R.S., Liu, C., Zhou, Y., 1992. New Cambrian and Ordovician paleomagnetic poles for the North China Block and their paleogeographic implications. J. Geophys. Res. Studi. Geol. 97, 1767–1788. https://doi.org/10.1029/91JB02742.
Zhao, G., Cawood, P.A., Wilde, S.A., Sun, M., 2002. Review of global 2.1–1.8 Ga orogens: implications for a pre-Rodinia supercontinent. Earth-Sci. Rev. 59, 125–162. https://doi.org/10.1016/S0012-8252(02)00073-9.
Zhao, P., Chen, Y., Zhan, S., Xu, B., Faure, M., 2014. The Apparent Polar Wander Path of the Tarim block (NW China) since the Neoproterozoic and its implications for a long-term Tarim–Australia connection. Precambrian Res. 242, 39–57. https://doi.org/10.1016/j.precamres.2013.12.009.
Zhao, G., Wang, Y., Huang, B., Dong, Y., Li, S., Zhang, G., Yu, S., 2018. Geological reconstructions of the East Asian blocks: From the breakup of Rodinia to the assembly of Pangea. Earth-Sci. Rev. 186, 262–286. https://doi.org/10.1016/j.earscirev.2018.10.003.
Zhong, S., Liu, X., 2016. The long-wavelength mantle structure and dynamics and implications for large-scale tectonics and volcanism in the Phanerozoic. Gondwana Res. 29, 83–104. https://doi.org/10.1016/j.gr.2015.07.007.
Zhong, S., Rudolph, M.L., 2015. On the temporal evolution of long-wavelength mantle structure of the Earth since the early Paleozoic. Geochem. Geophys. Geosyst. 16 (5), 1599–1615. https://doi.org/10.1002/2015GC005782.
Zhong, S., Zhang, N., Li, Z.-X., Roberts, J.H., 2007. Supercontinent cycles, true polar wander, and very long-wavelength mantle convection. Earth Planet. Sci. Lett. 261, 551–564. https://doi.org/10.1016/j.epsl.2007.07.049.
Zhu, D.-C., Zhao, Z.-D., Niu, Y., Dilek, Y., Mo, X.-X., 2011. Lhasa terrane in southern Tibet came from Australia. Geology 39, 727–730. https://doi.org/10.1130/G31895.1.
Zhu, D.-C., Zhao, Z.-D., Niu, Y., Dilek, Y., Hou, Z.-Q., Mo, X.-X., 2013. The origin and pre-Cenozoic evolution of the Tibetan Plateau. Gondwana Res. 23, 1429–1454. https://doi.org/10.1016/j.gr.2012.02.002.
Zhu, G.-Y., Ren, R., Chen, F.-R., Li, T.-T., Chen, Y.-Q., 2017. Neoproterozoic rift basins and their control on the development of hydrocarbon source rocks in the Tarim Basin, NW China. J. Asian Earth Sci. 150, 63–72. https://doi.org/10.1016/j.jseaes.2017.09.018.